

1-1-2006

# Fatigue damage modeling based on cracking progress in unidirectional and cross-ply FRP composites

Alireza Shirazi  
*Ryerson University*

Follow this and additional works at: <http://digitalcommons.ryerson.ca/dissertations>



Part of the [Mechanical Engineering Commons](#)

---

## Recommended Citation

Shirazi, Alireza, "Fatigue damage modeling based on cracking progress in unidirectional and cross-ply FRP composites" (2006). *Theses and dissertations*. Paper 382.

This Thesis is brought to you for free and open access by Digital Commons @ Ryerson. It has been accepted for inclusion in Theses and dissertations by an authorized administrator of Digital Commons @ Ryerson. For more information, please contact [bcameron@ryerson.ca](mailto:bcameron@ryerson.ca).

# **FATIGUE DAMAGE MODELING BASED ON CRACKING PROGRESS IN UNIDIRECTIONAL AND CROSS-PLY FRP COMPOSITES**

By

**Alireza Shirazi**

**Bachelor of Science in Mechanical Engineering**

**Iran University of Science and Technology, October 1999**

**A thesis to the Ryerson University**

**in fulfillment of the**

**thesis requirement for the degree of**

**Master of Applied Science**

**in**

**Mechanical Engineering**

**Toronto, Ontario, Canada, 2006**

**© Alireza Shirazi**

**PROPERTY OF  
RYERSON UNIVERSITY LIBRARY**

UMI Number: EC54181

## INFORMATION TO USERS

The quality of this reproduction is dependent upon the quality of the copy submitted. Broken or indistinct print, colored or poor quality illustrations and photographs, print bleed-through, substandard margins, and improper alignment can adversely affect reproduction.

In the unlikely event that the author did not send a complete manuscript and there are missing pages, these will be noted. Also, if unauthorized copyright material had to be removed, a note will indicate the deletion.



---

UMI Microform EC54181  
Copyright 2009 by ProQuest LLC  
All rights reserved. This microform edition is protected against  
unauthorized copying under Title 17, United States Code.

---

ProQuest LLC  
789 East Eisenhower Parkway  
P.O. Box 1346  
Ann Arbor, MI 48106-1346

A problem worthy of attack proves its worth by fighting back.

E. G. HARDY.

The Ryerson University requires the signatures of all persons using or photocopying this thesis. Please sign below, and give address and date.

## ACKNOWLEDGEMENTS

Writing a thesis can be considered as a solitary work, but research and implementation are clearly collaborative. Therefore, I first would like to thank all the people that contribute in a variety of ways to make the completion of this work possible.

My deepest thanks go to my supervisor Professor A. Varvani-Farahani for his support, encouragement and advice through my Masters program in the Department of Mechanical and Industrial Engineering at Ryerson University. He guided me through this work with clear-sightedness, drove me into very fruitful discussions and definitely contributed to the success of this work.

Thanks are extended to my friends who morally supported me over period of this study particularly, Dr. H. Haftchenari for his availability and constructive comments.

The Financial support of NSERC through Professor A. Varvani-Farahani of Department of Mechanical and Industrial Engineering, Ryerson University is greatly appreciated.

My gratitude goes to my love Jananeh who patiently encouraged and accompanied me during all the moments of my studies. This work undoubtedly owes a lot to her love, presence and support.

I have a special appreciation to my parents who directed me on this path and undoubtedly without their mercy nothing could have been done.

And, Thanks God for all the blessings has given me.

Alireza Shirazi, August 2006

## ABSTRACT

**Fatigue Damage Modeling based on Cracking Progress in Unidirectional and Cross-ply FRP Composites, Alireza Shirazi, Master of Applied Science Thesis in Mechanical Engineering, Ryerson University, Toronto, Canada, 2006.**

The present study intends to investigate the fatigue damage response of various off-axis unidirectional and cross-ply fiber-reinforced polymer (FRP) composite laminates. A fatigue damage analysis for these composites has been developed based on (i) a cracking mechanism and damage progress in the matrix (Region I), the matrix-fiber interface (Region II) and the fiber (Region III) and (ii) the corresponding stiffness reduction of the composite laminate as the number of cycles progresses. The characteristics of damage growth in unidirectional and cross-ply GRP and CFRP composites materials have been studied and compared with those of available experimental data for the respective materials. Experimentally obtained damage data versus stress cycles was found to be in good agreement with the predicted values.

The predicted fatigue damage results based on the proposed damage model for FRP composites were also found to be in good agreement with experimentally obtained values of fatigue damage at various cyclic stress levels, stress ratios, and off-axis angles for this material reported in the literature. In the cross-ply (0/90) system, the damage function is found to be dependent on the mechanical properties of the fiber and the matrix in 0° and 90° plies.

The proposed damage analysis also puts forward the effect of matrix-fiber interface bonding by introducing the parameter “ $f$ ”. This parameter varies between zero and unity. As  $f$  approaches zero, the interface strength drops and the load transfer from the matrix to the fiber decreases, while for  $f$  approaching unity, the bonding gets stronger and the load from matrix to the fiber is transferred efficiently. A finite element model (FEM) has been developed to estimate the efficiency parameter by using the displacement method in the concentric cylinders model. A comparison between  $f$  values



obtained from FEM and the experimental data is also carried out. The predicted parameter agrees well with the experimental data.

## TABLE OF CONTENTS

<b>AUTHOR'S DECLARATION.....</b>	<b>iii</b>
<b>AKCNOLEGMENTS.....</b>	<b>v</b>
<b>ABSTARCT.....</b>	<b>vii</b>
<b>TABLE OF CONTENTS.....</b>	<b>ix</b>
<b>LIST OF FIGURES.....</b>	<b>xiii</b>
<b>LIST OF TABLES.....</b>	<b>xxi</b>
<b>NOMENCLATURE.....</b>	<b>xxiii</b>
<b>OBJECTIVE AND SCOPE OF THE THESIS.....</b>	<b>xxv</b>
<b>PREFACE.....</b>	<b>xxvi</b>

### **Chapter 1: Introduction and Background**

1.1	Introduction.....	1
1.2	Importance and Application of Unidirectional and Cross-ply FRP Composites in Industries.....	2
1.3	Mechanistic Fatigue Damage Evolution Models and Constituents Cracking in FRP Composites.....	4
1.3.1	Philippidis-Vassilopoulos Model.....	4
1.3.1.1	Shokrieh-Lessard Model.....	6
1.3.2	Ramakrishnan and Jayaraman Model.....	8

### **Chapter 2: Material Characteristics and Properties of Unidirectional and Cross-ply FRP Composites**

2.1	Unidirectional Fiber Reinforced Composite.....	12
2.1.1	Transverse Strength.....	14
2.1.2	Orientation-Dependence of Composite Strength.....	15

2.1.3	Glass Fiber –Reinforced Polymers.....	16
2.1.4	Carbon Fiber-Reinforced Polymers.....	20
2.2	Cross-ply Fiber Reinforced Composite.....	21
2.3	Progressive Damage and Failure in Unidirectional Composites.....	23
2.4	Progressive Damage and Failure in Cross-ply Composites.....	26

### **Chapter 3: Stress and Strain Constituent Relationship in FRP**

3.1	Strains and Stresses.....	27
3.2	Stress-Strain Relationships.....	29
3.2.1	Generally Anisotropic Material.....	29
3.2.2	Transversely Isotropic Material.....	31
3.3	Macro-mechanical Analysis of A Unidirectional Lamina.....	37

### **Chapter 4: Fatigue Damage Analysis and Modelling**

4.1	The fundamental of Damage in Unidirectional FRP Composite.....	43
4.2	Elements of Damage Analysis.....	46
4.2.1	On-axis and Off-axis presentation.....	49
4.3	Modifications on Proposed Equation.....	51
4.3.1	Number of Cycles to Failure and Stiffness drop.....	51
4.3.2	Mean Stress Effect.....	52
4.3.3	Variation of Interface Shear Strength Parameter $f$ with Life Cycles.....	52
4.3.4	Effect of Off-axis Angle $\theta$ .....	54
4.4	Algorithm/Flowchart of Analysis for Unidirectional Composite.....	56
4.5	Elements of Fatigue Damage Analysis for Cross-ply Composite.....	58
4.5.1	Algorithm/Flowchart of Analysis for Cross-ply Composite.....	59

### **Chapter 5: Finite Element Analysis**

5.1	Efficiency of Fiber/Matrix interface in Unidirectional FRP Composite.....	61
-----	---	----

5.2	Numerical Analysis.....	62
5.2.1	Finite Element Model.....	62
5.2.2	Material Property Degradation.....	66
5.3	Nodal Displacement.....	71

**Chapter 6: Evaluation of Fatigue Damage Model**

6.1	GRP and CFRP Unidirectional Fatigue data.....	76
6.1.1	Agarwal and Joneja Data.....	76
6.1.2	Pauchard Data.....	77
6.1.3	Philippidis and Vassilopoulos Data.....	78
6.1.4	Plumtree and Shi Data.....	79
6.1.5	Oever Data.....	80
6.2	Variation of Interfacial Efficiency Parameter f.....	81
6.2.1	Variation of Parameter f for Longitudinal Direction ( $\theta = 0^\circ$ ).....	81
6.2.2	Variation of Parameter f for Off-axis Loading Direction ( $0<\theta<90$ ).....	82
6.2.3	Variation of parameter f for transverse direction.....	86
6.3	Variation of Damage Versus Life.....	87
6.3.1	Variation of Damage Parameter for Unidirectional Longitudinal Direction ( $\theta = 0^\circ$ ).....	87
6.3.2	Variation of Damage Parameter for off-axis angles, $0<\theta<90$ .....	88
6.3.3	Variation of Damage Parameter for Transverse Direction.....	90
6.4	Fatigue data and Properties of Cross-Ply GRP and CFRP Composites.....	93
6.4.1	Corum et al. Data.....	93
6.4.2	Daniel et al. Data.....	93
6.4.3	Boniface and Ogin Data.....	94
6.5	Variation of Damage Versus Life.....	94
6.5.1	Variation of parameter f for Plies of $0^\circ$ and $90^\circ$ .....	94
6.5.2	Variation of Damage Parameter.....	95
6.6	Variation of Interfacial Efficiency Factor.....	102

## **Chapter 7: Discussion of Results**

7.1	Fatigue Damage Evaluation for GRP Composites.....	104
7.1.1	Philippidis-Vassilopoulos GRP Data ( $\theta=0^\circ$ ).....	104
7.1.2	Philippidis-Vassilopoulos GRP Data ( $\theta=75^\circ$ ).....	105
7.1.3	Agarwal- Joneja GRP Composite Fatigue Data ( $\theta=0^\circ$ ).....	106
7.1.4	Pauchard and Oever GRP Composite Fatigue Data ( $\theta=0^\circ$ ).....	107
7.1.5	Agarwal- Joneja GRP Composite Fatigue Data ( $\theta=90^\circ$ ).....	108
7.1.6	Oever GRP Composite Fatigue Data ( $\theta=10^\circ$ ).....	109
7.2	Fatigue Damage Evaluation for CFRP Composites.....	111
7.2.1	Plumtree-Shi CFRP Composite Fatigue Data ( $\theta=0^\circ$ ).....	111

## **Chapter 8: Conclusion and Recommendations**

8.1	Conclusions.....	112
8.2	Recommendation.....	113

<b>References.....</b>	<b>115</b>
------------------------	------------

<b>Appendix A: Material Property and Data.....</b>	<b>120</b>
--	------------

<b>Appendix B: Programming Code.....</b>	<b>181</b>
--	------------

## LIST OF FIGURES

<b>Figure 2.1:</b> A simple unidirectional composite lamina under tensile load .....	13
<b>Figure 2.2:</b> Schematic illustration of the stress/strain curves of composite and its fiber and matrix phases .....	13
<b>Figure 2.3:</b> Schematic variation of Tensile strength versus off-axis angles for FRP composite.....	15
<b>Figure 2.4:</b> Variation of Tensile strength versus off-axis angles for CFRP.....	15
<b>Figure 2.5:</b> Variation of Tensile strength versus off-axis angles for GRP.....	16
<b>Figure 2.6:</b> Stress-strain curves of glass fiber and polyester resin and GRP	
(a) Matrix: Polyester.....	18
(b) Fiber: Glass fiber.....	19
(c) GRP composite.....	19
<b>Figure 2.7:</b> Stress-strain response for CFRP composite	
(a) Tensile test.....	21
(b) Shear test .....	22
<b>Figure 2.8:</b> Schematic diagram of orientation of fibers in cross-ply laminates with plies oriented at $0^\circ/90^\circ$ .....	22
<b>Figure 2.9:</b> Stress-strain response for CFRP cross-ply composite.....	23

**Figure 2.10:** Schematic representation of the development of damage during the fatigue life of composite materials .....25

**Figure 2.11:** Schematic diagram of damage mechanism in a cross-ply laminates.....27

**Figure 3.1:** The global x, y, z and the local 1,2,3 coordinate systems.....28

**Figure 3.2:** The stresses in the global x, y, z and the local 1, 2, 3 coordinate systems.... 29

**Figure 3.3a:** Material with three planes of symmetry .....34

**Figure 3.3b:** Example of a fiber-reinforced, transversely isotropic composite.....34

**Figure 3.4:** An off-axis unidirectional specimen under uniaxial tension the on-axis stresses are found by transforming the off-axis stress from the off-axis to on-axis directions.....38

**Figure 3.5:** The elastic modulus response as off-axis angle changes for a typical unidirectional GRP.....40

**Figure 3.6:** The shear modulus response as off-axis angle changes for a typical unidirectional GRP .....41

**Figure 3.7:** The elastic modulus response as off-axis angle changes for a typical unidirectional CFRP.....41

**Figure 3.8:** The -shear modulus response as off-axis angle changes for a typical unidirectional CFRP .....42

**Figure 4.1:** Three regions of cracking mechanism in unidirectional composites.....44

**Figure 4.2:** An off-axis unidirectional specimen under uniaxial tension the on-axis stresses are found by transforming the off-axis stress form the off-axis to on-axis directions.....49

**Figure 4.3:** The elastic modulus response as off-axis angle changes for unidirectional GRP composite.....51

**Figure 4.4:** Variation of parameter f with number of cycles in logarithmic scale.....53

**Figure 4.5:** Flowchart of generalized material property degradation technique.....56

**Figure 4.6:** Flowchart of identifying f parameter versus life.....57

**Figure 4.7:** Flowchart of generalized material property degradation technique.....60

**Figure 5.1:** The composite cylinder model, (b) cross-section of continuous fiber reinforced composite.....62

**Figure 5.2:** Axisymmetric model of the composite with crack.....63

**Figure 5.3:** Finite element mesh and boundary conditions.....64

**Figure 5.4:** Six nodes triangular quarter point elements at interface of crack tip.....64

**Figure 5.5:** Schematic of 2-Dimensional model used for FEM analysis,  $U_{fx}$  and  $U_{mx}$  are direction of nodal displacements respectively within the fiber and matrix surfaces.....66

**Figure 5.6:** Three regions of cracking mechanism in unidirectional composites.....67

**Figure 5.6 (Cont.):** Fatigue damage curve related to crack development in region I,II and III.....68



<b>Figure 5.7: Fatigue damage versus life in</b>	
GRP composite with cyclic applied load of 120 MPa..	69
CFRP composite with cyclic applied load of 1.306GPa.....	69
<b>Figure 5.8: Flowchart of the finite element implementation in fiber-matrix interfacial debonding study.....</b>	<b>71</b>
<b>Figure 5.9: Selected nodes around the tip of crack: Nodes (a), (c) and (e) on the upper face of crack in fiber surface and (b), (d) and (e) on the lower face of crack in matrix surface.....</b>	<b>73</b>
<b>Figure 5.10: Nodal displacement in x direction for the selected nodes cyclic applied load 120MPa for GRP composite for 5 cyclic intervals.....</b>	<b>74</b>
<b>140MPa for CFRP composite for 8 cyclic intervals.....</b>	<b>75</b>
<b>Figure 6.1: Parameter f versus number of cycles for UD GRP composite (<math>\theta = 0^\circ</math>) tested with stress ratio of <math>R=-1</math>.....</b>	<b>83</b>
<b>Figure 6.2: Parameter f versus number of cycles for UD GRP composite (<math>\theta = 0^\circ</math>) tested with stress ratios of <math>R=0.1</math> and <math>R=0.7</math>.....</b>	<b>84</b>
<b>Figure 6.3: Parameter f versus number of cycles for UD CFRP composite (<math>\theta = 0^\circ</math>) tested with stress ratio of <math>R = 0.1</math>.....</b>	<b>84</b>
<b>Figure 6.4: Parameter f versus number of cycles for UD GRP composite with off-axis angles of <math>0&lt;\theta\leq 90^\circ</math> tested with stress ratio of <math>R = 0.1</math>.....</b>	<b>85</b>
<b>Figure 6.5: Parameter f versus number of cycles for UD GRP composite (<math>\theta=90^\circ</math>) tested with stress ratio of <math>R = -1</math>.....</b>	<b>86</b>

**Figure 6.6:** Predicted damage-life cycles plotted versus experimental values of damage-life cycles for UD GRP composites tested under various cyclic stress magnitudes when off-axis angle and stress ratio are  $\theta = 0^\circ$  and  $R = -1$ , respectively.....88

**Figure 6.7:** Predicted damage-life cycles plotted versus experimental values of damage-life cycles for UD GRP composites tested under various cyclic stress magnitudes when off-axis angle and stress ratios are  $\theta = 0^\circ$  and  $R = 0.1, 0.7$ , respectively.....89

**Figure 6.8:** Predicted damage-life cycles plotted versus experimental values of damage-life cycles for UD CFRP composites tested under various cyclic stress magnitudes when off-axis angle and stress ratio are  $\theta = 0^\circ$  and  $R = 0.1$ , respectively.....90

**Figure 6.9:** Variation of Damage parameter versus life for UD GRP composite, at different cyclic stress magnitude for various off-axis angles of (a)  $\theta = 10^\circ$ , (b)  $\theta = 75^\circ$ , (c)  $\theta = 75^\circ$ , (d)  $\theta = 75^\circ$ and (e)  $\theta = 75^\circ$  .....91

**Figure 6.10:** Predicted damage-life cycles plotted versus experimental values of damage-life cycles for UD GRP composites tested under various cyclic strain magnitudes when off-axis angle and stress ratio are  $\theta = 90^\circ$  and  $R = -1$ , respectively.....92

**Figure 6.11:** Proposed damage of

(a)  $0^\circ$  and  $90^\circ$  plies versus experimental values of damage-life tested under 412.9MPa cyclic stress .....97

(b) 0/90 degree cross-ply and experimental values of damage-life tested under 412.9MPa cyclic stress .....97

(c)  $0^\circ$  and  $90^\circ$  plies versus experimental values of damage-life tested under 662MPa cyclic stress .....97

(d) 0/90 degree cross-ply and experimental values of damage-life tested under 662MPa cyclic stress.....97

**Figure 6.12: Proposed damage of**

(a) 0° and 90° plies versus experimental values of damage-life tested under 140 MPa cyclic stress .....	98
(b) 0/90 degree cross-ply and experimental values of damage-life tested under 140 MPa cyclic stress .....	98
(c) 0° and 90° plies versus experimental values of damage-life tested under 95 MPa cyclic stress .....	98
(d) 0/90 degree cross-ply and experimental values of damage-life tested under 95 MPa cyclic stress.....	98

<b>Figure 6.13: (a) and (c) Proposed damage of 0° and 90° plies versus experimental values of damage-life tested under 448.4 MPa cyclic stress.....</b>	<b>99</b>
(b) and (d) Proposed damage of 0/90 degree cross-ply and experimental values of damage-life tested under 448.4 MPa cyclic stress.....	99

<b>Figure 6.14: (a) and (c) Proposed damage of 0° and 90° plies versus experimental values of damage-life tested under 424.8 MPa cyclic stress.....</b>	<b>100</b>
(b) and (d) Proposed damage of 0/90 degree cross-ply and experimental values of damage-life tested under 424.8 MPa cyclic stress.....	100

<b>Figure 6.15: (a) and (c) Proposed damage of 0° and 90° plies versus experimental values of damage-life tested under 402.9 MPa cyclic stress .....</b>	<b>101</b>
(b) and (d) Proposed damage of 0/90 degree cross-ply and experimental values of damage-life tested under 402.9 MPa cyclic stress.....	101

<b>Figure 6.16: Comparison of Interfacial efficiency factor versus life in logarithmic scale for cyclic loads of (a) <math>\sigma_a=120\text{MPa}</math>, (b) <math>\sigma_a=140\text{MPa}</math>, during the region II of damage.....</b>	<b>102</b>
--	------------

<b>Figure 7.1: Comparison between Predicted damage-life cycles plotted versus experimental values of damage-life cycles for UD GRP composites tested under various</b>	
--	--

cyclic stress magnitudes when off-axis angle and stress ratio are $\theta = 0^\circ$ and $R = -1$ , respectively.....	105
---	-----

<b>Figure 7.2:</b> Comparison between Predicted damage-life cycles plotted versus experimental values of damage-life cycles for UD GRP composites tested under various cyclic stress magnitudes when off-axis angle and stress ratios are $\theta = 0^\circ$ and $R = 0.1$ ,respectively.....	106
---	-----

<b>Figure 7.3:</b> Comparison between Predicted Damage parameter versus life for UD GRP composite, at different cyclic stress magnitude for off-axis angle of $\theta = 75^\circ$ and stress ratio of $R = 0.1$ .....	107
---	-----

<b>Figure 7.4:</b> Comparison between Predicted damage-life cycles plotted versus experimental values of damage-life cycles for UD GRP composites tested under various cyclic strain magnitudes when off-axis angle and stress ratio are $\theta = 0^\circ$ and $R = -1$ , respectively.....	108
--	-----

<b>Figure 7.5:</b> Comparison between Predicted damage-life cycles plotted versus experimental values of damage-life cycles for UD GRP composites tested under various cyclic stress/strain magnitudes when off-axis angle and stress ratios are $\theta = 0^\circ$ and $R = 0.1, 0.7$ , respectively.....	109
--	-----

<b>Figure 7.6:</b> Comparison between Predicted damage-life cycles plotted versus experimental values of damage-life cycles for UD GRP composites tested under various cyclic strain magnitudes when off-axis angles and stress ratio are $\theta = 90^\circ$ and $R = -1$ respectively.....	110
--	-----

<b>Figure 7.7:</b> Comparison between Predicted damage-life cycles plotted versus experimental values of damage-life cycles for UD GRP composites tested under cyclic stress magnitudes when off-axis angle and stress ratios are $\theta = 10^\circ$ and $R = 0.1$ , respectively.....	110
---	-----

**Figure 7.8:** Comparison between Predicted damage-life cycles plotted versus experimental values of damage-life cycles for UD CFRP composites tested under various cyclic strain magnitudes when off-axis angle and stress ratios are  $\theta = 0^\circ$  and  $R = 0.1$  respectively.....111

## LIST OF TABLES

<b>Table 2.1:</b> E-glass fibers properties .....	18
<b>Table 2.2:</b> Carbon fibers properties .....	20
<b>Table 2.3:</b> Average properties for cross-ply composite with 0/90° fiber orientation .....	24
<b>Table 3.1:</b> The elements of the compliance matrix in the x, y, z systems .....	32
<b>Table 3.2:</b> Elements of the compliance matrix in terms of the engineering constants....	35
<b>Table 5.1:</b> Typical engineering properties of fiber, matrix and GRP composite .....	65
<b>Table 5.2:</b> Typical engineering properties of fiber, matrix and CFRP composite. ....	65
<b>Table 5.3:</b> Fatigue testing conditions for 0° directions, $R = -1$ and $V_f = 0.6$ .....	65
<b>Table 5.4:</b> Fatigue testing conditions for 0° directions, $R = 0.1$ and $V_f = 0.58$ .....	66
<b>Table 5.5:</b> Fiber and matrix stiffness during region II of fatigue life for $\sigma_a = 120\text{MPa}$ ...	70
<b>Table 5.6:</b> Fiber and matrix stiffness during region II of fatigue life for $\sigma_a = 1.306\text{GPa}$ ..	70
<b>Table 5.7:</b> Position of selected nodes in matrix and fiber faces.....	72
<b>Table 6.1:</b> Specimen dimensions of the different composites, by Oever .....	80

**Table 6.2:** Variation of  $\alpha$  and  $\beta$  for various sets of GRP and CFRP composite data with on-axis loading direction ( $\theta = 0^\circ$ ).....82

**Table 6.3:** Variation of  $\alpha$  and  $\beta$  for various sets of GRP composite data with off-axis loading direction ( $0<\theta<90$ ) .....83

**Table 6.4:** Variation of n parameter for various UD GRP and CFRP composite fatigue data with various off-axis angles and stress ratios.....87

**Table 6.5:** Variation of n and  $\eta$  for various cross-ply CFRP and GRP composites.....96

**Table 6.6:** Variation of  $\alpha$  and f for GRP composite data with on-axis loading direction ( $\theta = 0^\circ$ ).....102

## NOMENCLATURE

$A_f$	Final cross-sectional area of the composite
$A_0$	Original cross-sectional area of the composite
CFRP	Carbon Fiber Reinforced Polymer
CSM	Chop Stand Mat Fibrous Composites
$\bar{C}_{ij}$	Elements of the Stiffness Matrix $[\bar{C}]$ in x, y, z Coordinate System
$E_f$	Fiber Young's modulus
$E_c$	Composite Young's modulus
$E_f^*$	Fiber Young's modulus ratio
$E_m^*$	Matrix Young's modulus ratio
$E_{f\theta}^*$	Fiber Young's modulus ratio in off axis angle
$E_{m\theta}^*$	Matrix Young's modulus ratio in off axis angle
$E_x$	Composite Young's modulus along off-axis direction
$E_1$	Composite Young's modulus along fiber direction
$E_2$	Composite Young's modulus normal to fiber direction
$f$	Efficiency of the interface
FRP	Fiber Reinforced Plastics
GRP	Glass Fiber Reinforce Polymer
GRE	Glass Fiber Reinforced Epoxy
$G_{12}$	Interlaminar Shear modulus
$G_f$	Shear modulus of fiber
$G_m$	Shear modulus of matrix
$N$	Cycles
$n$	Fatigue life correction factor
$N_f$	Fatigue failure life
$N_f^*$	Modified fatigue failure life
$R$	Stress-ratio (minimum stress/maximum stress)



$r^*$	Modified stress ratio(mean stress/ultimate stress)
$\bar{S}_{ij}$	Elements of the compliance matrix $[\bar{S}]$ in x, y, z coordinate system
UD	Unidirectional fibrous composites
$V_f$	Volume fraction of fiber
$\alpha$	Ratio of normalized shear stress $\tau^*$ to interfacial shear strength ( $\alpha = \tau_s^* / \tau_i$ )
$\epsilon_{11}, \epsilon_{22}, \epsilon_{33}$	Global strain components ( $\epsilon_{11} > \epsilon_{22} > \epsilon_{33}$ )
$\nu_{12}$	Poisson's ratio
$\Theta$	Off-axis angle from fiber direction
$\sigma_a$	Amplitude cyclic stress
$\sigma_{uts}$	Ultimate tensile stress
$\sigma_{app}$	Applied tensile fatigue stress
$\sigma_f$	Stress in fibers
$\sigma_m$	Stress in matrix
$\sigma'_m$	Stress in matrix at the fiber's failure strain
$\sigma_{11}, \sigma_{22}, \sigma_{33}$	Global stress components ( $\sigma_{11} > \sigma_{22} > \sigma_{33}$ )
$\tau_s^*$	Normalized shear stress
$\tau_i$	Interfacial shear strength
$\tau_{12}$	Shear stress along the fiber

## OBJECTIVE AND SCOPE OF THE THESIS

Fiber-reinforced polymer (FRP) composites are broadly used in various industries to manufacture load-bearing engineering components with a high strength/weight ratio. FRP components are extensively used in the aerospace and automotive industries. Durability and fatigue damage assessment of these materials under cyclic loading conditions is of a prime concern and requires an extensive research investigation.

As the number of fatigue cycle increases, cracks are first initiated within the matrix (Region I). Multiple cracks within the matrix grow in length and continue growing along the matrix-fiber interface in Region II. An intensive damage within the composite lamina results in fiber failure in Region III.

The fatigue damage of unidirectional FRP composites was evaluated based on a stiffness reduction damage parameter. It has been found that stiffness change can be quantitatively related to the number of fatigue life cycles in composite laminates and the direction of plies in composite materials. The proposed damage analysis postulates the effect of matrix-fiber interface bonding by introducing the parameter  $f$ . Parameter  $f$  is described as a function of number of cycles  $N$ , interface shear strength, volume fraction of matrix and fiber, and the applied shear stress along the interface

To simulate propagation of a crack at the interface and the bonding efficiency of fiber and matrix under cyclic loading, a FEM study has been employed by using a 2-dimensional axisymmetric finite element model. Results obtained from the analysis help to understand the debonding phenomenon between fiber and matrix interface.

To predict the stiffness degradation and fatigue life of (0/90) cross-ply laminates, the experimentally determined S-N curves for individual unidirectional composite specimens with off axis angles of  $0^\circ$  and  $90^\circ$  laminates have been used. The predicted fatigue damage results based on the proposed damage model for FRP composites were also found to be in good agreement with those of experimentally obtained values at various cyclic stress levels, stress ratios, and off-axis angles.

## PREFACE

The following provides a brief description of materials covered in the chapters of this thesis.

Chapter 1 covers a review of the importance and the application of unidirectional and cross-ply FRP composites in industry. In this chapter, mechanistic fatigue damage evolution models and constituent cracking in FRP composites are introduced.

Chapter 2 addresses the Graphite Reinforced Polymer (GRP) and Carbon Fiber Reinforced Polymer (CFRP) composite characteristics and shows how the mechanical properties of these materials are influenced by the matrix, fiber, volume fraction and orientation of the fiber. This chapter also shows the cracking and damage mechanism in FRP composites.

Chapter 3 reviews the stress and strain relationship and constitutive models for FRP composites.

Chapter 4 represents fatigue damage analysis and modeling. This chapter develops a fatigue damage criterion based on the physics and mechanism of cracking in three regions namely matrix, fiber, and fiber-matrix interface and presents the procedure of fatigue damage analysis in a stepwise algorithm.

Chapter 5 analyzes the matrix-fiber in interface bonding using FEM modeling.

Chapter 6 evaluates the results of fatigue damage model in this thesis. The available experimental data from various laboratories were used to evaluate the capability of the proposed model. The results of damage assessment by the proposed model have been compared with stress-life data extracted from the literature and have shown how closely

the proposed model unifies the fatigue data in unidirectional GRP and CFRP over various off-axis and R-ratios. Also comparison of the matrix-fiber interface friction “  $f$  ” results of FEM with experimentally obtained values has been achieved.

Chapter 7 evaluates the proposed model and compares the capability of the proposed model in correlating fatigue data in unidirectional and cross-ply GRP and CFRP composites. This chapter shows the superiority of the proposed damage model is over other models in evaluating unidirectional GRP and CFRP composites.

Chapter 8 summarizes the conclusion obtained by this study. It gives the key points related to the fatigue assessment of unidirectional and cross-ply GRP and CFRP composites and includes recommendations at the end.

# CHAPTER ONE

## Introduction and Background

### 1.1 Introduction

The prediction of fatigue damage of laminated composite materials has been the subject of many investigations. Different approaches have been adopted, based on different damage parameter for measuring fatigue damage accumulation. The aim of such studies was to establish a process requiring a minimum of experimental data while reliably predicting the condition of the material. Existing fatigue theories can be classified in four categories [1]:

1. Macroscopic failure theories based on static strength criteria modified to account for cyclic loading.
2. Strength degradation fatigue theories, where the damage parameter is the residual strength of the composite material after a cyclic program. According to these, failure occurs when the residual strength decreases to the maximum applied cyclic stress.
3. Stiffness-change fatigue theories are those assuming stiffness degradation as a fatigue damage parameter. The superiority of stiffness degradation damage method over strength degradation damage method lies in its non-destructive inspection option of fatigue damage growth. This is simply coming from the fact that residual strength demonstrates minimal decreases with the number of cycles until a stage close to the end of lifetime when it begins to change rapidly. While stiffness exhibits greater changes during fatigue life therefore one can have a better control over the fatigue test using this method [1–3]. Stiffness based criteria can be established in order to use this method as a design tool, which has been demonstrated by Andersen et al. [4] in their method to design wing blades made of GRP composites.
4. Finally, actual damage mechanisms fatigue theories are based on the modeling of intrinsic defects in the matrix of the composite material that can be treated as matrix

cracks. Cracks can be initiated in the matrix, perpendicular to the direction of loading. Cracks can also be initiated in the interface along the directions of fibers between the fibers and matrix due to debonding. Many experimental fatigue tests have been carried out to study the crack growth in composites when there is only one dominant crack that is propagating. The crack propagates in the same plane and direction as the initial crack. The Paris law [1] is used to describe this fatigue crack propagation behavior. But this is limited to unidirectional aligned fiber reinforced composites. For more general laminates, a similar mode of crack propagation cannot be obtained even under simple loading. Thus, traditional fracture mechanics cannot be used for the fatigue analysis of composite materials. The concept of damage accumulation may be used as a more suitable approach to predict the fatigue life of structures of composite materials.

However, fatigue damage cannot be measured directly. Therefore, for quantitative evaluation of fatigue damage, Young's modulus or the stiffness of composite materials is often used to evaluate the fatigue damage due to cyclic loading [5]. As an instance, the present fatigue damage assessment based on stiffness degradation in unidirectional FRP composite materials, can be called. Available experimental data in the literature has been used to further assess fatigue damage of GRP and CFRP composites using different models developed earlier and the one presented in this study.

## **1.2 Importance and Application of Unidirectional and Cross-ply FRP Composites in Industries**

Composite materials are widely used in aerospace, automotive, and construction applications because of their high specific stiffness and strength, which results in a better performance of materials.

Composite materials were first used in aircraft engine rotor blades in the 1960s [6]. Since then, numerous researches have been conducted to improve the properties of composite materials. Composite materials are also considered for many high-temperature applications in advanced aerospace vehicles and gas turbine engine components. The use of composite materials has been shown to reduce major cost due to failure of components

and structures [7]. Some of these applications involve components that are subjected to cyclic loading. Cyclic loading causes damage and stiffness degradation in a cumulative manner. Composite laminates consist of several layers of fiber-reinforced resin arranged at different angles to each other to control the mechanical properties in different directions. In fact the ability to tailor the mechanical properties is one of the features that make fiber-reinforced composites particularly attractive in car industries. Over the past three decades, the terminology of composite materials has been well acknowledged by the technical community, and composite materials have been gaining exponential acceptance in many industries, serving as competitive candidates for traditional structural and functional materials to realize current and future trends imposed on high performance structures. Striking examples of breakthroughs based on the utilization of composite materials are increasingly found nowadays in transportation vehicles (aircraft, space shuttle and automobile), civil infrastructure (buildings, bridge and highway barriers), and sporting goods (tennis racket, golf club, sailboat) etc., owing to an improved understanding of their performance characteristics and application potentials, especially innovative, cost-effective manufacturing processes.

FRP composites are also finding application in the oil and gas industry, both onshore and offshore. The most significant advances have been made in the areas of pipework and fluid handling, driven by lightweight and corrosion resistance compared to metals. Modest, but significant progress has also been made in structural applications. Lessons are being learned from successful applications with the result that operators, designers and contractors are now beginning to take a serious interest in their wider use. Expansion is therefore expected to continue into all sectors of the oil and gas industry. Research results and new developments have been summarized in a number of references [8-10].

The most successful offshore applications for composites have been in pipework for aqueous liquids. Performance-based guidelines for the design of glass fiber reinforced epoxy (GRP) pipes have significantly accelerated these applications. The chemical resistance of GRP and the maximum use temperature in a particular fluid depends on the type of resin and hardener used. GRP tubes are largely immune to the effects of hydrogen sulphide and carbon dioxide. The most damaging chemical component is often water,

rather than oil, although some highly aromatic species such as toluene and xylene can be damaging. General guidance on suitability for use in particular fluids are given by Stringfellow [11] and by individual pipe manufacturers. Standards for the use of composite piping, such as ISO/DIS 14692 [12], and qualification procedures, such as ASTM 2992[13] and ISO 109281 [14] are facilitating the wider use of these products.

Composites have been used for some time for the manufacture of tanks for water and diesel storage. There are effective and conservative codes that enable both tanks and pressure vessels to be designed for moderate pressures [15-17]. Since a key feature of most pressure vessel codes for composites is the allowable strain, it is probable that future construction will place greater emphasis on resin systems that display improved levels of elongation before cracking occurs in the composite.

The future is expected to bring more widespread use in tanks, as well as in vessels operating at higher pressures than at present. This will probably lead eventually to applications in separators and other high pressure processing equipment where thermal and corrosion requirements can be very demanding.

### **1.3 Mechanistic Fatigue Damage Evolution Models and Constituents Cracking in FRP Composites**

#### **1.3.1 Philippidis-Vassilopoulos Model**

Philippidis and Vassilopoulos [5] have evaluated the fatigue damage of unidirectional GRP composites based on stiffness degradation. They adopted a linear relation between stiffness reduction and number of fatigue cycles.

The damage progress in GRP composite specimens was evaluated by measuring stiffness degradation,  $E_N/E_1$ , defined as:

$$\frac{E_N}{E_1} = 1 - K \left( \frac{\sigma_a}{E_0} \right)^c \frac{N}{N_f} \quad (1.1)$$



where

$E_1$  : modulus of elasticity of the material measured at the first cycle,

$E_0$  : monotonic modulus of elasticity,

$E_N$  : modulus of elasticity corresponding to the  $N^{\text{th}}$  cycle, and

$N_f$  : Number of cycles to failure.

Material constants,  $K$  and  $c$ , in Equation (1.1), are determined by means of the respective experimental data for stiffness degradation, which is assumed to depend on the number of stress cycles,  $N$ , and the applied cyclic stress amplitude,  $\sigma_a$ . Constants  $K$  and  $c$  are obtained from experiment.

For a specific case where  $E_N$  and  $N$  are respectively replaced with  $E_L$  and  $N_L$  values corresponding to a specific, relatively short, life interval, e.g., 60% of  $N_f$ , Equation (1.1) becomes:

$$\frac{E_L}{E_1} = 1 - K \left( \frac{\sigma_a}{E_0} \right)^c \frac{N_L}{N_f} \quad (1.2)$$

Solving Equation (1.2) for  $\left( \frac{\sigma_a}{E_0} \right)^c$  and substituting it into Equation (1.1), the stiffness degradation ratio,  $E_N/E_1$ , is given as:

$$\frac{E_N}{E_1} = 1 - \left( 1 - \frac{E_L}{E_1} \right) \frac{N}{N_L} \quad (1.3)$$

The ratio  $E_N/E_1$  is calculated together with Equation (1.1), and after determination of constants  $K$  and  $c$ ; the stress-life data are extrapolated for a specific stiffness degradation level.

### 1.3.2 Shokrieh-Lessard Model

Shokrieh et al. [18] developed a model that is not dependent on the state of stress; alternatively damage equation must be usable for various states of stress. For this purpose, a normalized damage parameter was introduced. The residual stiffness of a unidirectional CFRP composite ply under arbitrary uniaxial state of stress was proposed as:

$$E = \left( 1 - \frac{\check{D}}{f(\sigma, \sigma_{ult})} \right) E_0 \quad (1.4)$$

where

$E$  : residual stiffness,

$E_0$  : static stiffness,

$\check{D}$  : normalized damage parameter, and

$f(\sigma, \sigma_{ult})$ : function of stress level that can be determined using experimental data.

Function  $f(\sigma, \sigma_{ult})$  for unidirectional ( $\theta = 0^\circ$ ) ply under fatigue loading conditions was defined as:

$$f(\sigma, \sigma_{ult}) = S^m (1 - S)^{m-1} (1 + 3.1Cm) \quad (1.5)$$

While this function for unidirectional ( $\theta = 90^\circ$ ) ply under fatigue loading conditions was given as:

$$f(\sigma, \sigma_{ult}) = (1 - S)^{2m-1} (1 + 3.1Cm) \quad (1.6)$$

where

$$S = \sigma_{max} / \sigma_{ult} = \text{maximum stress / ultimate strength} \quad (1.7)$$

$$m = S(1 - S) \quad (1.8)$$

$$C = \sigma_c / \sigma_t \quad (1.9)$$

Shokrieh et al. [18-20] reformulated the parameter  $C$  defined earlier by Adam et al. [21] to address damage analysis of unidirectional CFRP data tested under transverse fatigue loading conditions. It has been found that for CFRP composite specimens tested under  $\theta = 90^\circ$  off-axis loading, a suitable curve fitting can be obtained by defining  $C = \sigma_t / \sigma_c$ . Utilizing this parameter, the model was able to calculate residual stiffness degradation of a unidirectional ply under uniaxial state of stress.

In Shokrieh et al. model, the normalized damage parameter,  $\check{D}$ , was defined as a function of the normalized number of cycles  $\check{N}$  and independent of stress level. It is noteworthy that  $\check{D}$  versus  $\check{N}$  diagrams of tested CFRP composite were reported to be approximately the same for all states of stress. They also reported that the normalized damage growth was very slow and approximately linear, from the beginning of cyclic loading to about 0.67 (a threshold point) of the normalized fatigue life. Beyond this threshold, damage progressed nonlinearly. Experimental results of damage growth before the threshold point corresponds to  $\check{D} = 0.1493\check{N}$  for unidirectional CFRP composites with  $\theta = 0^\circ$ . While for transversely tested components ( $\theta = 90^\circ$ ), damage growth as number of cycles progress corresponds to  $\check{D} = 0.0361\check{N}$ .

Damage progress as the number of fatigue cycles increases beyond the threshold point ( $0.67 < \check{N} \leq 1$ ) for CFRP components tested with off-axis angles of  $\theta = 0^\circ$  and  $\theta = 90^\circ$  were represented by Equations (1.10) and (1.11) respectively:

$$\check{D} = 5.788\check{N}^4 - 6.8785\check{N}^3 + 2.4153\check{N}^2 - 0.2654\check{N} + 0.0061 \quad (1.10)$$

$$\check{D} = -242.72\check{N}^4 + 715.04\check{N}^3 - 768.3\check{N}^2 + 358.19\check{N} - 61.22 \quad (1.11)$$

where,  $\check{N}$  is the normalized number of cycles where is defined as [19,20]:

$$\check{N} = \frac{\log(N) - \log(0.25)}{\log(N_f) - \log(0.25)} \quad (1.12)$$

where  $N$  is defined as number of applied cycles and  $N_f$  describes the fatigue life of a unidirectional ply under uniaxial state of stress.

$N_f$  was calculated using the following equation, developed by Adam et al. [21].

$$u = \frac{\ln\left(\frac{a}{z}\right)}{\ln[(1-q)(C+q)]} = A + B \log N_f \quad (1.13)$$

where

$$a = \sigma_a / \sigma_t \quad (1.14)$$

$$q = \sigma_m / \sigma_t \quad (1.15)$$

$$\sigma_a = (\sigma_{\max} - \sigma_{\min}) / 2 = \text{Alternating stress} \quad (1.16)$$

$$\sigma_m = (\sigma_{\max} + \sigma_{\min}) / 2 = \text{Mean stress} \quad (1.17)$$

Terms  $\sigma_t$  and  $\sigma_c$  were defined as tensile and compressive strength respectively, and  $z$  and  $u$  are curve fitting parameters. The parameter  $z$  considered as a constant value  $z = 1.06$  [19,20]. The parameter  $u$  for a unidirectional CFRP ply tested under fatigue loading with off-axis angles of  $\theta = 0^\circ$  and  $\theta = 90^\circ$  were respectively given by Equations (1.18) and (1.19) [19,20] as:

$$u = 1.3689 + 0.1097 \log(N_f) \quad (1.18)$$

$$u = 0.999 + 0.096 \log(N_f) \quad (1.19)$$

### 1.3.3 Ramakrishnan and Jayaraman Model

It has been discovered by many researchers that the mechanical behavior of the composite all together depends upon the response of its constituents, namely, the fiber,

the matrix and the their interface. Ramakrishnan and Jayaraman [22] have developed a stiffness-based damage model based on individual constituents as building blocks to determine the overall damage to the composite. In their model, a combination of logarithmic and linear decay functions of time (or cycles) was associated with the stiffness drops for the different damage processes. The total stiffness drop as a function of the number of fatigue cycles was described by a general equation of the form:

$$\frac{E}{E_c} = 1 - A[\{(1-f)\ln(N+1)\} + f(N)] - B \ln\left(1 - \frac{N}{N_f}\right) \quad (1.20)$$

where A, B and f are constants that will be shown to be related to composite constituent properties and  $N_f$  is the number of cycles to failure at the given applied fatigue stress. In Equation (1.20), the parameter f represents the fiber/matrix interface shear strength and varies between 0 to 1. In the specific case of  $f = 0$  interface strength is very small. The Equation (1.20) is then simplified to:

$$\frac{E}{E_c} = 1 - A \ln(N+1) - B \ln\left(1 - \frac{N}{N_f}\right) \quad (1.21)$$

At  $N=N_f-1$ , Equation (1.21) is also simplified as:

$$\frac{E}{E_c} = 1 - \left\{ A \ln(N_f) + B \ln\left(\frac{1}{N_f}\right) \right\} \quad (1.22)$$

Examination of Equation (1.22) indicated that the stiffness of the composite just prior to failure is obtained by subtracting two terms from the initial stiffness ( $E/E_c = 1$ ). It has been assumed at a time just prior to final failure that the matrix is entirely degraded and the fibers are degraded up to a point where the composite can no longer withstand the applied load. It can be further concluded from Equation (1.22) that:

$$A \ln(N_f) = \frac{E_m V_m}{E_c} \quad (1.23)$$

and,

$$B \ln \left( \frac{1}{N_f} \right) = \left( \frac{E_f V_f}{E_c} \right) (1 - r) \quad (1.24)$$

where  $(1-r)$ , represents the fraction of the remaining net cross-section at the time of failure. It is observed that, this has been applied only to the damage term for fibers because matrix cracking occurs early in the fatigue process when the overall composite is intact, while during the fiber breakage process, the effect due to the reduction of cross-section and the load-carrying capability of the composite is significantly affected. This fraction of the net cross-section of the composite at the time of failure can be calculated. If the ultimate tensile strength of the composite is denoted by  $\sigma_{uts}$ , the applied tensile fatigue stress and load are denoted by  $\sigma_{appl}$  and  $P_{appl}$  respectively, and  $A_0$  and  $A_{fail}$  are the original and final cross-sectional area of the composite then  $P_{appl}/A_0 = \sigma_{appl}$  and  $P_{appl}/A_{fail} = \sigma_{uts}$  or

$$\sigma_{appl} / \sigma_{uts} = A_{fail} / A_0 = r \quad (1.25)$$

Equations (1.23) and (1.24) predict the stiffness drops due to each of the damage processes. The damage evolution equation can then be written as:

$$\frac{E}{E_c} = 1 - \frac{E_m V_m}{E_c} \left\{ \frac{\ln (N + 1)}{\ln (N_f)} \right\} - \frac{E_f V_f}{E_c} (1 - r) \left\{ \frac{\ln \left( 1 - \frac{N}{N_f} \right)}{\ln \left( \frac{1}{N_f} \right)} \right\} \quad (1.26)$$

In the general case of composite systems with strong fiber/matrix interfaces,  $(0 < f < 1)$  varying fiber/matrix interface strength, Equation (1.20) can be rewritten by substituting for  $A$  and  $B$  from Equations (1.23) and (1.24) to give:

$$\frac{E}{E_c} = 1 - \left[ \frac{E_m V_m}{E_c} \left[ (1-f) \left\{ \frac{\ln(N+1)}{\ln(N_f)} \right\} + f \left( \frac{N}{N_f} \right) \right] + \frac{E_f V_f}{E_c} (1-r) \left\{ \frac{\ln \left( 1 - \frac{N}{N_f} \right)}{\ln \left( \frac{1}{N_f} \right)} \right\} \right] \quad (1.27)$$

The stiffness reduction due to matrix damage appears to be partitioned between the two rate processes, one logarithmic, and the other linear. The partitioning is done through a fiber/matrix interface strength parameter,  $f$ . The interface is the least understood but the most influential factor in the determination of composite properties. Equation (1.27) thus represents the mechanistically based damage equations that can be used for predicting stiffness drops as a function of cycles in a unidirectional brittle matrix fiber-reinforced composites for two cases: one a general case with variable fiber/matrix interface strength and another a specific case where the interface region is very weak, leading to the physical damage model. All the parameters used in these equations are mechanical properties of the constituents used in the composite.

## CHAPTER TWO

### Material Characteristics and Properties of Unidirectional and Cross-ply FRP Composites

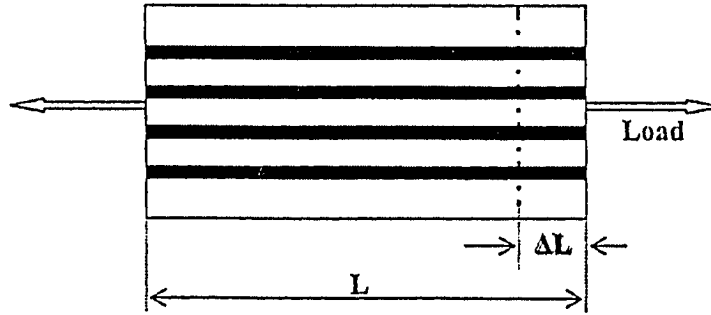
#### 2.1 Unidirectional Fiber Reinforced Composite

Figure 2.1 schematically shows a simple unidirectional composite lamina reinforced with continuous fibers which are initially well bonded to the matrix so that under load fibers and matrix deform together. The applied load is transferred to the matrix and fibres, and the stress on the composite,  $\sigma_c$ , can be expressed by the rule of mixtures:

$$\sigma_c = \sigma_f V_f + \sigma_m (1 - V_f) \quad (2.1)$$

where  $\sigma_f$  and  $\sigma_m$  are the stresses in the fiber and the matrix, respectively. In Equation (2.1),  $V_f$  corresponds to the volume fraction of the fiber. In most practical composites, the high-performance reinforcing fibers are regarded as being brittle, i.e., they deform elastically to failure, showing little or no non-linear deformation. In metal- and polymer-matrix composites, the matrix is usually capable of some irreversible plastic deformation and in such materials the matrix failure strain is usually much greater than that of the fibers.



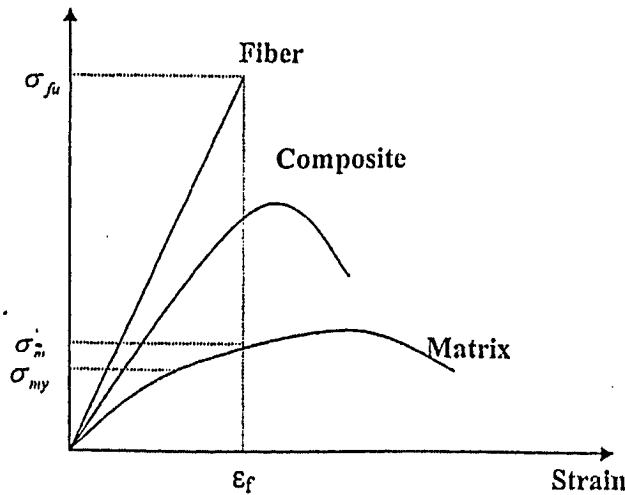


**Figure 2.1:** A simple unidirectional composite lamina under tensile load.

As Figure 2.2 shows, when the stress in the ductile matrix reaches the matrix yield stress,  $\sigma_{my}$ , the matrix continues to bear load, although the slope of the stress/strain curve falls somewhat. If the fibers are carrying most of the load, when the stress on the fibers reaches  $\sigma_{fu}$  (the fiber tensile strength), failure will occur and the stress on the composite at this point,  $\sigma_c$  defines the composite strength:

$$\sigma_c = \sigma_{fu} V_f + \sigma'_m (1 - V_f) \quad (2.2)$$

where  $\sigma'_m$  is the stress in the matrix at the fiber failure strain [24].



**Figure 2.2:** Schematic illustration of the stress/strain curves of composite and its fiber and matrix phases.

### 2.1.1 Transverse Strength

Perpendicular to the reinforcing fibers most composites are weak and failure is controlled by rupture or plastic flow of the matrix, or by fiber /matrix separation. Therefore, to load a composite material perpendicularly to the fiber direction is to load the fiber in the soft and weak diametral direction of the fiber. In addition, if a composite material is loaded perpendicularly to the fiber direction, commonly referred to as the transverse direction, not the entire load is transmitted through the fiber. Since the strengths of unidirectional composites are highly anisotropic, the damage mechanism in FRP composites will depend on the capacity of matrix for plastic deformation and the strength of the fiber/matrix bond. In other words, transverse properties of the composite depend on the strength of the interface bond between the fibers and the matrix. If this bond is weak, the transverse properties of the composite material are poor, and poor interface leads to poor transverse strength. Progressive failure of the interfaces leads to what can be interpreted as low stiffness in the transverse direction. A poor interface results in high resistance to thermal and electrical conduction. Considerable research is directed toward improving the bond at the interface between the fiber and matrix by treating the surface of the fiber before it is combined with the matrix material to form a composite [23].

### 2.1.2 Orientation-Dependence of Composite Strength

Figure 2.3 schematically demonstrates the strength of composite material based on the fiber angle with respect to the tensile axis. Figures 2.4 and 2.5 also represent the tensile strength for CFRP and GRP composites, respectively. It can be observed that tensile strength is maximum for  $0^\circ$  unidirectional and drops rapidly with increasing off-axis angles to  $90^\circ$ . The initial dominant failure is due to fiber failure while higher off-axis angles failure of composite is mainly due to matrix cracking.

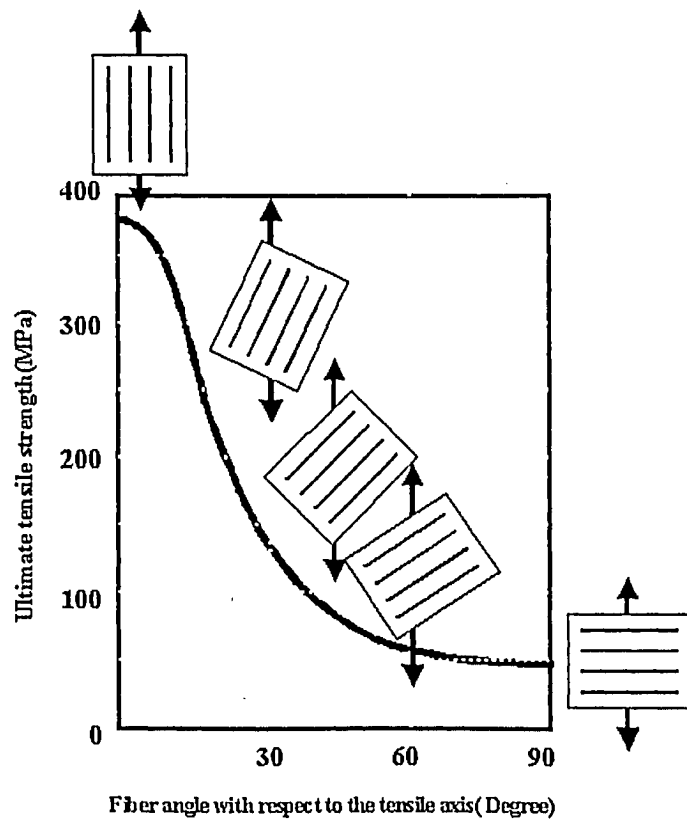


Figure 2.3: Schematic variation of Tensile strength versus off-axis angles for FRP composite.

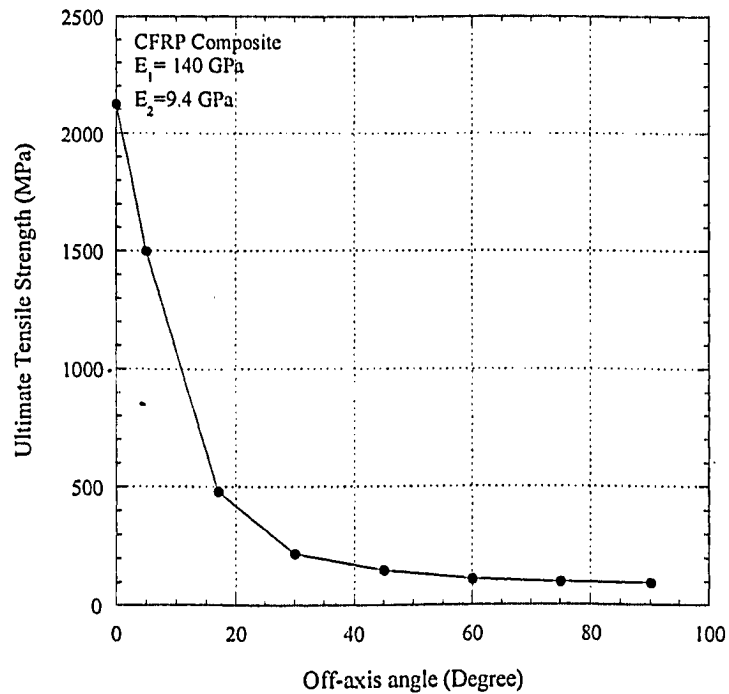
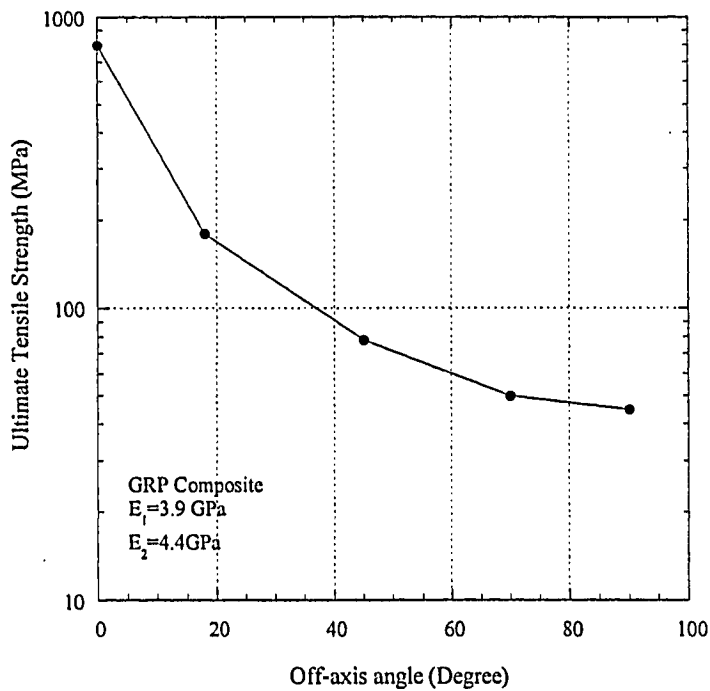


Figure 2.4: Variation of Tensile strength versus off-axis angles for CFRP [23].



**Figure 2.5:** Variation of Tensile strength versus off-axis angles for GRP [23].

### 2.1.3 Glass Fiber –Reinforced Polymers

Glass reinforced Polymer (GRP) is a versatile, durable and economic product. Like graphite-reinforced plastic, the composite material is commonly referred to by the name of its reinforcing fibers (fiberglass), an example of part-for-whole metonymy. Glass fibers or filaments of 8-15  $\mu\text{m}$  in diameter are produced by drawaing molten glass through a suitable orifice [25]. Most fibers for plastics reinforcement are made of a special low alkaline glass, alkali content of less than 1% termed E glass, which draws well and has good strength, stiffness and electrical and weathering properties.

The plastic is most often polyester or vinylester, but other plastics, like epoxy (GRE), are also sometimes used. The glass is mostly in the form of chopped strand mat (CSM), but woven fabrics are also used. Combining high-quality chopped strand mat glass-fiber, retardant resin and often structural-reinforcement, can produce a product with a life expectancy in excess of thirty years. GRP/GRE is a versatile material with many

uses. Although GRP was originally developed in the UK during the second world war as a replacement for the molded plywood used in aircraft radomes (GRP being transparent to microwaves), its first main civilian application was for building boats, where it gained acceptance in the 1950s, and now plays a dominant role. But its use has broadened over the years, and it is used extensively within the automotive and sport equipment sectors, although its use there is being taken over by carbon fiber because of its lower weight. GRE is also used to make hot tubs, pipes for drinking water, sewers, chemicals, and so on. Advanced manufacturing techniques such as pre-pregs and fiber rovings extend the applications and the tensile strength possible with fiber-reinforced plastics.

GRP is also widely used in the telecommunications industry for shrouding the visual appearance of antennas, due to its radio frequency permeability and low signal attenuation properties. It may also be used to shroud the visual appearance of other equipment where no signal permeability is required, such as equipment cabinets and steel support structures, due to the ease with which it can be moulded, manufactured, and painted to custom designs, to blend in with existing structures or brickwork.

GRP is also manufactured in sheet form and used for manufacturing electrical insulators and other structural components commonly found in the power industries. GRP materials for these uses are marketed under the trade name Glastic, or referred to generically as GPO materials like GPO-3. Parts manufactured from these materials are generally machined instead of formed to guarantee dielectric consistency from part to part [23].

Of many other types of glass fibers which are available, the main ones are: A glass, which has an alkali content of 10-15% , is inferior to E glass, but cheaper; S glass ,which is stronger and more temperature resistant than E glass, but more expensive. In this thesis, GRP composite with E glass fiber have been studied. Some typical properties of E glass fiber are given in Table 2.1.

The stress-strain curves resulted from tensile test on polyester resin, glass fiber and GRP composite are presented in Figures 2.6 a, b, and c, respectively. These curves show that the glass fiber is a brittle material and has a linear behavior until failure but the polyester resin is ductile and shows a nonlinear stress-strain curve.

Table 2.1: E-glass fibers properties [23].

Properties	Value	Properties	Value
Specific garvity	2.56 g/m <sup>3</sup>	Coefficient of thermal expansion	4.7-5× 10 <sup>-6</sup> /° C
Tensile strength	1.4-3.45 GPa	Dielectric constant at 1 MHZ	6.4
Elongation	1.8-3.2 %	Thermal conductivity	1.04-1.3 W/m/°C
Tensile modulus	72.4 GPa	Density	2540 Kg/m <sup>3</sup>
Poisson ratio	0.2	Hardness(Vickers 50g-15g)	5.6

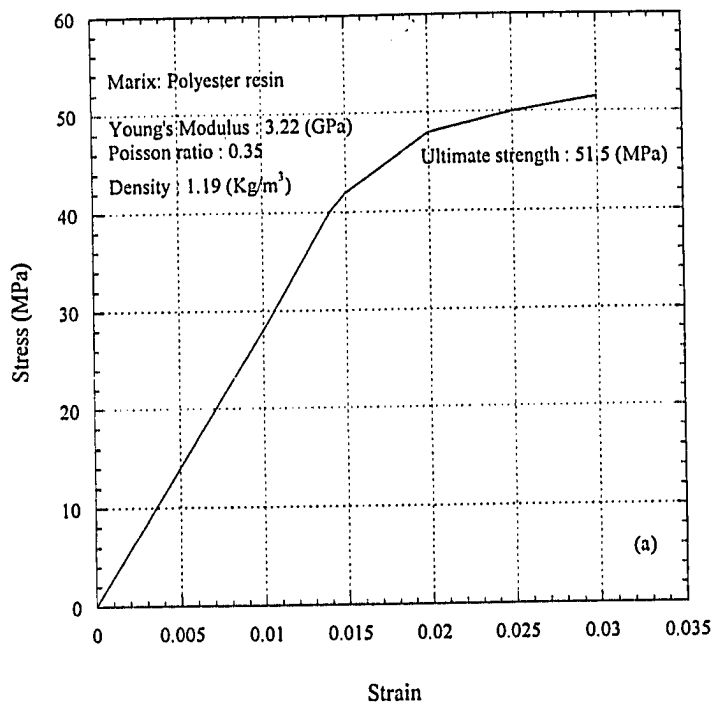


Figure 2.6: Stress-strain curves of glass fiber and polyester resin and GRP [23]

(a) Matrix: Polyester.

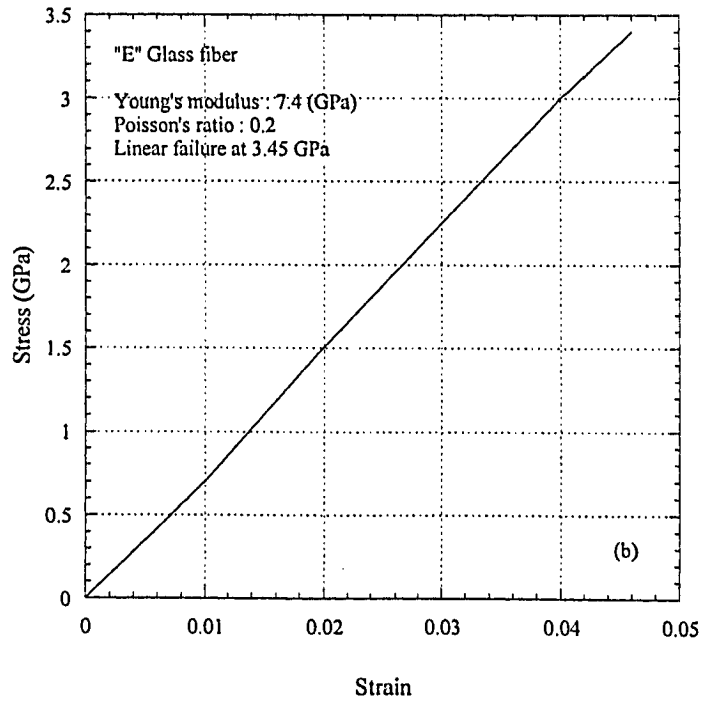


Figure 2.6 (Cont.): Stress-strain curves of glass fiber, polyester resin and GRP [23]

(b) Fiber: Glass fiber.

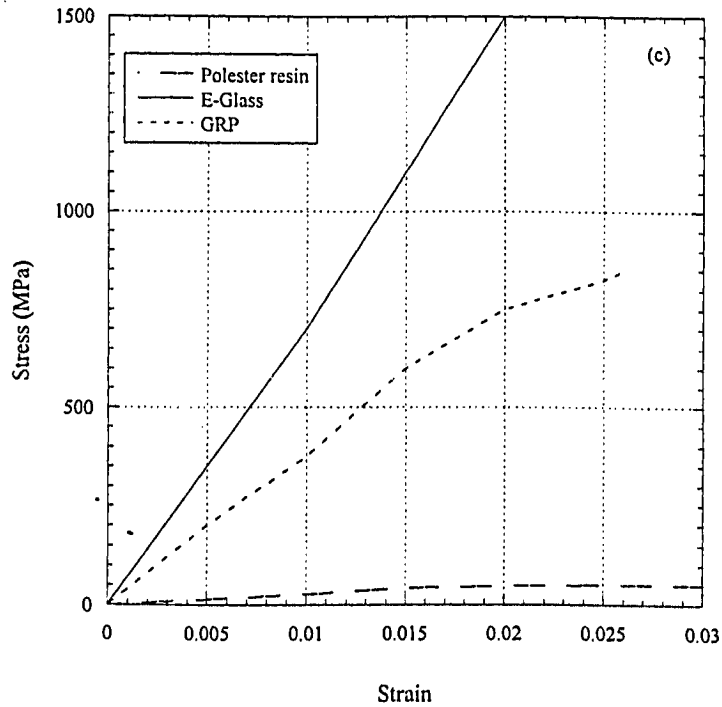


Figure 2.6 (Cont.): Stress-strain curves of glass fiber, polyester resin and GRP [23]

(c) GRP Composite.

#### 2.1.4 Carbon Fiber-Reinforced Polymers

The advent of high-modulus carbon (graphite) fibers obtained from continuous polyacrylonitrile (PAN) filaments has caused considerable technical interest in recent years. Although a continuous spectrum of fiber strength and modulus values can be obtained by varying the process details, especially the maximum temperature at which the fibers are pyrolyzed, they are usually marked in the three basic forms often referred to as Types I, II, III fibers. For practical purposes, the fibers can only be used in conjunction with polymeric matrices such as epoxy and polyester resins. Typical properties of carbon fibers are given in Table 2.2.

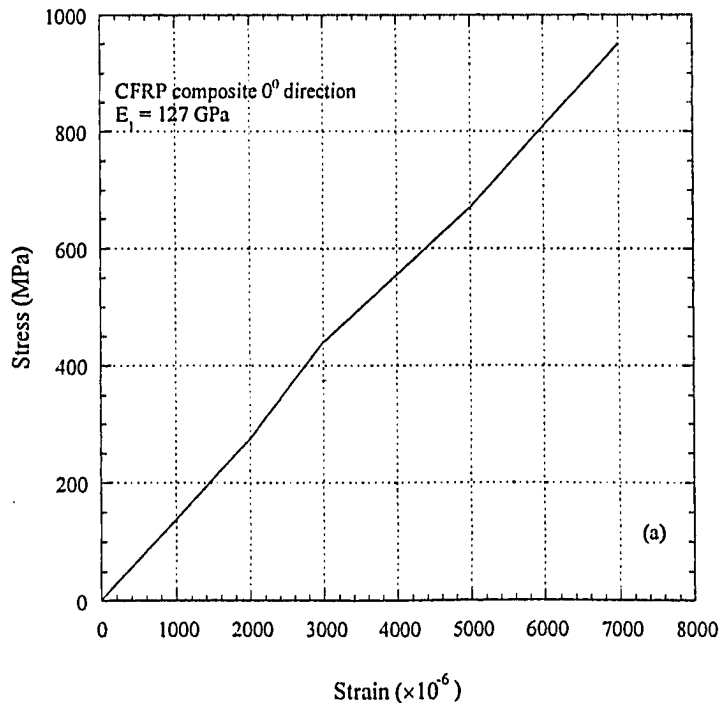
**Table 2.2:** Carbon fibers properties [23].

Properties	Value	Properties	Value
Filament diameter	8-9 $\mu\text{m}$	Coefficient of thermal expansion	$7-12 \times 10^{-6} / ^\circ\text{C}$
Tensile strength	2.4-2.9 GPa	Specific heat	950 J/Kg/ $^\circ\text{K}$
Elongation	1 %	Thermal conductivity	20 W/m/ $^\circ\text{C}$
Tensile modulus	228-276 GPa	Density	1950 Kg/m <sup>3</sup>
Poisson's ratio	0.3	Shear modulus	5.5 GPa

It should be noted that the high modulus of carbon fibers causes more anisotropy in strength, modulus, and thermal expansion coefficients than similar composites incorporating glass fibers. For a given type of fiber, the axial tensile strength and modulus of a composite depends on the volume fraction of fibers and only to a slight



extent on the resin system employed. The axial compressive strength is substantially lower than the tensile strength. Figure 2.7a presents the tensile stress-strain curve, which is almost linear until failure so fiber properties are dominant. Figure 2.7b presents the shear stress-strain curve of CFRP composite, which is non-linear, and this non-linearity is due to matrix ductility.



**Figure 2.7:** Stress-strain response for CFRP composite, (a) tensile test.

## 2.2 Cross-ply Fiber Reinforced Composite

A laminate is said to be a cross-ply laminate if every layer has its fibers oriented at either  $0^\circ$  or  $90^\circ$ . This implies that the laminate consists of plies, which are unidirectional fiber composites. Figure 2.8 schematically demonstrates a cross-ply composite material laminated so that one layer is oriented at a perpendicular angle to the other layer with respect to the laminate grain. A cross-ply composite consists of an arbitrary number of layers of the same material and thickness but with alternating orientations of  $0^\circ$  and  $90^\circ$ .

This bi-directional laminate is orthotropic and has a Poisson's ratio of nearly zero. In the tensile loading case, the behavior of specimens with the 0/90° fiber orientation is fiber dominated [2]. Typical properties of CFRP cross-ply composite are given in Table 2.3.

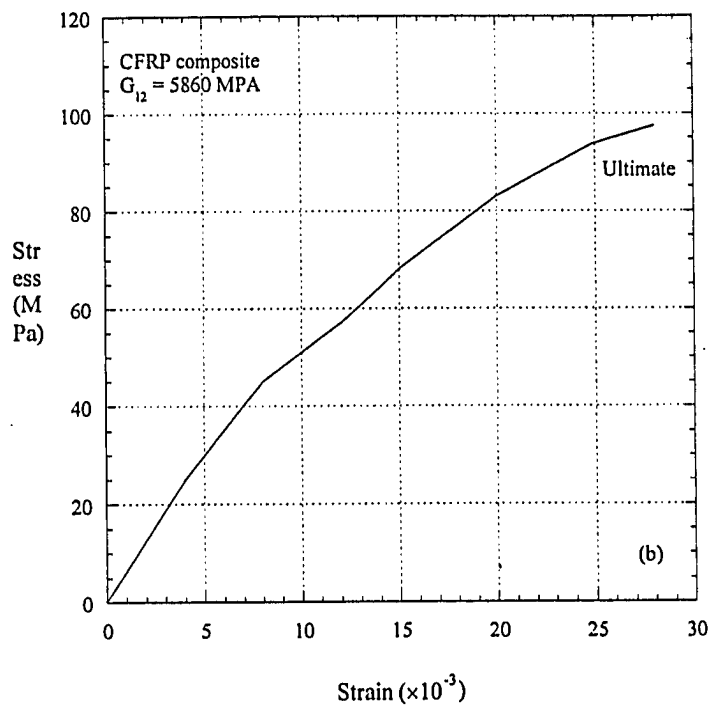


Figure 2.7 (Cont.): Stress-strain response for CFRP composite, (b) Shear test [24]

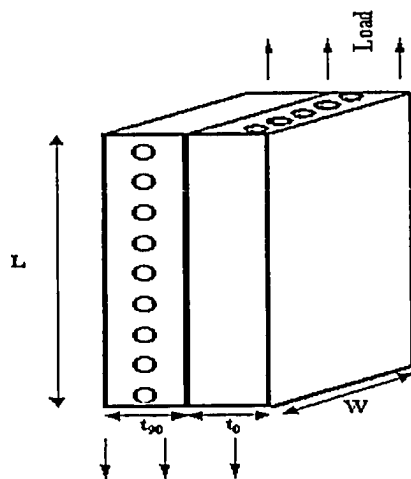
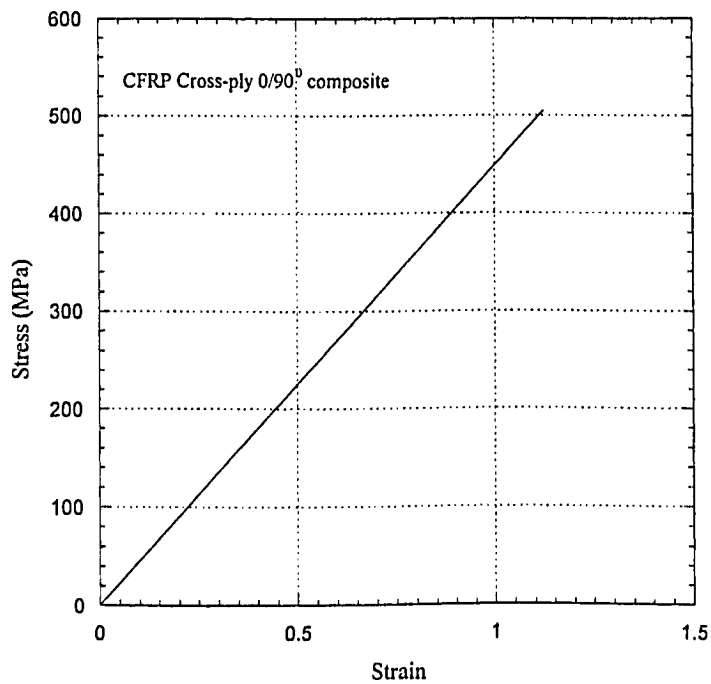


Figure 2.8: Schematic diagram of orientation of fibers in cross-ply laminates with plies oriented at 0/90°.

Many observations have confirmed that the first form of damage in cross-ply laminates loaded in tension is matrix cracking or micro cracking in the off-axis plies [26]. Microcracks are observed in  $90^\circ$  plies in which they are termed transverse cracks. Microcracks are observed during static loading, fatigue loading, thermal loading or any combination of these loadings. At the further stages of loading, the transverse microcracks can promote delamination between the off-axis ply and the adjacent ply, longitudinal splitting in the  $0^\circ$  plies and, finally, the laminate failure. Figure 2.9 presents the tensile stress-strain curve for a cross-ply composite, which is almost linear until failure, so fiber properties are dominant.



**Figure 2.9:** Stress-strain response for CFRP cross-ply composite [24]

### 2.3 Progressive Damage and Failure in Unidirectional Composites

Fatigue loading of composite laminates consists of the application of loads or strains that vary with time, usually in a cycle. By definition, the loads or strains reach amplitudes that are less than the values required to fracture the laminates in monotonic loading tests. If

eventual failure due to cyclic loading occurs, then damage must have been developed in the laminate during the fatigue damage progress.

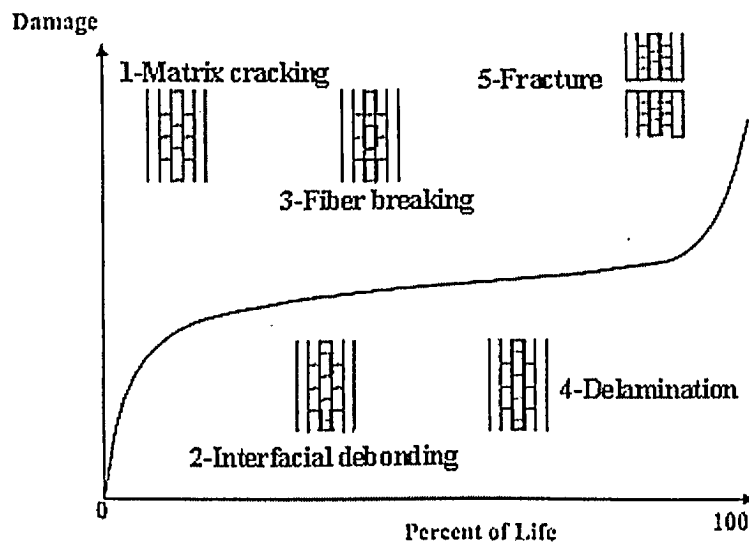
**Table 2.3:** Average properties for cross-ply composite with 0/90° fiber orientation [23].

Property	Value	Property	Value
Tensile modulus	44.9 GPa	Poisson's ratio	0.076
Tensile strength	474 MPa	Shear modulus	2.96 GPa
Shear strength	92.8 MPa	Tensile strain	1.01

The damage process in composite laminates consists of the initiation and growth of several different damage modes and complex interactions between damage modes. The number of unique damage modes and the interactions between damage modes and subsequent effects on fatigue behavior are dependent on material, load, geometry, and environment. The progressive development of damage during fatigue life can be overviewed with the aid of Figure 2.10, which traces the damage process as a function of percentage of life of composite laminates which contain 0° plies and off-axis plies subjected to cyclic tension-compression loading. Under such conditions, there is some combination of damage modes to occur as illustrated schematically in Figure 2.10.

Cracks are initially initiated within the matrix and upon cyclic loading. These cracks are the source of subsequent damage development and form the interfacial debonding and delaminations in stages 2 and 3. In the stages 2 and 3, cracks develop in directions parallel to fibers in continuous-fiber-reinforced materials. In duration between stages 1-4, a fiber bundle embedded in a matrix does not behave like a free fiber bundle. When the local load level reaches the failure stress at a weak point in a given fiber it breaks and the carried load is transferred back into the neighboring matrix regions. But away from the broken ends the fiber carries its full share of the load, by contrast with

what happens in an unbounded bundle. The stress carried by neighboring fibers in the vicinity of the break will be disturbed, but the stress concentration may not be great enough to break a neighboring fiber (or fibers). As the load on the composite increases, more fibers will fail, but without seriously damaging the overall load-bearing ability of the composite. This is mainly due to the fact that the tensile load supported by the broken fiber within a short distance, will rapidly build up again to its original level.

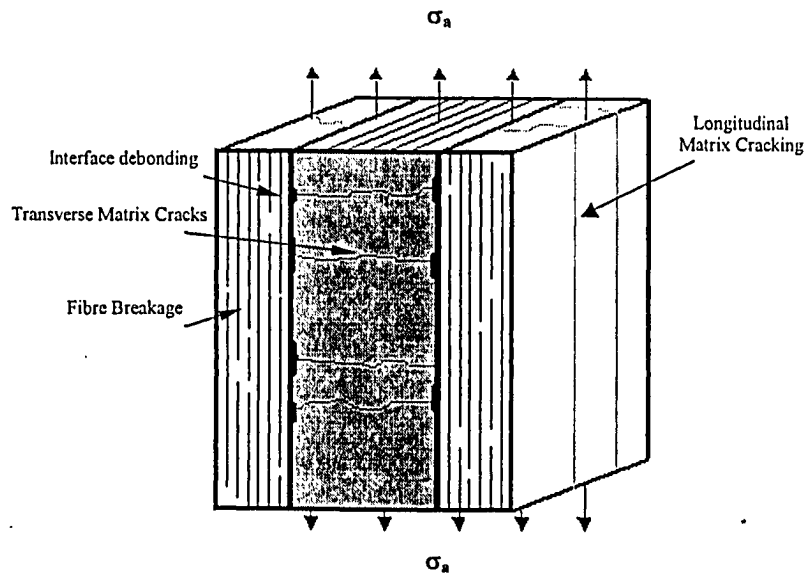


**Figure 2.10:** Schematic representation of the development of damage during the fatigue life of composite materials.

If the process is repeated a number of times, the cross section where the breaks are occurring will rapidly become too weak to support the applied load and catastrophic brittle failure will follow in stage 5. Fiber breaks accumulate randomly throughout the whole sample or structure. The final failure may then occur when the number of breaks in any one cross-section has effectively reduced the local  $V_f$  below that required supporting the applied load [26].

## 2.4 Progressive Damage and Failure in Cross-ply Composites

The framework for the discussion of damage is laminate stiffness reduction as the number of fatigue cycles increases. In each laminate, damage progress under cyclic loading follows three stages of cracking respectively within the matrix, the matrix-fiber interface and the fiber: Stage I, a rapid initial decrease in stiffness; Stage II, a larger, intermediate period of approximately linear stiffness reduction; and Stage III, a final rapid stiffness decrease resulting in failure of component. These stages in fatigue damage development in the cross-ply  $0/90^\circ$  laminate can be characterized as follows: in stage I, the predominant mode is transverse cracking; in stage II, longitudinal cracks nucleate and grow along the specimen length in the  $0^\circ$  plies and produce interior delaminations at the  $0/90^\circ$  degree interface; in stage III, these delaminations join together in regions between longitudinal cracks, separating small volumes of material in the  $0^\circ$  plies which become longitudinal splits, and ultimately fiber breakage of the load-carrying ( $0^\circ$ ) plies occurs, as shown schematically in Figure 2.11[27]. Fatigue damage, which develops during the first stage in a laminate, consists of the development of transverse cracks, which ultimately form a saturated pattern of cracks in the  $90^\circ$  layer, then grow slowly across the specimen width as a function of cycle number. This well-defined and predictable condition at early stage of damage development for matrix cracking is called as CDS (Characteristic Damage State). The subsequent two stages are related to an advanced damage state. This first stage is followed by longitudinal matrix crack splitting, local delamination at intersections of transverse and longitudinal cracks and ultimately by fiber fracture of the  $0^\circ$  layers carrying the load applied to laminates [27].



**Figure 2.11:** Schematic diagram of damage mechanism in a cross-ply laminates.

## **CHAPTER THREE**

### **Stress and Strain Constituent Relationship in FRP**

#### **3.1 Strains and Stresses**

Fiber reinforced polymer (FRP) composites consist of continuous or discontinues brittle fibers embedded in a matrix. Such a composite is heterogeneous (i.e., the properties vary from point to point). On a scale that is large with respect to the fiber diameter, the fiber and matrix properties may be averaged, and the material may be treated as homogeneous.

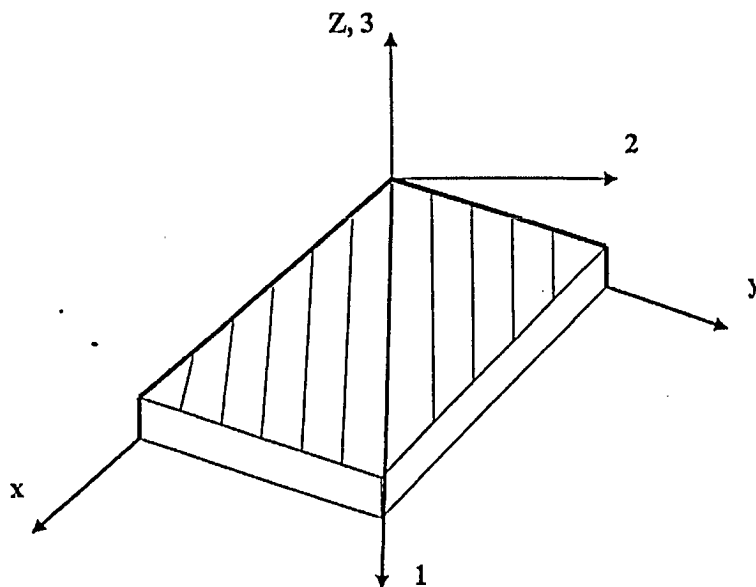
The material is considered to be quasi-homogeneous, which implies that the properties are taken to be the same at every point. These properties are not the same as the properties of either the fiber or the matrix but are a combination of the properties of the constituents.

The study of the stress-strain response of a single layer is assumed to be equivalent to determining the relations between the stresses applied to the bonding surfaces of the layer and the deformations of the layer as a whole. The strain of an individual fiber or element of matrix is no consequence to this level of analysis. The effect of the fiber reinforcement is smeared over the volume of material, and it is assumed that the two-materials, fiber-matrix system, is equivalent to a single homogenous material. This is an important concept because it makes the analysis of a fiber-reinforced composite easier. Equally important is the fact that this single material does not have the same properties in all directions. Composite system is obviously stronger and stiffer in the fiber direction (direction 1) than in the matrix directions (directions 2 and 3). In addition, just because the matrix directions are both perpendicular to the fiber direction, the properties in these two directions are not necessarily equal to each other. A material with different properties in three mutually perpendicular directions is called an orthotropic material. As a result, a layer is said to be orthotropic [23]. The 1-

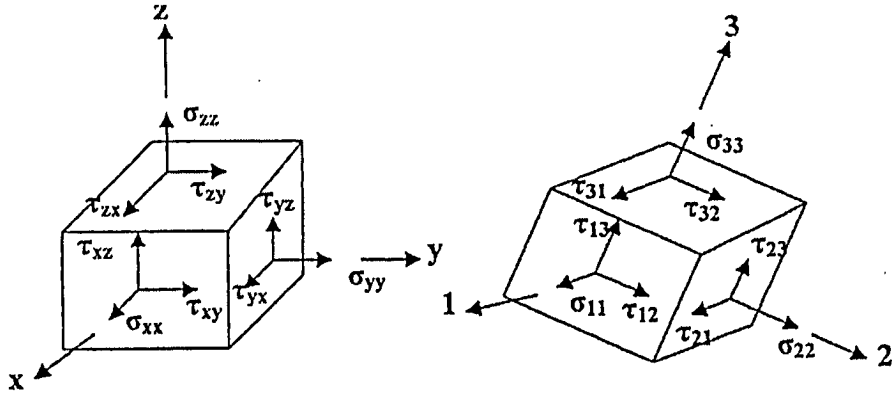


2, 1-3 and 2-3 are three planes, and the material properties are symmetric with respect to each of these planes.

In this chapter, equations are presented for calculating the stress, and strains when the structure undergoes only small deformations and the material behaves in a linearly elastic manner. A unidirectional FRP composite consists of fibers reinforced within the matrix phase with an off-axis angle  $\theta$  with respect to the applied loading axis. It is therefore convenient to employ two coordinate systems: a local coordinated system aligned, at a point with the fibers and a global coordinate system attached to a fixed reference point. Figure 3.1 presents global and local coordinate systems used for fibrous composites. The local and global Cartesian coordinate systems are designated respectively by 1,2,3, and the x, y, z-axes designate the local and global Cartesian coordinate systems respectively. In the x, y, z coordinate system the normal stresses are denoted by  $\sigma_{xx}$ ,  $\sigma_{yy}$ ,  $\sigma_{zz}$  and the shear stresses by  $\tau_{yz}$ ,  $\tau_{xz}$ ,  $\tau_{xy}$ . The corresponding normal and shear strains are  $\epsilon_{xx}$ ,  $\epsilon_{yy}$ ,  $\epsilon_{zz}$  and  $\gamma_{yz}$ ,  $\gamma_{xz}$ ,  $\gamma_{xy}$  respectively. In the 1,2, 3 principal material coordinate system the normal stresses are denoted by  $\sigma_{11}$ ,  $\sigma_{22}$ ,  $\sigma_{33}$  and the shear stresses are denoted by  $\tau_{23}$ ,  $\tau_{13}$ ,  $\tau_{12}$ . The corresponding normal and shear strains are  $\epsilon_{11}$ ,  $\epsilon_{22}$ ,  $\epsilon_{33}$  and  $\gamma_{23}$ ,  $\gamma_{13}$ ,  $\gamma_{12}$  respectively. The symbol  $\gamma$  represents engineering shear stain. Figure 3.2 presents all tonsorial stresses in x, y, z and 1, 2, 3 coordinates.



**Figure 3.1:** The global x, y, z and the local 1,2,3 coordinate systems.



**Figure 3.2:** The stresses in the global  $x, y, z$  and the local  $1, 2, 3$  coordinate systems.

## 3.2 Stress-Strain Relationships

In a composite material, the fibers may be oriented in an arbitrary manner. Depending on the arrangements of the fibers, the material may behave differently in different directions. According to their behavior, composites may be characterized as generally anisotropic, monoclinic, orthotropic, transversely isotropic or isotropic. In the following, the stress-strain relationships for these types of materials under linearly elastic conditions are presented.

### 3.2.1 Generally Anisotropic Material

When there are no symmetry planes with respect to the alignment of the fibers, the material is referred to as generally anisotropic. A fiber-reinforced composite material is generally anisotropic when the fibers are aligned in three non-orthogonal directions. For a generally anisotropic linearly material in the  $x, y$ , and  $z$  global coordination the stress-strain relationships are presented in Equation (3.1) [23]:

$$\begin{Bmatrix} \sigma_{xx} \\ \sigma_{yy} \\ \sigma_{zz} \\ \tau_{yz} \\ \tau_{xz} \\ \tau_{xy} \end{Bmatrix} = \begin{bmatrix} \bar{C}_{11} & \bar{C}_{12} & \bar{C}_{13} & \bar{C}_{14} & \bar{C}_{15} & \bar{C}_{16} \\ \bar{C}_{21} & \bar{C}_{22} & \bar{C}_{23} & \bar{C}_{24} & \bar{C}_{25} & \bar{C}_{26} \\ \bar{C}_{31} & \bar{C}_{32} & \bar{C}_{33} & \bar{C}_{34} & \bar{C}_{35} & \bar{C}_{36} \\ \bar{C}_{41} & \bar{C}_{42} & \bar{C}_{43} & \bar{C}_{44} & \bar{C}_{45} & \bar{C}_{46} \\ \bar{C}_{51} & \bar{C}_{52} & \bar{C}_{53} & \bar{C}_{54} & \bar{C}_{55} & \bar{C}_{56} \\ \bar{C}_{61} & \bar{C}_{62} & \bar{C}_{63} & \bar{C}_{64} & \bar{C}_{65} & \bar{C}_{66} \end{bmatrix} \begin{Bmatrix} \epsilon_{xx} \\ \epsilon_{yy} \\ \epsilon_{zz} \\ \gamma_{yz} \\ \gamma_{xz} \\ \gamma_{xy} \end{Bmatrix} \quad (3.1)$$

where  $\bar{C}_{ij}$  are the elements of the stiffness matrix  $[\bar{C}]$  in the x, y, and z coordinate system. Inversion of Equation (3.1) results in the following strain-stress relationship in Equation (3.2):

$$\begin{Bmatrix} \epsilon_{xx} \\ \epsilon_{yy} \\ \epsilon_{zz} \\ \gamma_{yz} \\ \gamma_{xz} \\ \gamma_{xy} \end{Bmatrix} = \begin{bmatrix} \bar{S}_{11} & \bar{S}_{12} & \bar{S}_{13} & \bar{S}_{14} & \bar{S}_{15} & \bar{S}_{16} \\ \bar{S}_{21} & \bar{S}_{22} & \bar{S}_{23} & \bar{S}_{24} & \bar{S}_{25} & \bar{S}_{26} \\ \bar{S}_{31} & \bar{S}_{32} & \bar{S}_{33} & \bar{S}_{34} & \bar{S}_{35} & \bar{S}_{36} \\ \bar{S}_{41} & \bar{S}_{42} & \bar{S}_{43} & \bar{S}_{44} & \bar{S}_{45} & \bar{S}_{46} \\ \bar{S}_{51} & \bar{S}_{52} & \bar{S}_{53} & \bar{S}_{54} & \bar{S}_{55} & \bar{S}_{56} \\ \bar{S}_{61} & \bar{S}_{62} & \bar{S}_{63} & \bar{S}_{64} & \bar{S}_{65} & \bar{S}_{66} \end{bmatrix} \begin{Bmatrix} \sigma_{xx} \\ \sigma_{yy} \\ \sigma_{zz} \\ \tau_{yz} \\ \tau_{xz} \\ \tau_{xy} \end{Bmatrix} \quad (3.2)$$

where  $\bar{S}_{ij}$  are the elements of the compliance matrix  $[\bar{S}]$  in the x, y, z coordinate system and are defined in Table 3.2. In the 1, 2, 3 coordinate system, the stress-strain relationships can be defined by Equation (3.3):

$$\begin{Bmatrix} \sigma_{11} \\ \sigma_{22} \\ \sigma_{33} \\ \tau_{23} \\ \tau_{13} \\ \tau_{12} \end{Bmatrix} = \begin{bmatrix} C_{11} & C_{12} & C_{13} & C_{14} & C_{15} & C_{16} \\ C_{21} & C_{22} & C_{23} & C_{24} & C_{25} & C_{26} \\ C_{31} & C_{32} & C_{33} & C_{34} & C_{35} & C_{36} \\ C_{41} & C_{42} & C_{43} & C_{44} & C_{45} & C_{46} \\ C_{51} & C_{52} & C_{53} & C_{54} & C_{55} & C_{56} \\ C_{61} & C_{62} & C_{63} & C_{64} & C_{65} & C_{66} \end{bmatrix} \begin{Bmatrix} \epsilon_{11} \\ \epsilon_{22} \\ \epsilon_{33} \\ \epsilon_{23} \\ \gamma_{13} \\ \tau_{12} \end{Bmatrix} \quad (3.3)$$

where  $C_{ij}$  are the elements of the stiffness matrix  $[C]$  in the 1,2,3 coordinate system. By inverting Equation (3.3) the following strain-stress relationships can be obtained:

$$\begin{Bmatrix} \epsilon_{11} \\ \epsilon_{22} \\ \epsilon_{33} \\ \gamma_{23} \\ \gamma_{13} \\ \gamma_{12} \end{Bmatrix} = \begin{bmatrix} S_{11} & S_{12} & S_{13} & S_{14} & S_{15} & S_{16} \\ S_{21} & S_{22} & S_{23} & S_{24} & S_{25} & S_{26} \\ S_{31} & S_{32} & S_{33} & S_{34} & S_{35} & S_{36} \\ S_{41} & S_{42} & S_{43} & S_{44} & S_{45} & S_{46} \\ S_{51} & S_{52} & S_{53} & S_{54} & S_{55} & S_{56} \\ S_{61} & S_{62} & S_{63} & S_{64} & S_{65} & S_{66} \end{bmatrix} \begin{Bmatrix} \sigma_{11} \\ \sigma_{22} \\ \sigma_{33} \\ \tau_{23} \\ \tau_{13} \\ \tau_{12} \end{Bmatrix} \quad (3.4)$$

where  $S_{ij}$  are the elements of the compliance matrix  $[S]$  in the 1,2,3 coordinate system (Table 3.1). It is evident from Equation (3.2) – (3.3) that the compliance matrix  $[S]$  is the inverse of the stiffness matrix  $[C]$ :

$$[\bar{S}] = [\bar{C}]^{-1} \text{ and } [S] = [C]^{-1} \quad (3.5)$$

It can be shown that, for an elastic material, the stiffness and compliance matrices are symmetrical in the x, y, z and 1, 2, 3 coordinate systems as Equation (3.6):

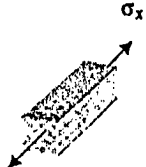
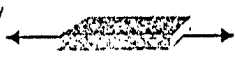



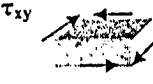
$$\bar{S}_{ij} = \bar{S}_{ji}, S_{ij} = S_{ji} \text{ and } \bar{C}_{ij} = \bar{C}_{ji}, C_{ij} = C_{ji} \quad ij=1,2\dots6 \quad (3.6)$$

Because of symmetry, in the  $[\bar{S}]$  and  $[\bar{C}]$  matrices, only 21 of the 36 elements are independent [23].

### 3.2.2 Transversely Isotropic Material

A transversely isotropic material has three planes of symmetry. These planes are illustrated in Figures 3.3a –3.3b. In one of the planes of symmetry, the material is treated

**Table 3.1:** The elements of the compliance matrix in the x, y, z systems [23].

	$S_{11} = \epsilon_{xx} / \sigma_{xx}$	$S_{41} = \gamma_{yz} / \sigma_{xx}$
	$S_{21} = \epsilon_{yy} / \sigma_{xx}$	$S_{51} = \gamma_{xz} / \sigma_{xx}$
	$S_{31} = \epsilon_{zz} / \sigma_{xx}$	$S_{61} = \gamma_{xy} / \sigma_{xx}$
	$S_{12} = \epsilon_{xx} / \sigma_{yy}$	$S_{42} = \gamma_{yz} / \sigma_{yy}$
	$S_{22} = \epsilon_{yy} / \sigma_{yy}$	$S_{52} = \gamma_{xz} / \sigma_{yy}$
	$S_{32} = \epsilon_{zz} / \sigma_{yy}$	$S_{62} = \gamma_{xy} / \sigma_{yy}$
	$S_{13} = \epsilon_{xx} / \sigma_{zz}$	$S_{43} = \gamma_{yz} / \sigma_{zz}$
	$S_{23} = \epsilon_{yy} / \sigma_{zz}$	$S_{53} = \gamma_{xz} / \sigma_{zz}$
	$S_{33} = \epsilon_{zz} / \sigma_{zz}$	$S_{63} = \gamma_{xy} / \sigma_{zz}$
	$S_{14} = \epsilon_{xx} / \tau_{yz}$	$S_{44} = \gamma_{yz} / \tau_{yz}$
	$S_{24} = \epsilon_{yy} / \tau_{yz}$	$S_{54} = \gamma_{xz} / \tau_{yz}$
	$S_{34} = \epsilon_{zz} / \tau_{yz}$	$S_{64} = \gamma_{xy} / \tau_{yz}$
	$S_{15} = \epsilon_{xx} / \tau_{xz}$	$S_{45} = \gamma_{yz} / \tau_{xz}$
	$S_{25} = \epsilon_{yy} / \tau_{xz}$	$S_{55} = \gamma_{xz} / \tau_{xz}$
	$S_{35} = \epsilon_{zz} / \tau_{xz}$	$S_{65} = \gamma_{xy} / \tau_{xz}$
	$S_{16} = \epsilon_{xx} / \tau_{xy}$	$S_{46} = \gamma_{yz} / \tau_{xy}$
	$S_{26} = \epsilon_{yy} / \tau_{xy}$	$S_{56} = \gamma_{xz} / \tau_{xy}$
	$S_{36} = \epsilon_{xz} / \tau_{xy}$	$S_{66} = \gamma_{xy} / \tau_{xy}$

as isotropic. An example of a transversely isotropic material is a composite reinforced with continuous unidirectional fibers with all the fibers aligned in the direction 1 (See Figure 3.3b). In this case, the material in the plane perpendicular to the fibers (2-3 plane) is treated as isotropic. For a transversely isotropic material, the stiffness and compliance matrices in a 1, 2, 3 coordinate system are chosen in such a way that the axes are perpendicular to the planes of symmetry and the material properties in this system are:

$$E_3 = E_2 \quad G_{13} = G_{12} \quad \nu_{13} = \nu_{12} \quad (3.7)$$

For an isotropic material Equation (3.8) defines the shear modulus:

$$G = \frac{E}{2(1 + \nu)} \quad (3.8)$$

Correspondingly, for a material that is isotropic in the 2-3 plane, the relation between Young's modulus and Equation (3.9) can present shear modulus:

$$G_{23} = \frac{E_2}{2(1 + \nu_{23})} \quad (3.9)$$

Equations (3.7) and (3.9), together with the expressions in Table 3.2, yield the compliance matrix in terms of the engineering constants. The results are given in Equation (3.12 – 3.15). The zero and non-zero elements of the compliance matrix are given in Equation (3.10) [28]:

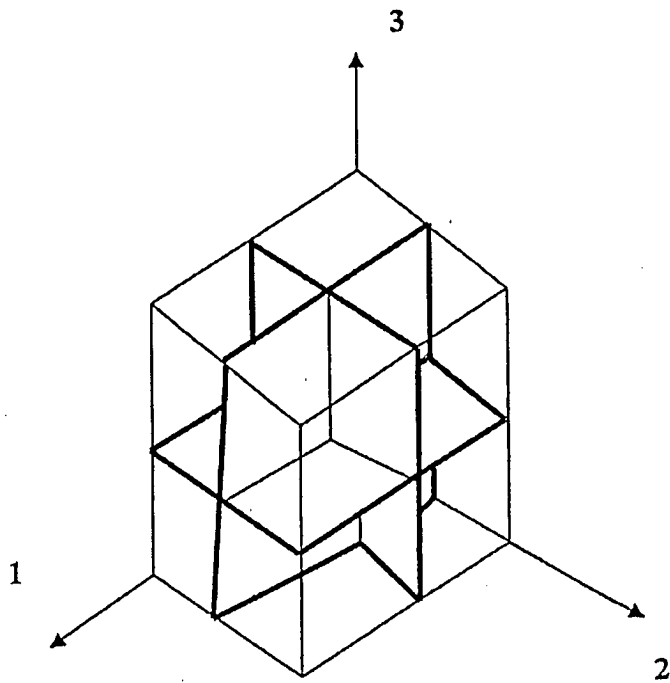
$$[S] = \begin{bmatrix} S_{11} & S_{12} & S_{13} & 0 & 0 & 0 \\ S_{12} & S_{22} & S_{23} & 0 & 0 & 0 \\ S_{13} & S_{23} & S_{33} & 0 & 0 & 0 \\ 0 & 0 & 0 & 2(S_{22} - S_{23}) & 0 & 0 \\ 0 & 0 & 0 & 0 & S_{66} & 0 \\ 0 & 0 & 0 & 0 & 0 & S_{66} \end{bmatrix} \quad (3.10)$$

The stiffness matrix is obtained by inverting the compliance matrix. The zero and non-zero elements of the stiffness matrix are defined by Equation (3.11):

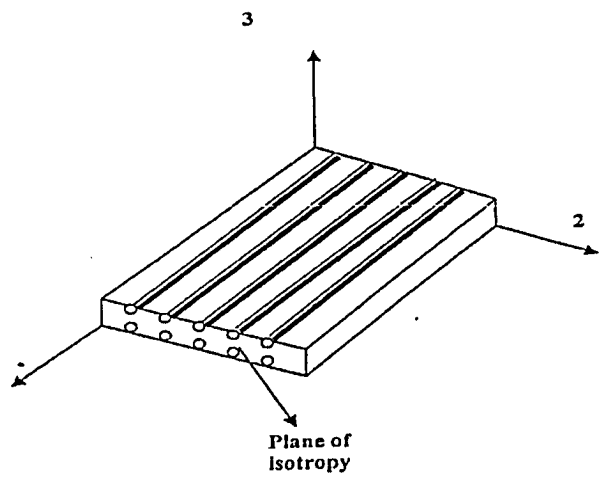
$$[C] = \begin{bmatrix} C_{11} & C_{12} & C_{12} & 0 & 0 & 0 \\ C_{12} & C_{22} & C_{23} & 0 & 0 & 0 \\ C_{12} & C_{23} & C_{22} & 0 & 0 & 0 \\ 0 & 0 & 0 & \frac{C_{22} - C_{23}}{2} & 0 & 0 \\ 0 & 0 & 0 & 0 & C_{66} & 0 \\ 0 & 0 & 0 & 0 & 0 & C_{66} \end{bmatrix} \quad (3.11)$$

The compliance matrices in terms of the engineering constants for monoclinic, orthotropic, transversely isotropic and isotropic materials can be shown as follows.

When there is a symmetry plane with respect to the alignment of the fibers, the monoclinic compliance matrix is defined by Equation (3.12).



**Figure: 3.3a:** Material with three planes of symmetry.



**Figure 3.3b:** Example of a fiber-reinforced, transversely isotropic composite.

**Table 3.2:** Elements of the compliance matrix in terms of the engineering constants.

$S_{11}=\epsilon_{11}/\sigma_{11}=$ $\epsilon_{11}/(\epsilon_{11}E_1) =$ $1/E_1$	$S_{12}=\epsilon_{11}/\sigma_{22}=$ $\epsilon_{11}/(\epsilon_{22}E_2) =$ $-\nu_{21}/E_2$	$S_{13}=\epsilon_{11}/\sigma_{33}=$ $\epsilon_{11}/(\epsilon_{33}E_1) =$ $-\nu_{31}/E_2$	$S_{14} = 0$	$S_{15} = 0$	$S_{16}=\epsilon_{11}/\tau_{12}=$ $\epsilon_{11}/(G_{12}\gamma_{12})$ $= \nu_{61}/G_{12}$
$S_{21}=\epsilon_{22}/\sigma_{11}=$ $\epsilon_{22}/(\epsilon_{11}E_1)=$ $-\nu_{12}/E_1$	$S_{22}=\epsilon_{22}/\sigma_{22}=$ $\epsilon_{22}/(\epsilon_{22}E_2)$ $= 1/E_2$	$S_{23}=\epsilon_{22}/\sigma_{33}=$ $\epsilon_{22}/(\epsilon_{33}E_3) =$ $-\nu_{32}/E_3$	$S_{24} = 0$	$S_{25} = 0$	$S_{26}=\epsilon_{22}/\tau_{12}=$ $\epsilon_{22}/(G_{12}\gamma_{12})$ $= \nu_{62}/G_{12}$
$S_{31}=\epsilon_{33}/\sigma_{11}=$ $\epsilon_{33}/(\epsilon_{11}E_1) =$ $-\nu_{13}/E_1$	$S_{32}=\epsilon_{33}/\sigma_{22}=$ $\epsilon_{33}/(\epsilon_{22}E_2) =$ $-\nu_{23}/E_2$	$S_{33}=\epsilon_{33}/\sigma_{33}=$ $\epsilon_{33}/(\epsilon_{33}E_3) =$ $1/E_3$	$S_{34} = 0$	$S_{35} = 0$	$S_{36}=\epsilon_{33}/\tau_{12}=$ $\epsilon_{33}/(G_{12}\gamma_{12})$ $= \nu_{63}/G_{12}$
$S_{41} = 0$	$S_{42} = 0$	$S_{43} = 0$	$S_{44}=\epsilon_{44}/\sigma_{44}=$ $\gamma_{23}/(\gamma_{23}G_{23})$ $= 1/G_{23}$	$S_{45}=\gamma_{23}/\tau_{13}=$ $\gamma_{23}/(\gamma_{13}G_{13})$ $= \nu_{54}/G_{13}$	$S_{46} = 0$
$S_{51} = 0$	$S_{52} = 0$	$S_{53} = 0$	$S_{54}=\gamma_{13}/\tau_{23}=$ $\gamma_{13}/(\gamma_{23}G_{23})$ $= \nu_{45}/G_{23}$	$S_{55}=\gamma_{13}/\tau_{13}=$ $\gamma_{13}/(\gamma_{13}G_{13})$ $= 1/G_{13}$	$S_{56} = 0$
$S_{61}=\gamma_{12}/\sigma_{12}=$ $\gamma_{12}/(E_1 \epsilon_{11})$ $= \nu_{16}/E_1$	$S_{62}=\gamma_{12}/\sigma_{22}=$ $\gamma_{12}/(E_2 \epsilon_{22})$ $= \nu_{26}/E_2$	$S_{63}=\gamma_{12}/\sigma_{33}=$ $\gamma_{12}/(E_3 \epsilon_{33})$ $= \nu_{36}/E_3$	$S_{64} = 0$	$S_{65} = 0$	$S_{66}=\gamma_{12}/\tau_{12}=$ $\gamma_{12}/(\gamma_{12}G_{12})$ $= 1/G_{12}$

The above table is also valid for orthotropic, transversely isotropic and isotropic materials with  $S_{16} = S_{61} = 0$ ,  $S_{26} = S_{62} = 0$ ,  $S_{36} = S_{63} = 0$ ,  $S_{45} = S_{54} = 0$  [23].



$$[S] = \begin{bmatrix} \frac{1}{E_1} & -\frac{\nu_{21}}{E_2} & -\frac{\nu_{31}}{E_3} & 0 & 0 & \frac{\nu_{61}}{G_{12}} \\ -\frac{\nu_{12}}{E_1} & \frac{1}{E_2} & -\frac{\nu_{32}}{E_2} & 0 & 0 & \frac{\nu_{62}}{G_{12}} \\ -\frac{\nu_{13}}{E_1} & -\frac{\nu_{23}}{E_2} & \frac{1}{E_3} & 0 & 0 & \frac{\nu_{63}}{G_{12}} \\ 0 & 0 & 0 & \frac{1}{G_{23}} & \frac{\nu_{54}}{G_{13}} & 0 \\ 0 & 0 & 0 & \frac{\nu_{45}}{G_{23}} & \frac{\nu_{21}}{G_{13}} & 0 \\ -\frac{\nu_{16}}{E_1} & \frac{\nu_{26}}{E_2} & \frac{\nu_{36}}{E_3} & 0 & 0 & \frac{\nu_{21}}{E_2} \end{bmatrix} \quad (3.12)$$

Equation 3.13 presents the orthotropic compliance matrix when there are three mutually perpendicular symmetry planes with respect to the alignment of the fibers:

$$[S] = \begin{bmatrix} \frac{1}{E_1} & -\frac{\nu_{21}}{E_2} & -\frac{\nu_{31}}{E_3} & 0 & 0 & 0 \\ -\frac{\nu_{12}}{E_1} & \frac{1}{E_2} & -\frac{\nu_{32}}{E_2} & 0 & 0 & 0 \\ -\frac{\nu_{13}}{E_1} & -\frac{\nu_{23}}{E_2} & \frac{1}{E_3} & 0 & 0 & 0 \\ 0 & 0 & 0 & \frac{1}{G_{23}} & 0 & 0 \\ 0 & 0 & 0 & 0 & \frac{1}{G_{13}} & 0 \\ 0 & 0 & 0 & 0 & 0 & \frac{1}{G_{12}} \end{bmatrix} \quad (3.13)$$

When there are three planes of symmetry and in one of them the material is treated as an isotropic material, Equation 3.14 presents transversely isotropic compliance matrix.

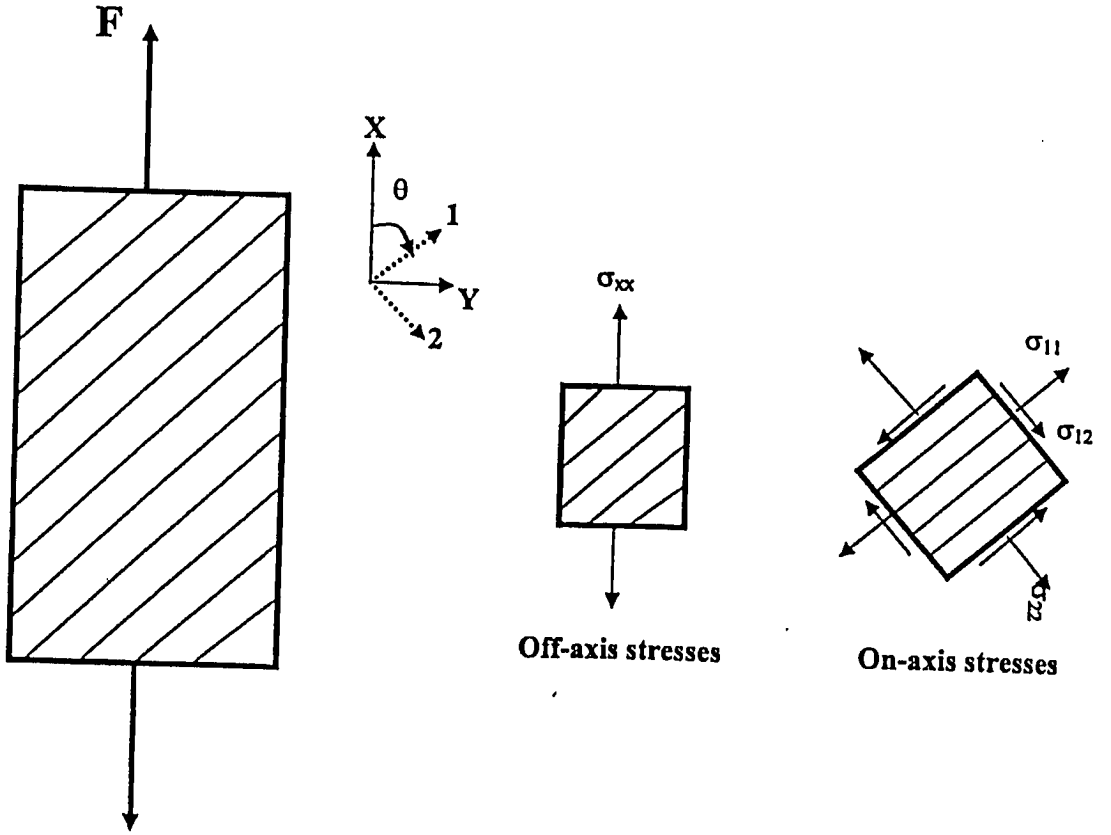
$$[S] = \begin{bmatrix} \frac{1}{E_1} & -\frac{\nu_{21}}{E_2} & -\frac{\nu_{31}}{E_3} & 0 & 0 & 0 \\ -\frac{\nu_{12}}{E_1} & \frac{1}{E_2} & -\frac{\nu_{32}}{E_2} & 0 & 0 & 0 \\ -\frac{\nu_{13}}{E_1} & -\frac{\nu_{23}}{E_2} & \frac{1}{E_3} & 0 & 0 & 0 \\ 0 & 0 & 0 & \frac{2(1+\nu_{12})}{E_2} & 0 & 0 \\ 0 & 0 & 0 & 0 & \frac{1}{G_{13}} & 0 \\ 0 & 0 & 0 & 0 & 0 & \frac{1}{G_{12}} \end{bmatrix} \quad (3.14)$$

There are no preferred directions and every plane is a plane of symmetry in isotropic materials. Equation (3.15) presents its compliance matrix.

$$[S] = \begin{bmatrix} \frac{1}{E_1} & -\frac{\nu_{21}}{E_2} & -\frac{\nu_{31}}{E_3} & 0 & 0 & 0 \\ -\frac{\nu_{12}}{E_1} & \frac{1}{E_2} & -\frac{\nu_{32}}{E_2} & 0 & 0 & 0 \\ -\frac{\nu_{13}}{E_1} & -\frac{\nu_{23}}{E_2} & \frac{1}{E_3} & 0 & 0 & 0 \\ 0 & 0 & 0 & \frac{2(1+\nu)}{E} & 0 & 0 \\ 0 & 0 & 0 & 0 & \frac{2(1+\nu)}{E} & 0 \\ 0 & 0 & 0 & 0 & 0 & \frac{2(1+\nu)}{E} \end{bmatrix} \quad (3.15)$$

### 3.3 Macro-Mechanical Analysis of A Unidirectional Lamina

The unidirectional composite ply can be considered as a transversely isotropic material and the elastic module for an angle lamina (See Figure 3.3b) are derived by compliance matrix in x-y coordination.



**Figure 3.4:** An off-axis unidirectional specimen under uniaxial tension. The on-axis stresses are found by transforming the off-axis stress from the off-axis to on-axis directions [18].

The relationships between stresses and strains in the  $x, y$  coordinate system are written in Equation (3.16).

$$\begin{bmatrix} \epsilon_{xx} \\ \epsilon_{yy} \\ \epsilon_{zz} \end{bmatrix} = \begin{bmatrix} \bar{S}_{11} & \bar{S}_{12} & \bar{S}_{13} \\ \bar{S}_{21} & \bar{S}_{22} & \bar{S}_{23} \\ \bar{S}_{31} & \bar{S}_{32} & \bar{S}_{33} \end{bmatrix} \begin{bmatrix} \sigma_{xx} \\ \sigma_{yy} \\ \sigma_{zz} \end{bmatrix} \quad (3.16)$$

where the transformation matrix  $S_{ij}$  in 1 – 2 coordination ( Figure 3.4), can be defined as Equation (3.17) [23].

$$[S_{ij}] = \begin{bmatrix} \cos^2 \theta & \sin^2 \theta & -\cos \theta \sin \theta \\ \sin^2 \theta & \cos^2 \theta & \cos \theta \sin \theta \\ 2 \cos \theta \sin \theta & -2 \cos \theta \sin \theta & \cos^2 \theta - \sin^2 \theta \end{bmatrix} \quad (3.17)$$

From Equations (3.16) and (3.17) the relationships between the stresses and strains in the arbitrary x-y coordinate system can be derived from  $[\bar{S}_{ij}]_0$  elements through following transformations:

$$\begin{aligned} \bar{S}_{11} &= S_{11} \cos^4 \theta + S_{22} \sin^4 \theta + (2S_{12} + S_{33}) \sin^2 \theta \cos^2 \theta \\ \bar{S}_{12} &= \bar{S}_{21} = S_{12} (\sin \theta + \cos \theta) + (S_{11} + S_{22} - S_{33}) \sin^2 \theta \cos^2 \theta \\ \bar{S}_{13} &= S_{31} + (2S_{11} - 2S_{12} - S_{33}) \sin \theta \cos^3 \theta \\ \bar{S}_{22} &= S_{11} \sin^4 \theta + S_{22} \cos^4 \theta + (2S_{12} + S_{33}) \sin^2 \theta \cos^2 \theta \\ \bar{S}_{32} &= \bar{S}_{23} = (2S_{11} - 2S_{12} - S_{33}) \sin^3 \theta \cos \theta - (2S_{22} - 2S_{12} - S_{33}) \sin \theta \cos^3 \theta \\ \bar{S}_{33} &= 2(2S_{11} + 2S_{22} - 4S_{12} - S_{33}) \sin^2 \theta \cos^2 \theta + S_{33} (\sin^4 \theta + \cos^4 \theta) \\ S_{11} &= \frac{1}{E_1}, S_{22} = \frac{1}{E_2}, S_{12} = -\frac{\nu_{21}}{E_2} = -\frac{\nu_{12}}{E_1}, S_{33} = \frac{1}{G_{12}} \end{aligned} \quad (3.17 \text{ a-g})$$

Thus the relationships between material properties in x - y and 1 - 2 coordinates can be calculated by Equations (3.18, 19, 20 and 21).

$$1/E_x = \cos^4 \theta / E_1 + (1/G_{12} - 2\nu_{12}/E_1) \sin^2 \theta \cos^2 \theta + \sin^4 \theta / E_2 \quad (3.18)$$

$$\nu_{xy} = E_x [\nu_{12} (\sin^4 \theta + \cos^4 \theta) / E_1 - (1/E_1 + 1/E_2 - 1/G_{12}) \sin^2 \theta \cos^2 \theta] \quad (3.19)$$

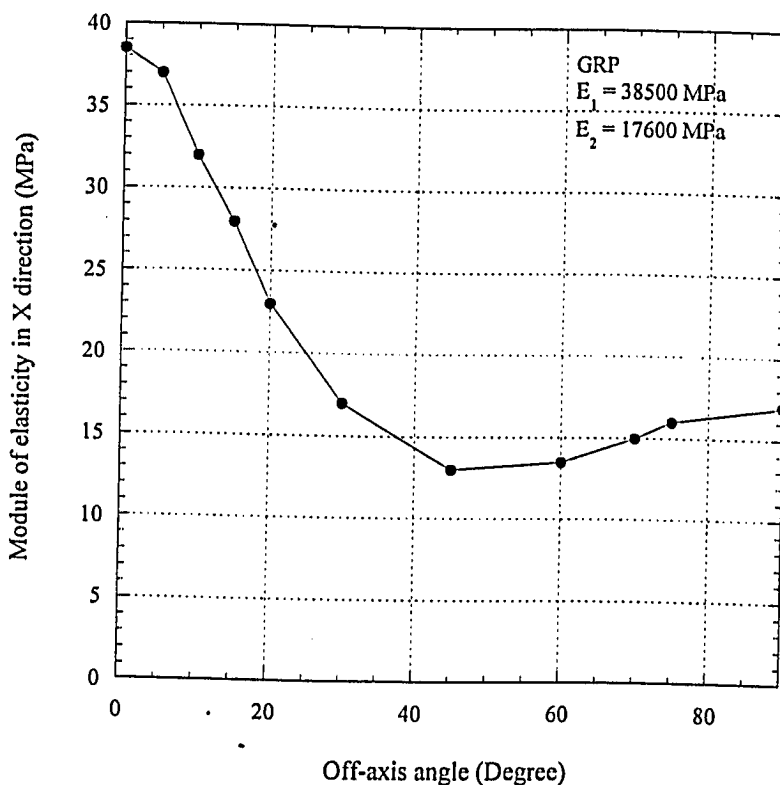
$$1/E_y = \sin^4 \theta / E_1 + (1/G_{12} - 2\nu_{12}/E_1) \sin^2 \theta \cos^2 \theta + \cos^4 \theta / E_2 \quad (3.20)$$

$$1/G_{xy} = 2(2/E_1 + 2/E_2 + 4\nu_{12}/E_1 - 1/G_{12}) \sin^2 \theta \cos^2 \theta + (\cos^4 \theta + \sin^4 \theta) / G_{12} \quad (3.21)$$

Transformation of the stress components in Equation 3.22 is expressed as:

$$\begin{bmatrix} \sigma_{11} \\ \sigma_{22} \\ \sigma_{33} \end{bmatrix} = \begin{bmatrix} \cos^2 \theta & \sin^2 \theta & 2 \cos \theta \sin \theta \\ \sin^2 \theta & \cos^2 \theta & -2 \cos \theta \sin \theta \\ -\sin \theta & \cos \theta \sin \theta & \cos^2 \theta - \sin^2 \theta \end{bmatrix} \begin{bmatrix} \sigma_{xx} \\ \sigma_{yy} \\ \sigma_{zz} \end{bmatrix} \quad (3.22)$$

Figures 3.5 – 3.8 represent the variations of the shear modulus and elastic modulus of GRP and CFRP composites as the off-axis angle increases. These variations were calculated using Equations (3.18 – 3.21). As Figures 3.5 and 3.7 show elastic modulus initially possesses the highest value at 0° off-axis angle where the fibers are oriented along the loading axis. The magnitude of the elastic modulus decreases as off-axis angle increases. Figures 3.6 and 3.8 represent an initial increase of the shear modulus as off-axis angle increases from zero to a maximum value of 45°. Beyond off-axis 45°: the shear modulus keeps decreasing as off-axis angle increases from 45° to 90°. At 90° off-axis angle the shear modulus becomes as small as the shear modulus achieved at 0° off-axis.



**Figure 3.5:** The elastic modulus response as off-axis angle changes for a typical unidirectional GRP [23].

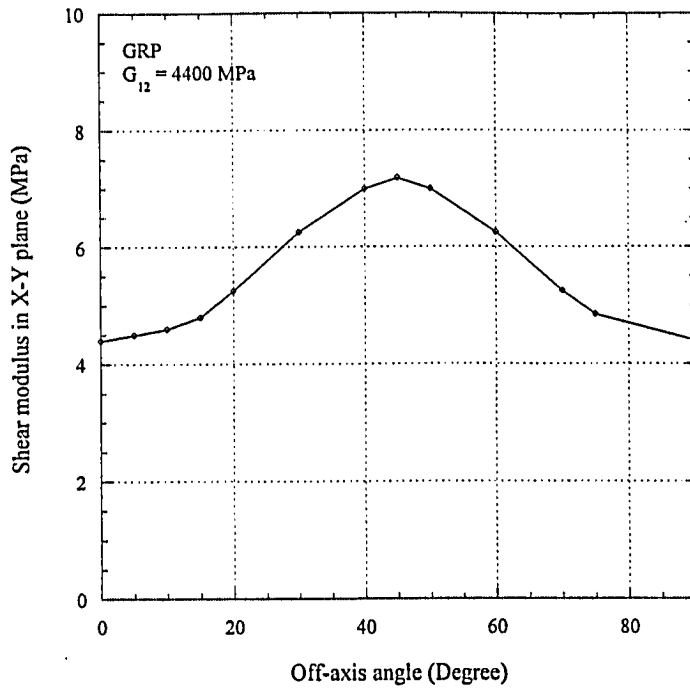


Figure 3.6: The shear modulus response as off-axis angle changes for a typical unidirectional GRP [23].

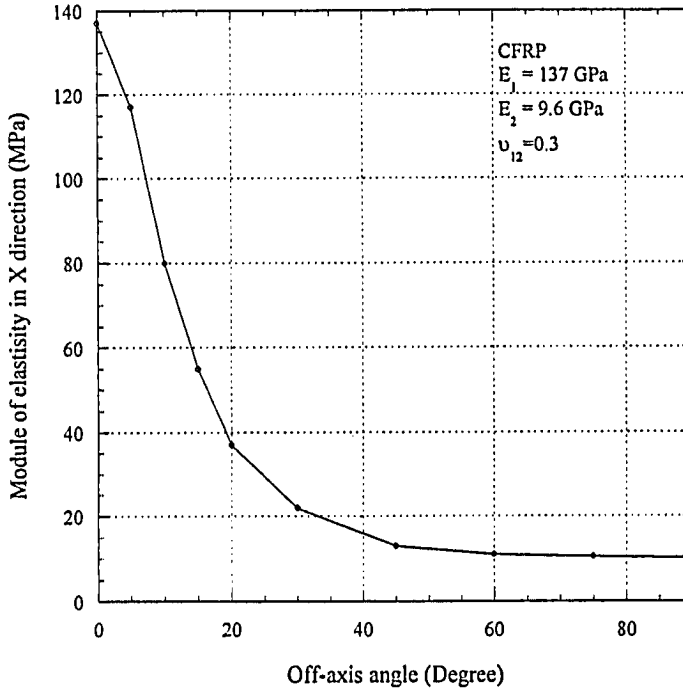
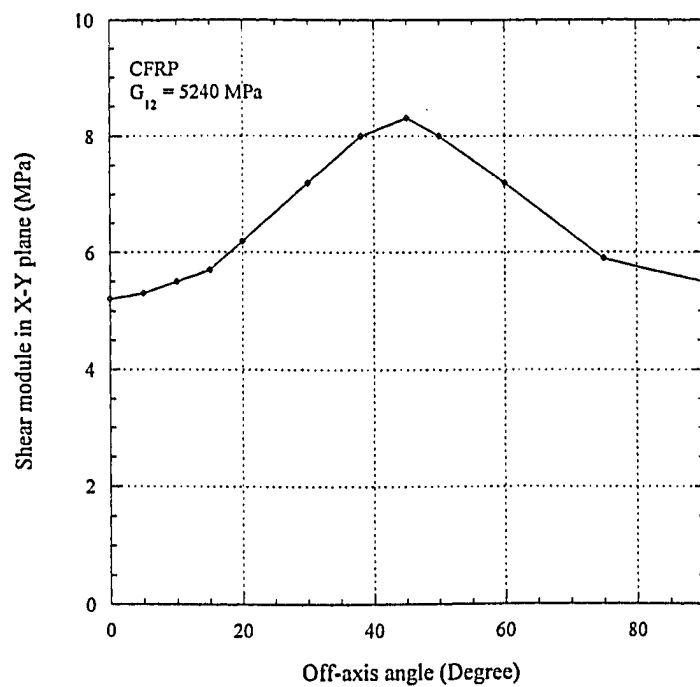


Figure 3.7: The elastic modulus response as off-axis angle changes for a typical unidirectional CFRP [23].



**Figure 3.8:** The shear modulus response as off-axis angle changes for a typical unidirectional CFRP [23]

## **CHAPTER FOUR**

### **Fatigue Damage Analysis and Modeling**

#### **4.1 The Fundamental of Damage in Unidirectional FRP Composite**

Fatigue loading of composite laminates consists of the application of loads or strains that vary with time, usually in a cyclic or repetitive manner. By definition, the loads or strains reach amplitudes that are less than the values required to fracture the laminates in monotonic loading tests. If eventual failure due to cyclic loading occurs, then damage must have progressed in the laminate during the fatigue lifetime and caused degradation of properties such as strength and stiffness.

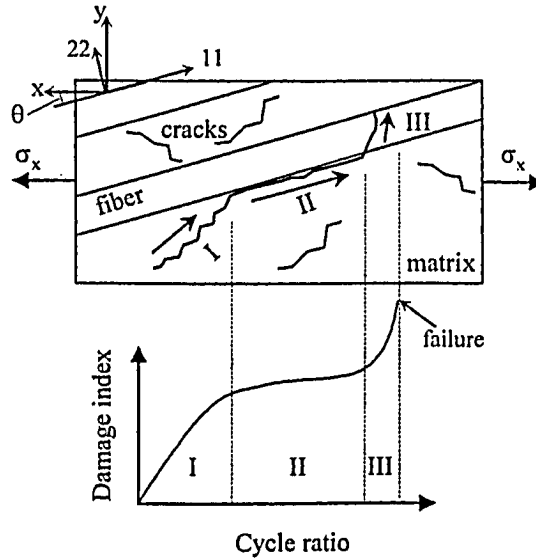
The damage process in composite laminates consists of the initiation and growth of different damage modes and interactions between them. The interactions between damage modes are dependent on material, load, geometry and environment.

The progressive development of damage during fatigue life can be overviewed with the aid of a schematic, Figure 4.1, which represents the development of damage during the fatigue life of 0°-ply composite coupon that is subjected to cyclic loading in the fiber direction.

The damage process can be classified into three regions: Region I occurs during the first 10 – 15% of life, during which damage develops at a very rapid rate. Region II corresponds to the next 70 – 80% of the fatigue life, during which time damage continues to initiate and grow, but at a slower rate than during region I. However, at the end of Region II, the laminate is severely damaged to the level where continued cyclic loading accelerates the damage process during Region III, the final 10 – 15% of life.

The major damage mode during region I is matrix cracking [25, 26]. Because the ply level stress fields are biaxial, matrix crack will usually initiate and grow in all plies, which have a tensile stress and perpendicular to the fibers. Matrix cracks that appears in some plies on the first cycle, are sufficiently large to produce so-called “first-ply failure”.





**Figure 4.1:** Three regions of cracking mechanism in unidirectional composites [29].

The term “first-ply failure” is misleading. Matrix cracks, initiate in the off-axis plies at low values (relative to the laminate strength) of applied stress, but these initial cracks are few in number and are widely spaced. Although the ply is damaged locally, it does remain effective in the laminate by providing strength and stiffness in the direction of the fibers and at locations away from the first cracks.

Throughout Region I, the number and density of matrix cracks increases until a uniform, saturation spacing is reached [5]. This state of damage, known as the Characteristic Damage State, is a laminate property, which is, achieved near the end of region I. The crack spacing in a given ply is a function of material properties and the constraints imposed on the ply by the surrounding plies.

As the loading history continues, Region II damage begins with turning and growth of matrix cracks along the interfaces between plies. Crack coupling produces interfacial debonding, which is confined to the material near the edge of the laminate or around a notch. With additional cycles, the interfacial debonds on interfaces with high interlaminar shear stress begin to grow in the plane of the laminates to form

delaminations. The remainder of region II of the damage process is taken up by the initiation and growth of delaminations and additional fiber fractures.

Not all delaminations during Region II are associated with laminate edges and notch boundaries. Some delaminations initiate internally at sites of crossing matrix cracks in adjacent plies. The tensile interlaminar normal stress and the large interlaminar shear stress associated with matrix cracks support the initiation and growth of delaminations during cyclic loading. The locally high stress field associated with crossing matrix cracks and the intersection of matrix cracks and ply interfaces is one of the factors responsible for fiber fracture. Fiber fracture is a major damage mode controlling the life of laminates subjected to tensile and compressive cyclic loads. However, it is the least studied and, therefore, the least understood of all fatigue damage modes. Although several probabilistic arguments have been presented for fiber fracture [30-32], the mechanisms of fiber fracture have not been described as extensively as other damage mechanisms [33, 34]. Under cyclic loading, fiber fractures occur during all three regions of fatigue life. Some failures are random fractures of statistically weak fibers; however, many more fiber fractures are associated with matrix cracks in adjacent plies.

The onset of Region III of life is characterized by an increase in the damage rate caused by damage localization and delamination growth. Under cyclic tensile loads, laminate fracture is coincident with the catastrophic fracture of the major load bearing plies. Under cyclic compressive loads, failure occurs when the laminate stiffness degrades to such an extent that the laminate cannot support the applied loads. Failure is usually due to buckling or micro-buckling and subsequent shear crippling, dependent on constraint conditions. In situations where the compressively loaded laminates are highly constrained, failure may occur in a crushing mode [35] initiated by local fiber kinking.

Laminates subjected to both tensile and compressive cyclic loads may exhibit either tensile or compressive fracture modes, depending on the response of competing example, delaminations may produce a greater reduction in the life of laminates subjected to reversed cyclic loads than in the life of similar laminates subjected to either tensile or compressive cyclic loads of the same amplitude. When loads are reversed, delaminations are subjected to a cyclic shear stress range, which is twice as large as the range under either cyclic tensile or compressive loads alone. Also delaminations isolate sub-laminates

from the parent laminate, and thereby reduce the stiffness of the laminate and promote compressive failures, especially in brittle matrix materials [36].

## 4.2 Elements of Damage Analysis

As was described earlier, the mechanical behavior of a composite as whole depends upon the response of its constituents, namely the matrix, the interface and the fiber. Thus, any physically based damage model must use the contributions from individual constituents as building blocks to determine the overall damage to the composite. It is generally known that the fatigue damage in brittle matrix composites consists of a sequence of events starting from matrix cracking, crack bridging fiber-matrix debonding and fiber breakage leading to final failure [26]. The presence or absence of any of the damage events depends on a number of materials factors, such as the relative mechanical and thermal properties of the fiber and matrix and the strength of the fiber/matrix bonding.

The concept of damage accumulation may be used as a more suitable approach to predict the fatigue life of structures of composite materials. However, fatigue damage cannot be measured directly. Therefore, for quantitative evaluation of fatigue damage, Young's modulus or the stiffness of composite materials are often used to evaluate the fatigue damage due to cyclic loading [37]:

$$D = 1 - \frac{E}{E_c} \quad (4.1)$$

where  $D$  is the accumulated fatigue damage,  $E_c$  is initial Young's modulus of the undamaged material, and  $E$  is the Young's modulus of the damaged material. Thus, the extent of damage can be quantified by measuring the Young's modulus of the material. The experimental results show that the measured Young's modulus or stiffness just before complete failure of the specimen is not zero. The final accumulated damage is

$1-E_f = E_c$  instead of unity when the material fails, where  $E_f$  is the Young's modulus when fracture occurs. Therefore, a new damage parameter can be defined with the final Young's modulus  $E_f$  as [5]:

$$D = \frac{(E_c - E)}{(E_c - E_f)} \quad (4.2)$$

According to Equation (4.2) the accumulated damage will be in the range between 0 and 1. As was previously mentioned, the complexity of composites leads to the presence of many modes of damage. These modes appear at the early regions of the fatigue life. The damage accumulates rapidly during the first few cycles. During this region, microcracks initiate in multiple locations in the matrix. Debonding occurs at the weak interfaces between fibers and matrix. Also, some fibers with low strength may break during this region. The next region shows a slow and steady damage growth rate. Finally, the damage again grows rapidly during the last region before the fracture occurs. Figure 4.1 is plotted in terms of damage index versus cycle ratio, where the stiffness degradation is defined in Equation (4.3). The cycle ratio is the number of cycles at a given instant divided by the fatigue life.

The present study is a further extension of an earlier developed fatigue damage model of Ramakrishnan [22] for the FRP composites. The backbone elements of this model (Equation (4.3)) are constructed based on the fact that the stiffness of the composite just prior to failure is obtained by subtracting two terms from the initial stiffness ( $E/E_c=1$ ). Intuitively, one might suspect that one of these terms might be due to the matrix and other due to the fiber. It is assumed that the matrix is severely damaged prior to final failure and fibers are degraded up to a point where the composite can no longer withstand the applied load. For continuous fiber-reinforced composite, the total stiffness cycle is described by a general equation of the form [22]:

$$\frac{E}{E_c} = 1 - \{E_m^*[(1-f)A + f(B)] + E_f^*(1-r)C\} \quad (4.3)$$

where

$$A = \frac{\ln(N+1)}{\ln(N_f)} \quad (4.4)$$

$$B = \left( \frac{N}{N_f} \right) \quad (4.5)$$

$$C = \frac{\ln\left(1 - \frac{N}{N_f}\right)}{\ln\left(\frac{1}{N_f}\right)} \quad (4.6)$$

$$E_m^* = 1 - E_f^* \quad (4.7)$$

$$E_f^* = \frac{E_f V_f}{E_c} \quad (4.8)$$

$$r = \frac{\sigma_{app}}{\sigma_{uts}} = \frac{A_f}{A_0} \quad (4.9)$$

where

N: Cycle,

N<sub>f</sub>: Fatigue life,

E<sub>f</sub>: Stiffness of fiber,

E<sub>c</sub>: Stiffness of composite,

V<sub>f</sub>: Volume fraction of fiber,

A<sub>f</sub>: Final cross-sectional area of the composite,

A<sub>0</sub>: Original cross-sectional area of the composite,

σ<sub>uts</sub> : Ultimate tensile stress,

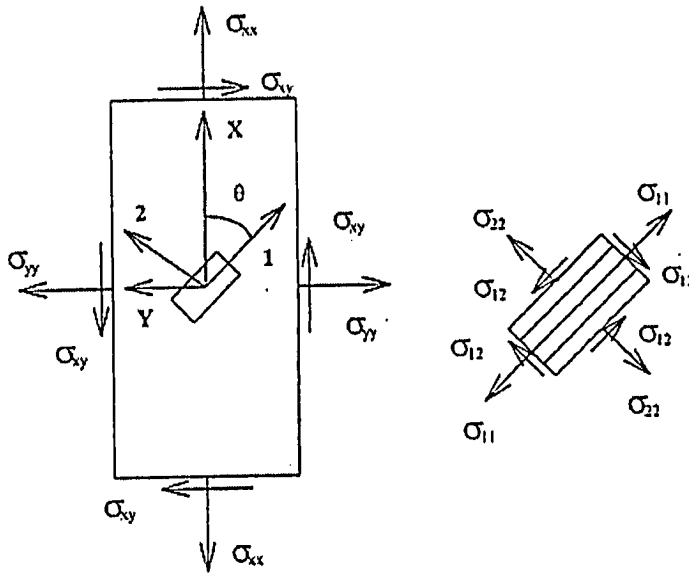
σ<sub>app</sub> : Applied tensile fatigue stress

N<sub>f</sub> is the number of cycles to failure at given applied fatigue stress and (1-r) represents the fraction of remaining net cross section at the time of failure, since A<sub>0</sub> and A<sub>f</sub> are the original and final cross-sectional area of the composite.

The factor  $f$  in Equation (4.3) was found to represent the fiber/matrix interface shear strength and varies between zero and unity, where  $f = 0$  corresponds v̆ery little fiber/matrix interface strength and for  $0 < f < 1$  considers the general case of composite systems with strong fiber/matrix interfaces. The interface is the least understood but the most influential factor in the determination of composite properties [38].

#### 4.2.1 On-axis and Off-axis Presentation

Figure 4.2 schematically indicates the normal and shear stresses on the plane parallel to the fibers. In this case the composite is loaded at an angle  $\theta$  to the fibers. Once a crack has formed in the matrix, its tip will be subjected to two displacements, an opening mode normal to the fibers ( $\sigma_{12}$ ) and an in-plane sliding or shear mode parallel to the fibers ( $\tau_{12}$  or  $\sigma_{12}$ ). This will lead to mixed-mode crack growth parallel to the fibers.



**Figure 4.2:** An off-axis unidirectional specimen under uniaxial tension the on-axis stresses are found by transforming the off-axis stress form the off-axis to on-axis directions.

As Figure 4.3 depicts principal material coordinates 1–2 represent the load along the fiber direction ( $\Theta = 0$ ) and perpendicular to the fiber direction ( $\Theta = 90^\circ$ ). The stress transformation for coordinates 1–2 are given by:

$$\begin{aligned}\sigma_{11} &= \sigma_{xx} \cos^2 \theta, \\ \sigma_{22} &= \sigma_{xx} \sin^2 \theta, \\ \sigma_{12} &= \tau_{12} = -\sigma_{xx} \sin \theta \cos \theta,\end{aligned}\tag{4.10}$$

The modulus of the composite along non-principal x direction is a function of properties of both the fiber and matrix constituents [23]:

$$\frac{1}{E_x} = \frac{1}{E_1} \cos^4 \theta + \left( \frac{1}{G_{12}} - \frac{2\nu_{12}}{E_1} \right) \sin^2 \theta \cos^2 \theta + \frac{1}{E_2} \sin^4 \theta \tag{4.11}$$

where

$$E_2 = E_m \frac{1 + \zeta \eta \nu_f}{1 - \eta \nu_f} \tag{4.12}$$

$$\eta = \frac{\frac{E_f}{E_m} - 1}{\frac{E_f}{E_m} + \zeta} \tag{4.13}$$

and  $\zeta = 2$  for circular fiber.

$E_x$ : Composite Young modulus along off-axis direction

$E_1$ : Composite Young modulus along fiber direction,

$E_2$ : Composite Young modulus normal to fiber direction,

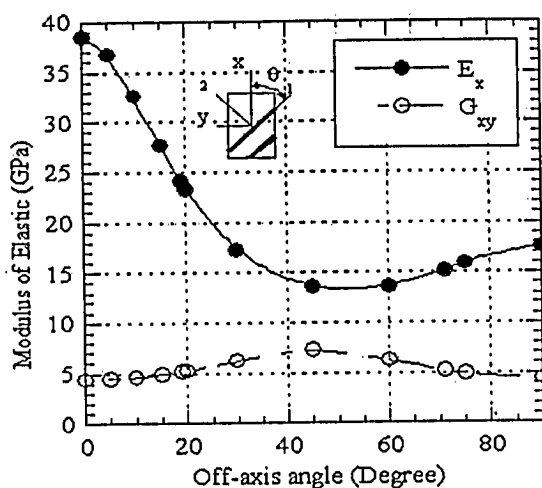
$G_{12}$ : Interlaminar Shear modulus,

$\nu_{12}$ : Poisson's ratio,

$\Theta$ : Off-axis angle from fiber direction.

Beyond  $45^\circ$ , the shear modulus decreases as the off-axis angle increases from  $45^\circ$  to  $90^\circ$ . At  $90^\circ$  off-axis angle the shear modulus becomes as small as the shear modulus

achieved at  $0^\circ$ . Values of elastic modulus at any given off-axis angle are extracted from Figure 4.3 and are used to calculate  $E_m^*$  and  $E_f^*$  in the proposed Equations, by substituting  $E_x$  as  $E_c$ . Obviously in the case of  $90^\circ$ ,  $E_c$  will be equal to  $E_2$ , which explains why the matrix is dominant in transverse direction.



**Figure 4.3:** The elastic modulus response as off-axis angle changes for unidirectional GRP composite [29].

## 4.3 Modifications on Proposed Equation

### 4.3.1 Number of Cycles to Failure and Stiffness Drop

Comparing the experimental data obtained from the literatures one can realize that in most cases the researchers usually impose two common conditions to discontinue the fatigue test, either reaching to certain percentage of drop in stiffness or certain number of cycles. When a specimen does not break at specific number of cycles, the specimen is assumed to be a run-out. Term  $n$  corresponds to the percentage of drop in stiffness recorded for a fatigue test. This mainly shows to what extent stiffness drop versus fatigue cycles has been controlled/ measured before final failure. For instance, by considering the



degradation up to the half of the real damage life (50%) term  $n=(0.5)^{-1}=2$ . Then, the number of cycles considering term  $n$  is modified as:

$$N_f^* = n.N_f \quad (4.14)$$

#### 4.3.2 Mean Stress Effect

In many analyses of composite, the effects of mean stress on the determination of damage are either ignored completely or characterized inadequately. It is been proved that higher mean stress results a faster damage progress in composites [29] and this effect has been implemented in the proposed damage analysis. To implement the effect of stress ratio  $R$  on fatigue damage model presented in this study,  $r = \frac{\sigma_{app}}{\sigma_{uts}}$  (Equation (4.9)) has been modified to:

$$r^* = \frac{\sigma_a}{\sigma_{uts}} = \frac{\sigma_{max}(1-R)}{2\sigma_{uts}} \quad (4.15)$$

where  $\sigma_a$  is the amplitude of the applied cyclic stress. Accordingly,  $R^*$  will be considered as:

$$R^* = 1 - r^* \quad (4.16)$$

#### 4.3.3 Variation of Interface Shear Strength Parameter $f$ with Life Cycles

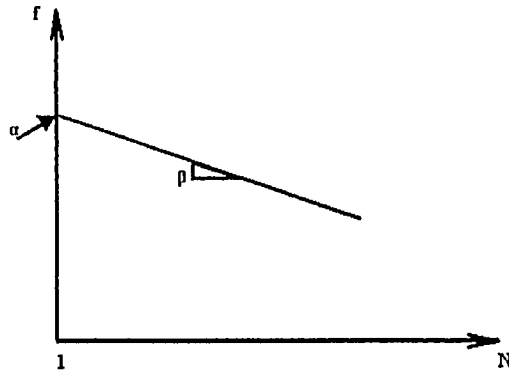
It is well known that the static strength of unidirectional laminates is related to fiber-matrix bonding. Many investigators using micromechanics models have predicted the influence of the fiber-matrix interface on the tensile strength of unidirectional laminates [40-42]. Subraminian et al. [38] also has introduced a parameter similar to  $f$ , called the

efficiency of the interface, to predict the influence of the interface on the tensile strength of unidirectional composites. The interfacial efficiency determines how well load is transferred from the matrix to the fiber. If the bonding is perfect and there is efficient load transfer from matrix to the fiber,  $f \rightarrow 1$ . If the bonding is imperfect and there is no load transfer from the matrix to the fiber then  $f \rightarrow 0$ .

Because of the large elastic shear stress concentrations at the interface, one anticipates that there will be interfacial failure such as shear yielding or debonding. It is assumed that if the applied longitudinal strain exceeds a certain value, the shear stress exerted at the fiber/matrix interface near a crack would reach the  $\tau_s$ , and shear yielding or debonding at the interface would occur and grow in the longitudinal direction.

The effect of interface shear strength parameter  $f$  as number of cycle's progresses was defined as:

$$f = \alpha N^\beta \quad (4.17)$$



**Figure 4.4:** Variation of parameter  $f$  with number of cycles in logarithmic scale.

where the coefficient  $\alpha$  is mathematically defined at  $N=1$  and the exponent  $\beta$  is the slope of curve presented in Figure 4.4.

The coefficient  $\alpha$  is defined as a ratio of normalized shear stress  $\tau_s^*$  of composite to interfacial shear strength  $\tau_i$  ( $\alpha = \tau_s^* / \tau_i$ ).

Zeng et al., [20] defined  $\tau_s^*$  as function of stress applied along fiber direction  $\sigma_{11}$  and fiber/matrix properties:

$$\tau_s^* = \sigma_{11} \left( \frac{V_f G_f G_m}{E_f (V_f G_m + V_m G_f)} \right)^{\frac{1}{2}} \quad (4.18)$$

where  $V_f$ ,  $E_f$  and  $G_f$  are volume fraction, tensile modulus and shear modulus of fiber, respectively,  $V_m$  and  $G_m$  are the matrix volume fraction and shear modulus of matrix, respectively.

It is noteworthy to point out that the modifications of damage equation by parameter  $f$  merely addresses matrix and matrix-fiber interface cracking and has no impact on fiber breakage region.

#### 4.3.4 Effect of Off-Axis Angle ( $\theta$ )

Last but not the least aspect needs to be considered in damage modeling is accountability of the equation for fatigue under off-axis loading. By considering the effect of angle on the Young's modulus of the composite, the other factors needed to be modified are the  $E_m^*$  and  $E_f^*$ .

By referring to Equation (4.7) and (4.8), it is realized that  $E_f^*$  modification is going to have direct effect on the  $E_m^*$ . It is assumed that just prior to final failure that the matrix is severely damaged and the fibers are degraded up to a point where the composite can no longer withstand the applied load. One can further conclude from Equation (4.3) that the effect of off-axis angle is applied only to the damage term for fibers because the matrix cracking occurs early in the fatigue process when the overall composite is intact, while during the fiber breakage process, the effect due to the reduction of cross-section and the load-carrying capability of the composite is significantly affected.

The damage equation is further modified for off-axis angle  $\theta$  as:

$$E_{f\theta}^* = E_f^* \times \cos \theta \quad (4.19)$$

$$E_{m\theta}^* = 1 - E_{f\theta}^* \quad (4.20)$$

The effect of off-axis angle on damage curves are distinctly pronounced, at  $\theta=0$ ,  $E_f^*$  stays unchanged, while as  $\theta$  increases in magnitude,  $E_m^*$  decreases and becomes zero at  $\theta=90$ .

In Equation (4.19), substituting off-axis angles  $\theta=0$  and  $\theta=90$  correspond to composites with fiber-dominancy and matrix-dominancy cases, respectively.

It is found that modifying the damage equation by implementing the effects of:

- (i) Stiffness drop as function of life cycles,
- (ii) Mean stress and stress ratio,
- (iii) Parameter  $f$  as function of fatigue cycles in regions I and II, and
- (iv) Off-axis angles

Successfully evaluates damage of FRP composites and can be described by a general equation of the form:

$$D = 1 - E/E_c = \{E_{m0}^* [A + f(A - B)] + E_{m0}^* R^* C\} \quad (4.21)$$

where

$$A = \frac{\ln(N+1)}{\ln(N_f^*)} \quad (4.22)$$

$$B = \left( \frac{N}{N_f^*} \right) \quad (4.23)$$

$$C = \frac{\ln\left(1 - \frac{N}{N_f^*}\right)}{\ln\left(\frac{1}{N_f^*}\right)} \quad (4.24)$$

4.4 Algorithm/Flowchart of Analysis for Unidirectional Composite

Figure 4.5 represents the procedure of fatigue damage analysis of unidirectional GRP and CFRP composites based on the proposed damage method in this study. The developed fatigue damage analysis method includes damage in three regions of matrix, matrix-fiber interface and fiber and reflects the cracking mechanism within the three regions from early region of growth to final failure. This figures stepwise the procedure of damage analysis in the following steps: (1) The material properties such as fiber stiffness, matrix stiffness, composite initial stiffness, fiber volume fraction, Poisson ratio, stress ratio, applied stress and number of applied cycle to failure, of unidirectional GRP and CFRP composites for various on- or off-axis angles are required as initial step of analysis. (2) For cycles smaller than fatigue life, calculate damage parameter for each stress state, and (3) Plot the damage parameter versus fatigue life.

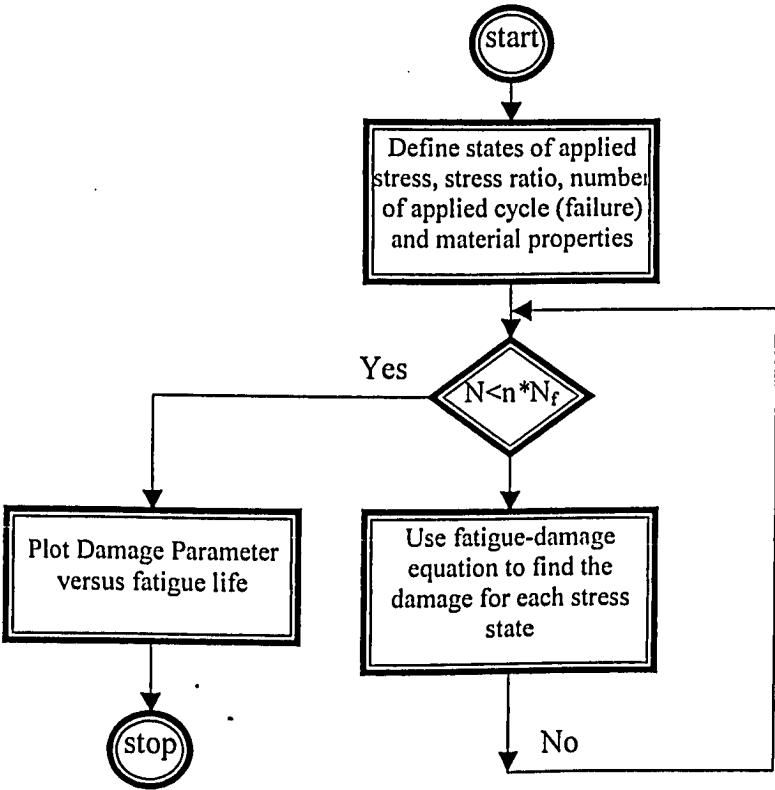


Figure 4.5: Flowchart of generalized material property degradation technique

Figure 4.6 also represents the steps to define the parameter  $f$  as a function of  $N$ , based on the damage equation, by substituting the material properties such as fiber stiffness, matrix stiffness, composite initial stiffness, fiber volume fraction, Poisson ratio, stress ratio, applied stress and number of applied cycle to failure, of unidirectional GRP and CFRP composites for various on- or off-axis angles are required as initial step of analysis. The following steps should make to define  $f$  parameter from the experimental data. (1) The material properties such as fiber stiffness, matrix stiffness, composite initial stiffness, fiber volume fraction, Poisson ratio, stress ratio, applied stress and number of applied cycle to failure, of unidirectional GRP and CFRP composites for various on- or off-axis angles are required as the initial step of analysis. (2) For life smaller than fatigue life, calculated  $f$  parameter for each stress state, and (3) Graph the  $f$  parameter versus fatigue life.

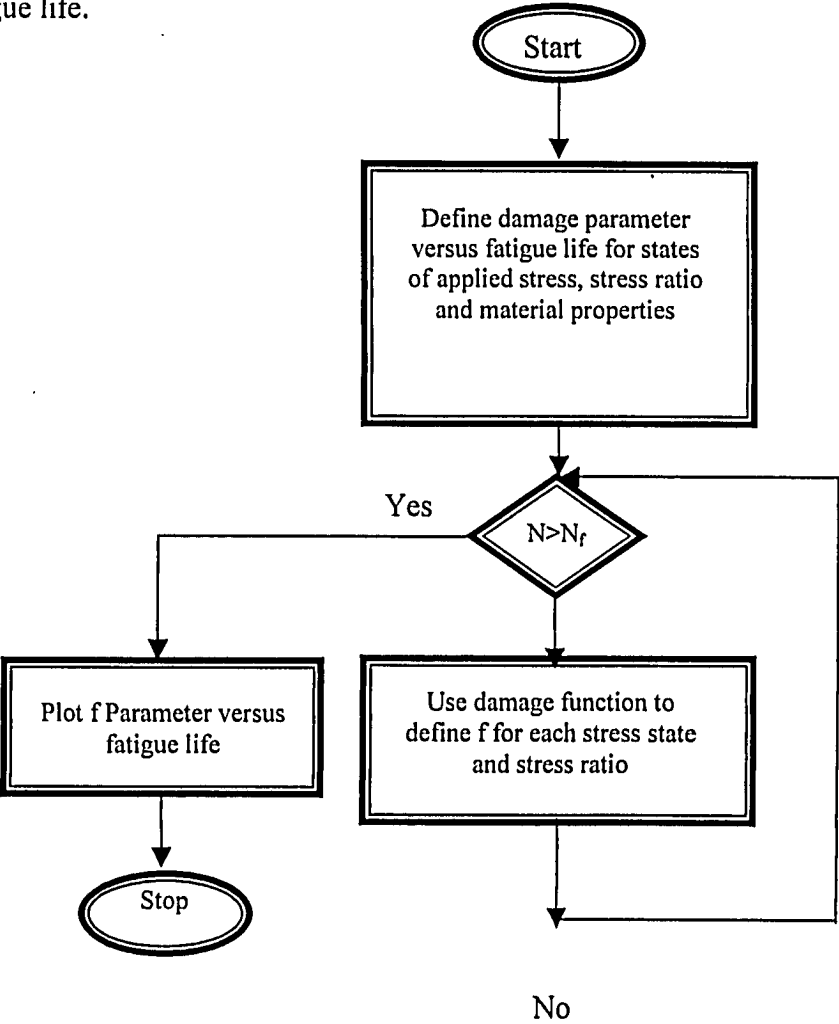


Figure 4.6: Flowchart of identifying  $f$  parameter versus life

#### 4.5 Elements of Fatigue Damage Analysis for Cross-ply Composite

As was discussed before, the transverse matrix cracking is the major damage mechanism in the early region (i.e., first 20% of fatigue life) of fatigue damage. After Characteristic Damage State (CDS) is attained, delamination induced from tips of the transverse matrix cracks gradually becomes the dominant damage mechanism until extensive fiber fracture occurs at the final region of fatigue damage. Due to damage accumulation, the local stress state in each lamina changes continuously with matrix cracking in  $90^\circ$  plies and delamination at tips of matrix cracks, which consequently reduces the stiffness of the entire laminate. Progressive failure is characterized by the manner of load redistribution/transfer to the  $0^\circ$  plies. Such mechanisms have to be addressed, to represent the physical process of fatigue failure and to predict the fatigue life of a composite laminate. The concept of damage accumulation may be used as a more suitable approach to predict the fatigue life of constituent plies of cross-ply composite materials. In cross-ply laminates subjected to uniaxial tensile fatigue loading, experimental investigations show that the predominant damage mechanisms are the initiation and propagation of transverse cracking in the  $90^\circ$  layers [39]. Most of the stiffness reduction occurs during the first 10%-20% of the life of the laminate [39].

During this region, the crack density increases in the  $90^\circ$  ply and reaches a saturation value. Transverse cracking in the  $90^\circ$  ply results in local stress redistribution in the laminate, with the  $0^\circ$  ply carrying additional load. These damage mechanisms are observed [68] to occur during the first 80% of the lifetime of the test specimen. Then, longitudinal matrix crack splitting follows this first region, local delamination at intersections of transverse and longitudinal cracks, and ultimately by fiber fracture of the  $0^\circ$  layers carrying the load applied to laminates.

The accumulation of damage of  $0^\circ$  ply and  $90^\circ$  ply to predict the life and damage of cross-ply composite can be generalized by the use of damage model equation presented in this study a weighting factor of  $\eta$  describes the efficiency of load carrying plies of  $0^\circ$  and  $90^\circ$  in cross-ply composite. Equation 4.25 demonstrates the accumulative

model that combines the damage from two unidirectional plies of 0° and 90° by employing the factor  $\eta$ :

$$(1 - E/E_c)_{[0/90]} = (1 - \eta)(1 - E/E_c)_0 + \eta(1 - E/E_c)_{90} \quad (4.25)$$

As described earlier, the contribution of the 90° ply in fatigue life of the composite is about 80%. Since, during the first 10% of composite life, most of the stiffness reduction is due to damage in the 90° ply, and there is very minor stiffness reduction in the 0° ply, the factor  $\eta$  is predicted to vary between 10%-20% depending on the type of the laminate and stacking sequences [39].

#### 4.5.1 Algorithm/Flowchart of Analysis for Cross-ply Composite

Figure 4.7 represents the cumulative damage scheme of fatigue damage analysis of a cross-ply composite based on the proposed damage method in this study. The proposed fatigue damage analysis method includes damage in different plies of 0/90 degree in three regions of matrix, matrix-fiber interface and fiber and reflects the cracking mechanism within three regions from early region of growth to final failure. This figure gives the procedure of damage analysis in the following steps: (1) The material properties such as fiber stiffness, matrix stiffness, composite initial stiffness, fiber volume fraction, Poisson ratio, stress ratio, applied stress and number of applied cycles to failure of 0° and 90° plies are required as initial step of analysis. (2) Calculating damage parameter for each stress state for 0° ply and 90° ply separately until the failure (Equation (4.3)). (3) Applied modified damage parameter for cross-ply composite (Equation (4.25)), and (4) Compare the predicted damage-fatigue-cycles curve with the experimental curve.



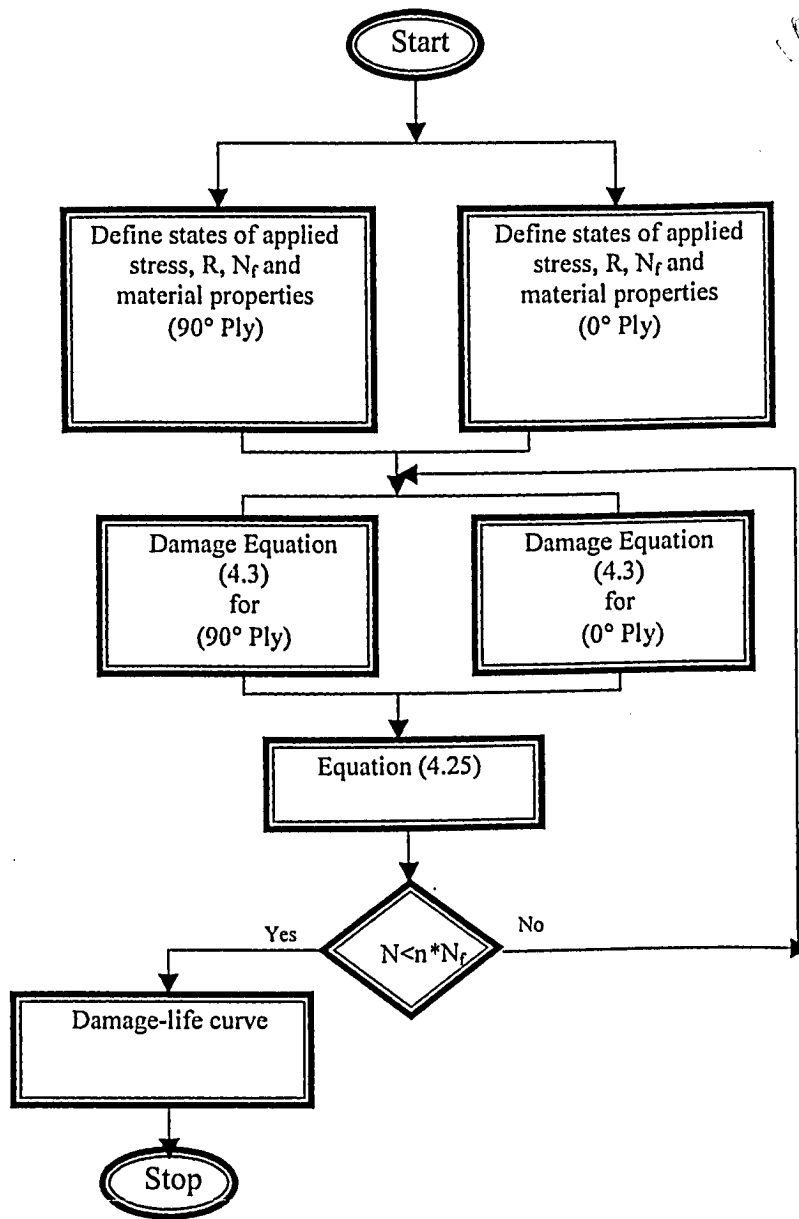


Figure 4.7: Flowchart of generalized material property degradation technique

## CHAPTER FIVE

### Finite Element Analysis

#### 5.1 Efficiency of Fiber/Matrix Interface in Unidirectional FRP Composite

As it was discussed earlier, the static strength of unidirectional laminates is related to the fiber-matrix bonding. Many investigators using micromechanics models have predicted the efficiency of the interface. The parameter  $f$  has been introduced to predict the influence of the interface on the tensile strength of unidirectional composites. As  $f \rightarrow 1$ , the stiffness of the composite approaches the value predicted by the rule of mixtures, which assumes perfect bonding. As  $f \rightarrow 0$ , the stiffness of the composite approaches the stiffness of the matrix. This is because no load is being transferred to the fiber and the matrix material is carrying the entire load.

A finite element solution to the problem of a single fiber embedded in matrix is outlined in this study to compare the “ $f$ ” parameter with values obtained through the experimental data. The methodology used in the FEM analysis is based on two assumptions conjectured from different studies [43]: (a) in each cycle only the maximum and minimum loads are applied based on the assumption that damage initiates and grows only at these loads, and (b) for the number of cycles equal to a chosen increment during the second stage of damage, only gradual degradation of the material at the end of each step is considered. The second assumption is vital in order to introduce the degradation of stiffness corresponding to any given cycles.

In the present study, a representative volume element (RVE) that consists of a single fiber in a matrix cylinder and containing a central interface crack is considered. The outer radius of the matrix cylinder is chosen to match the fiber volume fraction of the corresponding composite. Special contact elements, which have bonded features, are used between the fiber and the matrix. It is also assumed that the fiber and matrix are statistically homogeneous and linearly elastic materials. The matrix is assumed to be

isotropic and the fiber transversely isotropic. The displacement correlation method is used to calculate  $f$  based on a formula  $f = \frac{U_f}{U_m}$  introduced by Subramanian [44].

## 5.2 Numerical analysis

### 5.21 Finite element Model

Consider the RVE of a unidirectional composite of length  $L = 20\mu\text{m}$ , which has a fiber/matrix interface crack of length  $a = 5\mu\text{m}$  shown in Figure 5.1. The outer radius of the matrix is chosen such that the RVE has the same fiber volume fraction as the composite. Thus

$$r_f^2 = V_f * r_m^2 \quad (5.1)$$

Further, the outer matrix surface ( $r = r_m$ ) is assumed traction free. In the RVE, the fiber occupies the region,  $r < r_f$  and the matrix occupies the region,  $r_f < r < r_m$ . Along the crack surface the fiber is not bonded to the matrix, while outside this region, perfect bonding between fiber and matrix is assumed.

Figure 5.2 shows a small representative planar region (RPR) within the cylindrical specimen modeled in a two-dimensional plane strain setting using the ANSYS 8.0 Educational Version finite element program [45].

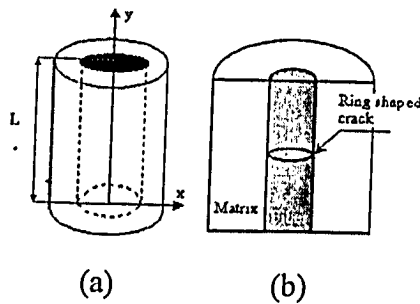
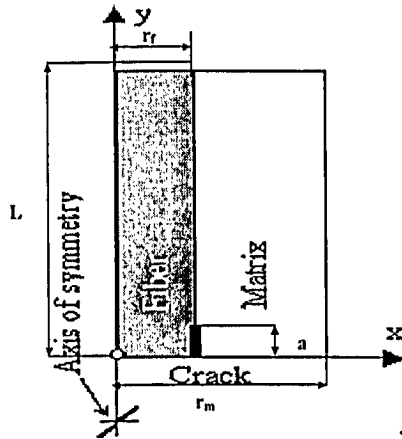


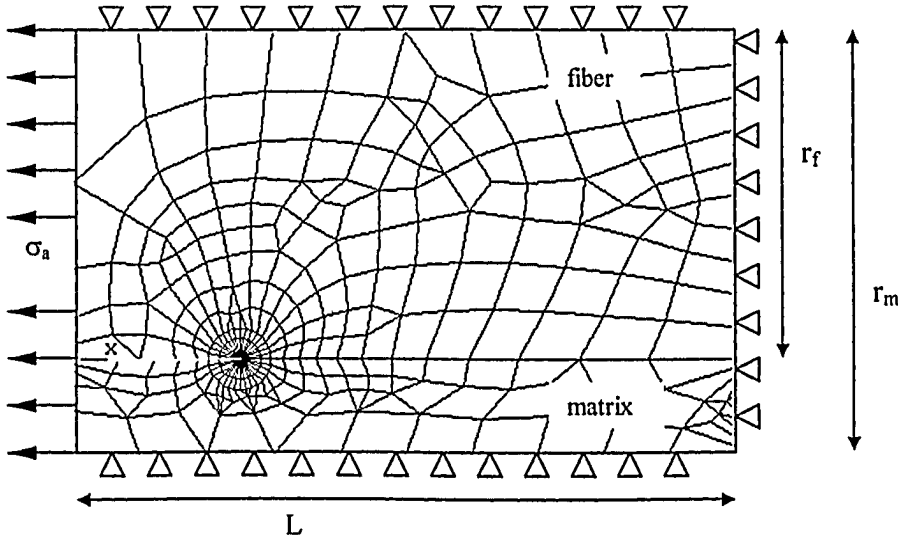
Figure 5.1: (a) The composite cylinder model; (b) Cross-section of continuous fiber reinforced composite



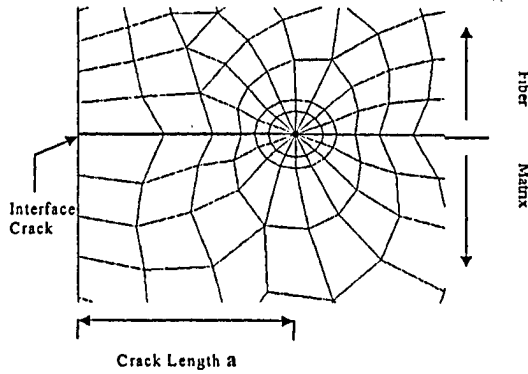
**Figure 5.2:** Axisymmetric model of the composite with crack.

Eight node isoparametric finite element elements (PLANE183) are used for the model of the solution domain except those contacting the crack tip. These elements are six node triangular quarter point elements. PLANE183 2-dimensional

The 8-node structural solid element is a high order two-dimensional 8-node element. PLANE183 has quadratic displacement behavior and is well suited to model irregular meshes. The 8 nodes having two degrees of freedom at each node define this element as translations in the nodal  $x$  and  $y$  directions. The element has been used as a plane element, plane stress in an axisymmetric element. The elements near the crack are taken as small as possible in order to simulate the stress distribution and deformation near the crack more accurately. The number of nodes and elements are 378 and 944, respectively. Contact elements, Conta178 and Target 169, are used to represent 2-dimensional contacting surface, respectively, between the matrix and the fiber. The contact surfaces are identified by a shared real constant set. Figures 5.3 and 5.4 depict the elements, the boundary conditions and direction of applied load for the finite element model.



**Figure 5.3:** Finite element mesh and boundary conditions



**Figure 5.4:** Six-node triangular quarter point elements at interface of crack tip.

The FRP composite materials used for the specimen are GRP composite with the CFRP of volume fraction of  $V_f = 0.58-0.6$  and radius of fiber  $r_f = 10\mu\text{m}$  where the ratio of the length of crack and the fiber radius is  $\frac{a}{r_f} = 0.5$ . The matrix material used for specimens is epoxy with the radius of  $r_m = 12.9\mu\text{m}$ . Tables 5.1-5.2 represent the material properties of GRP and CFRP composites used in the FEM model. Tables 5.3-5.4 also denote the

fatigue loading conditions extracted from the literatures [46, 47]. To illustrate the methodology two cyclic loading ( $R = -1$ ) and ( $R = 0.1$ ) are used with different applied stresses of  $\sigma_a=120$  MPa and  $\sigma_a=1.306$  GPa for GRP and CFRP composite materials, respectively.

**Table 5.1:** Typical engineering properties of fiber, matrix and GRP composite [46].

	Tensile Modulus (GPa)	Shear Modulus (GPa)	Poisson's Ratio
Glass Fiber	72.4	30	0.2
Epoxy Matrix	4.73	1.822	0.31
GRP Composite	45	4.17	0.29

**Table 5.2:** Typical engineering properties of fiber, matrix and CFRP composite. [47]

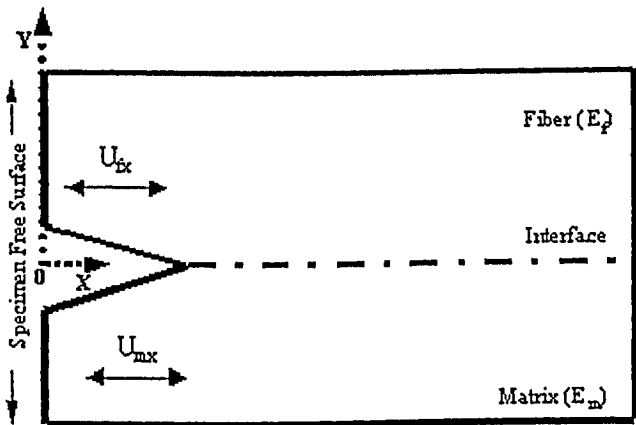
	Tensile Modulus (GPa)	Shear Modulus (GPa)	Poisson's Ratio
Carbon Fiber	296	5.5	0.28
Epoxy Matrix	3.3	2.9	0.31
CFRP Composite	173	5	0.3

**Table 5.3:** Fatigue testing conditions for 0° directions,  $R = -1$  and  $V_f=0.6$  by Philippidis et al. [46].

R=-1	
Longitudinal Direction 0°	
Applied Stress (MPa)	Life (Cycles)
120	313

**Table 5.4:** Fatigue testing conditions for 0° directions,  $R = 0.1$  and  $V_f = 0.58$  by Plumtree et al. [47].

R=0.1	
Longitudinal Direction 0°	
Applied Stress (GPa)	Life (Cycles)
1.306	4908



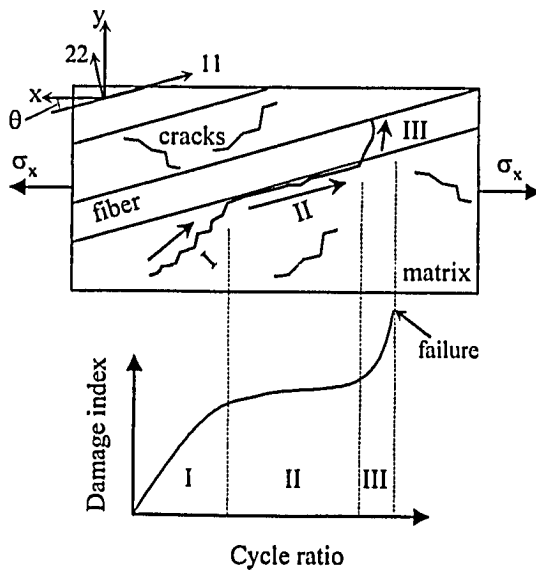
**Figure 5.5:** Schematic of 2-dimensional model used for FEM analysis,  $U_{fx}$  and  $U_{mx}$  are direction of nodal displacements respectively within the fiber and matrix surfaces.

### 5.2.2 Material Property Degradation

When composite structures are imposed to fatigue loading, the material is loaded by a stress state, which, during the first cycles of loading is smaller than the strength of the material. Thus, during the first cycle, there is no static mode of failure. By increasing the number of cycles, the stiffness of the material degrades due to the nature of cyclic loading. The degradation of stiffness leads to stress redistributions and thus, to higher stress states.

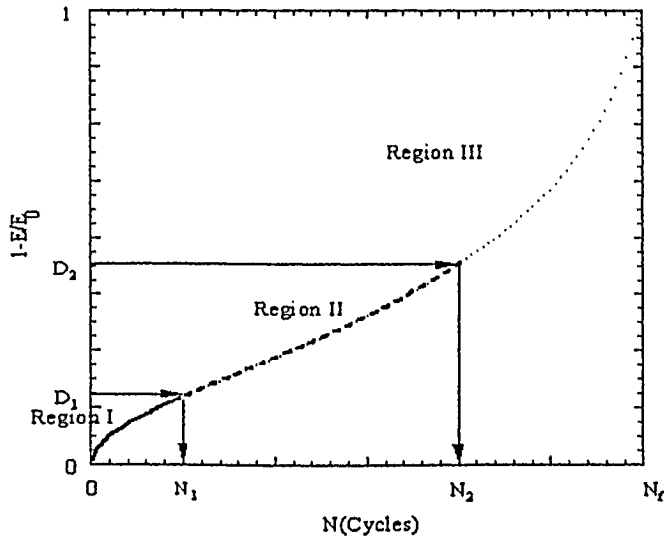
In fatigue loading cases, the nature of cyclic loading implies material degradation by the increased number of cycles, which happens gradually, hence the name called gradual material property degradation [48].

Gradual degradation of the composite materials is due to cyclic loading in three main regions and it is applied on the basis of material stiffness. During the finite element modeling of fiber-matrix interfacial debonding special attention was given to develop a technique, which requires small amount of experimental data and can be easily applied to different composite material systems. The experiments required for each material are those for the S–N curve and the stiffness reduction as a function of number of cycles [49]. In the present FEM analysis the stiffness reduction during stage II of damage of the FRP composite has been derived from the proposed damage model. The fatigue damage curves in Figure 5.6 are related to crack development throughout the life. In region I, the number and density of matrix cracks increases until a uniform, saturation spacing is reached. This state of damage, known as the characteristic damage state, is a laminate property, which is achieved near the end of region I. The crack spacing in a given ply is a function of material properties and the constraints imposed on the ply by the surrounding plies. It can be concluded that during this stage the matrix mechanical property degrades the most compared with the fiber, so the composite mechanical property degrades.



**Figure 5.6:** Three regions of cracking mechanism in unidirectional composites.





**Figure 5.6 (Cont.):** Fatigue damage curve related to crack development in region I,II and III.

As the loading history continues, region II damage begins with turning and growth of matrix cracks along the interfaces between plies. The tensile interlaminar normal stress and the large interlaminar shear stress associated with matrix cracks support the initiation and growth of delaminations during cyclic loading. The locally high stress field associated with crossing matrix cracks and the intersection of matrix cracks and ply interfaces is one of the factors responsible for fiber fracture. Some failures are random fractures of statistically weak fibers; however, many more fiber fractures are associated with matrix cracks in adjacent plies. So based on the degradation of composite stiffness during region II, degradation of the matrix and the fiber can be conducted by the use of proposed damage criterion.

Figure 5.7 represents the behavior of fiber and matrix along with the composite degradation curve. It can be observed that the rate of degradation in the matrix at the region I is higher compared with the other regions and gradually continues until the end of the life of the specimen. In the fiber, this rate slowly increases by applying load and eventually increases with a sharp slope toward the catastrophic failure of the specimen. It also concludes that during the debonding in region II the degradation of fiber and matrix

follows a steady state until the end of the region at which fiber breakage starts to happen more intensively.

For the finite element simulation, a cycle jump approach has been adopted which allows calculating stiffness degradation of the fiber and the matrix at deliberately chosen intervals in region II of the damage where the efficiency of bonding between the fiber and the matrix is evaluated. Tables 5.5 and Table 5.6 demonstrate the number of cycles related to each point of damage and related stiffness for the fiber and the matrix based on the degradation model presented in this study, for two cyclic applied loads.

The advantage of this method compare with the use of the Euler explicit integration formula is that it takes into consideration the mechanics of damage by using the damage model presented in this study, which helps to evaluate and understand the physics of fatigue damage thoroughly.

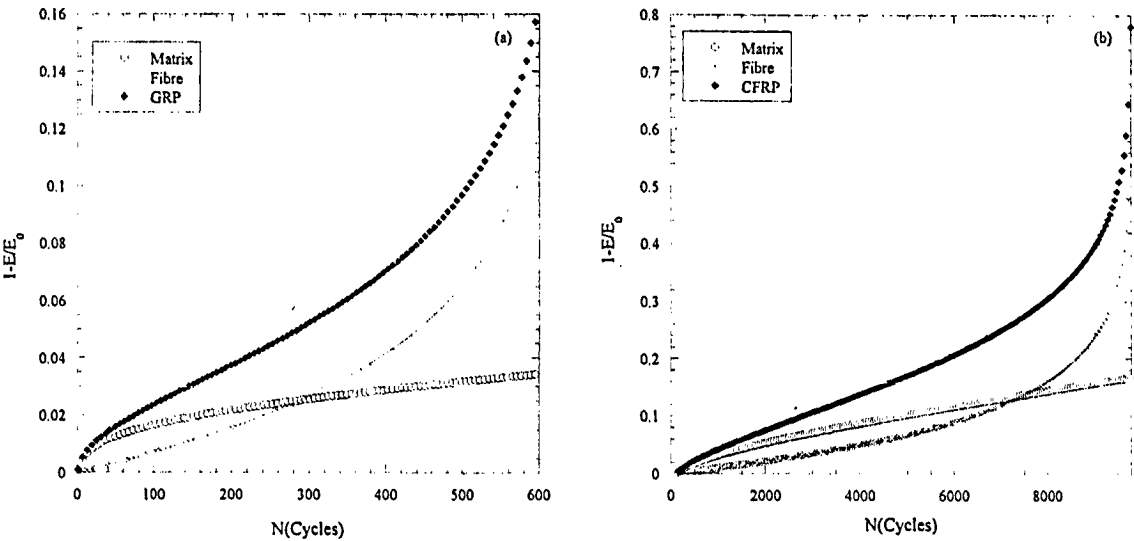


Figure 5.7: Fatigue damage versus life in (a) GRP composite with cyclic applied load of 120 MPa and (b) CFRP composite with cyclic applied load of 1.306GPa.

**Table 5.5:** Fiber and matrix stiffness during region II of fatigue life for  $\sigma_a=120\text{MPa}$ .

Number of cycle	Matrix Stiffness (GPa)	Fiber Stiffness (GPa)
97	2.5	71.9
151	2.1	71.5
205	1.8	71.2
259	1.5	70.8
313	1.2	70.3

**Table 5.6:** Fiber and matrix stiffness during region II of fatigue life for  $\sigma_a=1.306\text{GPa}$ .

Number of cycle	Matrix Stiffness (GPa)	Fiber Stiffness (GPa)
1500	2.4	291.9
2300	2.1	289.5
3100	1.9	286.8
3900	1.4	280.3
4700	1.4	280.3
5500	1.4	276.2
6300	0.9	271.2
7100	0.7	264.9

Figure 5.8 shows a detailed flowchart of the finite element implementation of the cycle jump approach during region II of the damage. There are three stages in the flowchart and two steps within the finite element procedure. During each cyclic loading interval, mechanical properties are assumed to be constant.

Results from FEM analysis in the form of nodal displacements after each number of loading cycles for specified nodes (Table (5.7)) are stored and the parameter  $f$  is

computed using these nodal displacements. The experimental data that have been used to evaluate the FEM model are extracted from the experimental data provided by Philippidis et al. and [46] and Plumtree et al. [47].

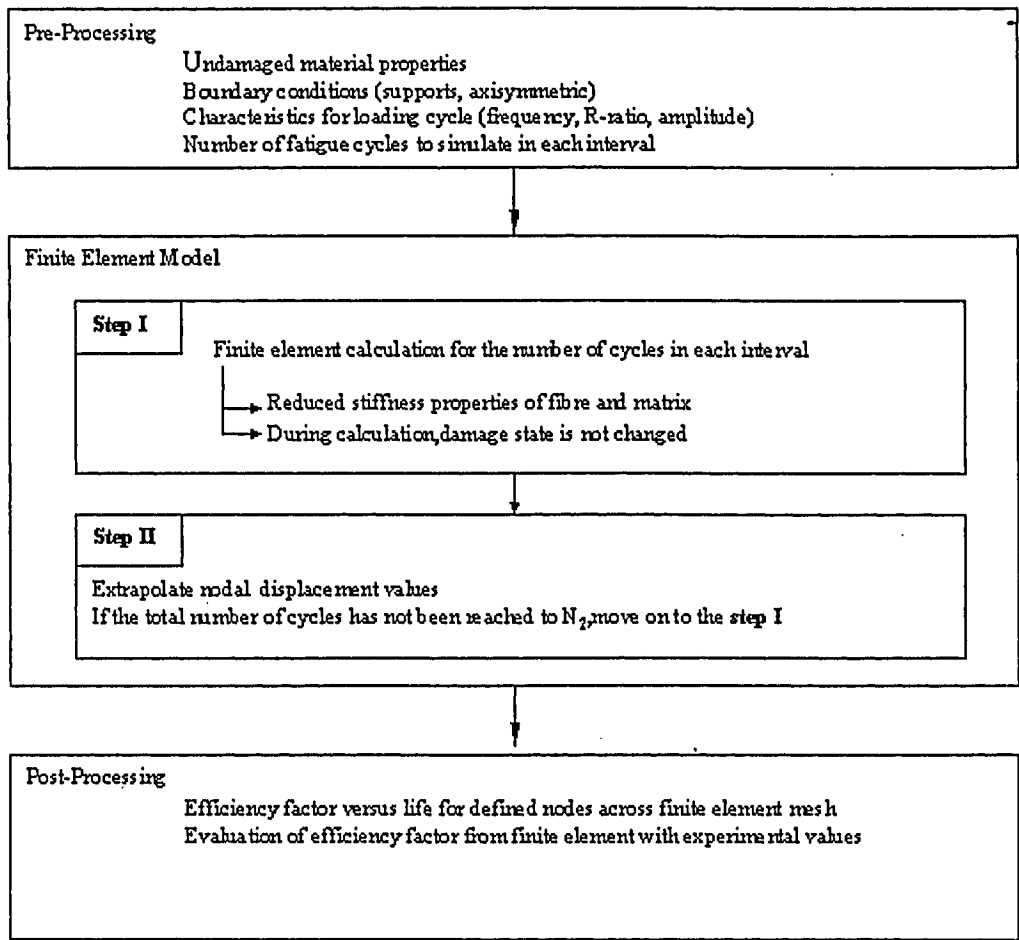


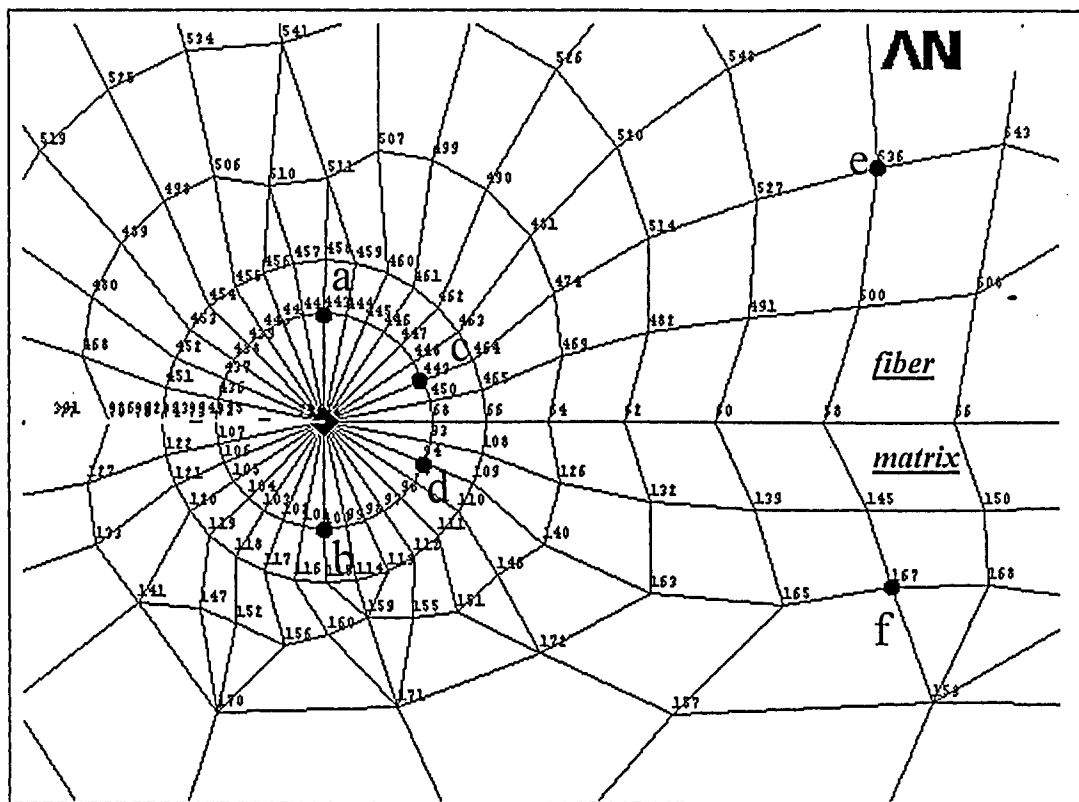
Figure 5.8: Flowchart of the finite element implementation in fiber-matrix interfacial debonding study

5.3 Nodal Displacement

For the evaluation of the efficiency factor, the relative displacements,  $U_x$  of selected nodes on upper and lower crack faces, in the fiber and matrix surfaces, as shown in Figure 5.9 are determined by using the ANSYS 8.0 finite element software. Figure 5.9 shows the nodes across the mesh. To get more accurate results from the displacement method, nodes have been selected to have the same x coordinates. Table 5.7 tabulates the nodes with their x coordinates with respect to the free surface of the specimen. As it has been explained before, the efficiency of the interface can be defined based on the formula that provides the relationship between fiber and matrix nodal displacements in the direction of the force. In this study, the constraint at the upper and lower edges of the model eliminates movements along the Y direction. Therefore pure x direction nodal displacements, can be extracted from the FEM results. Based on the location of the nodes from the specimen’s free surface (Figure 5.5), they have been plotted in different cyclic intervals during the region II of damage.

Table 5.7: Position of selected nodes in matrix and fiber faces.

Fiber Surface	(a)	(c)	(e)
Node#	443	449	536
Position ( $\mu\text{m}$ )	5.0031	5.577	8.3
Matrix Surface	(b)	(d)	(f)
Node#	100	94	167
Position ( $\mu\text{m}$ )	5.0031	5.577	8.3



**Figure 5.9:** Selected nodes around the tip of crack: Nodes (a), (c) and (e) on the upper face of crack in fiber surface and (b), (d) and (f) on the lower face of crack in matrix surface.

Figures 5.10a and 5.10b demonstrate the variation of displacements in different cycle intervals versus the position of each node respected to specimen free surface. It is observed that the nodal displacement increases with increasing number of cycles until damage reaches the end of region II, in both fiber and matrix surfaces. Also at the tip of crack nodes (a and b) the  $f$  has the lowest value compared with the other nodes. By going further away from the tip of the crack it is expected the value of  $f$  with increase.

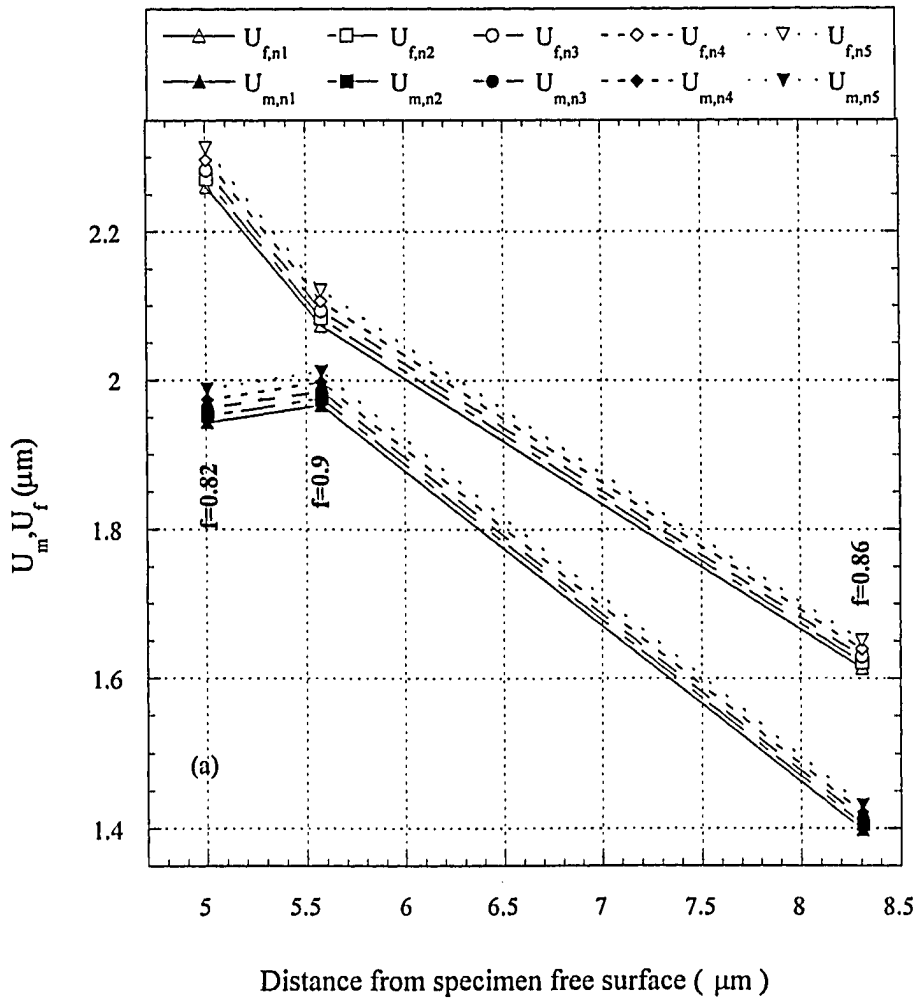
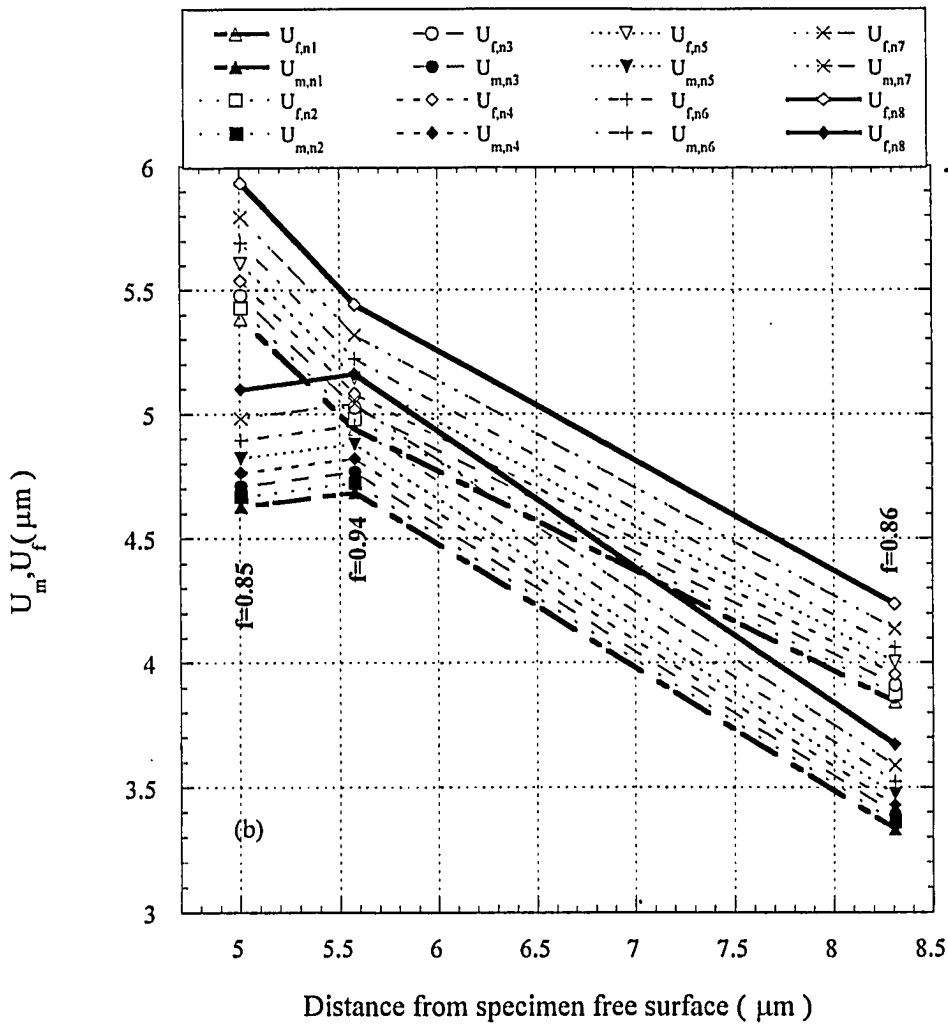


Figure 5.10a: Nodal displacement in x direction for the selected nodes and cyclic applied load of 120MPa for GRP composite for 5 cyclic intervals.



**Figure 5.10b:** Nodal displacement in x direction for the selected nodes and cyclic applied 1.306 GPa for CFRP composite for 8 cyclic intervals.



## CHAPTER SIX

### Evaluation of Fatigue Damage Model

This chapter discusses the results of fatigue damage assessment using the model proposed in this thesis. The available experimental data are first converted to terms required in the model and accordingly the values are submitted in the model. This chapter evaluates the model with unidirectional and cross-ply CFRP and GRP data obtained at different off-axis angles and R ratios.

#### 6.1 GRP and CFRP Unidirectional Fatigue Data

To evaluate the fatigue damage analysis proposed in this study, fatigue data of unidirectional and cross-ply GRP and CFRP composites at various off-axis angles and R-ratios have been extracted from the literature. Appendix A consists of material properties, fatigue damage-life and loading condition data. Available data are either stiffness degradation or damage parameters versus life or cycle ratio, which are first converted to damage-life data required in the analysis.

##### 6.1.1 Agarwal and Joneja Data

The experimental program conducted by Agarwal and Joneja [50-52] consisted of fatigue testing of on-axis and off-axis unidirectional glass fiber-reinforced polymers (GRP) under uniaxial loading conditions. The material tested was composed of epoxy resin (Araldite LY 553 cured by a hardener designated HY 551), reinforced by continuous E glass fiber. Plates of the unidirectional composite were fabricated by a hand layout technique in the laboratory. The plates were 3.3 mm thick and exhibited a fiber content of approximately 25%. Rectangular pieces were cut from the plates and specimens were machined to a width of 12.7 mm and a length of 130 mm. The specimens were tested in flexural fatigue with the load applied 90 mm away from the fixed end. A fatigue-testing machine was

specially designed, fabricated and instrumented in this study. Flat specimens were fixed at one end while the other end was cycled between fixed displacement limits with zero mean displacement. Thus, the fatigue tests were constant-strain-amplitude tests, and performed stress ratio considered to be  $R = -1$ . The fatigue tests were performed in three different angles as  $0^\circ$ ,  $45^\circ$  and  $90^\circ$  with different strain amplitudes. In the longitudinal direction, fatigue tests were conducted in alternating bending at four strain amplitudes of 0.77%, 0.88%, 1.07% and 1.35% at the fixed end of the specimens that the fatigue life varied from about 25 to  $10^6$  cycles. When a specimen did not break at  $10^6$  cycles, the test was discontinued and the specimen was assumed to be a run-out. The tests were performed at frequencies between 6 and 8 Hz, which cause no significant heating of the specimens.

These tests were also conducted on the off-axis angles  $45^\circ$  and  $90^\circ$  to the longitudinal edge of the specimen. Four different strain amplitudes, for the case of  $45^\circ$ , namely 0.22, 0.28, 0.38 and 0.53%, at the fixed end of the specimens, were chosen so that the fatigue life of specimens varied from less than 100 cycles to more than  $10^6$  cycles. Tests were discontinued at  $10^6$  cycles when specimens did not break at this life.

In the transverse direction,  $90^\circ$ , fatigue tests were also performed at four different maximum displacements that produced strains of 0.22, 0.27, 0.33 and 0.43% at the fixed end of the specimens. The fatigue life of the specimens was observed vary from about  $10^3$  cycles to more than  $10^6$  cycles. When a specimen broke at  $10^6$  cycles, the test was discontinued and the specimen, as mentioned earlier, was assumed to be run-out.

### 6.1.2 Pauchard Data

The composite material investigated by Pauchard [53] was a unidirectional glass/epoxy composite under longitudinal loading. The polymer matrix was based upon a Bisphenol-A epoxy prepolymer (DGEBA) cross-linked using an anhydride hardener. ECR glass fibers (Owens Corning Fiber Glass) have been used as reinforcement. Curved composite beams corresponding to the industrial application have been elaborated using a filament winding process. The specimens had a  $10 \times 5 \text{ mm}^2$  rectangular cross-section and their radius of curvature was ca. 700 mm. The average fiber volume fraction was 55 vol.%.

The fatigue properties of the curved composite beams have been determined under a three-point bending condition by means of a hydraulic fatigue machine, which operated at a frequency 5 Hz. A span to depth ratio of 26 ensured that the shear effects were minimized. The experiments were performed at an imposed deflection using strain ratios,  $R=\sigma_{\min}/\sigma_{\max}$ , which is considered to be 0.7. During the tests, the relative stiffness loss was continuously monitored from the measurement of the maximum load.

### 6.1.3 Philippidis and Vassilopoulos Data

Results from the fatigue behavior of an experimental program by Philippidis et al. [5,46] consisting of fatigue tests on flat coupons, cut at 75° off-axis direction and on-axis 0° from a unidirectional, (UD), Glass/Polyester, (GRP), laminate are presented in this thesis.

The material is similar to those used by GRP wind turbine rotor blade manufacturers, i.e., hand lay-up and room temperature curing and fiber content of approximately 60%. A comprehensive experimental program was carried out which consisted of fatigue tests on straight-edged coupons cut from a plate. The stacking sequence of the laminate consisted of two layers unidirectional lamina of 100% aligned fibers, with a weight of 700 g/m<sup>2</sup>. The material system was E-glass/polyester, E-glass from Ahlstrom Glass fiber, while the polyester resin was Chempol 80 THIX by Interchem. This resin is a thixotropic unsaturated polyester and was mixed with 0.4%, Cobalt naphthenate solution (6%Co), accelerator and 1.5% methyl ethyl ketone peroxide, MEKP, (50% solution), catalyst. Rectangular plates were fabricated by the hand lay-up technique and cured at room temperature. Considering as the 0° direction that of the UD layer fibers, Coupons were cut, by a diamond wheel, at 0°, on-axis, and 75° off-axis direction. All test data was used for the study of stiffness variation during fatigue life as a function of stress level, off-axis angle and stress ratio, R. The specimens were prepared according to ASTM 3039-76 standard, their edges were trimmed with sandpaper and aluminum tabs were glued at their ends. The coupons were 250 mm long and had a width of 25 mm. Their nominal thickness was 2.6 mm. The length of the tabs, with a thickness of 2 mm, was 45 mm leaving a gauge length of 160 mm for each one of the coupons. Static and fatigue tests were performed. Coupon stiffness during fatigue, defined by the

average slope of the stress/strain loop, was monitored continuously and stiffness changes for all coupons were recorded. Fatigue tests, of sinusoidal, constant amplitude, waveform, were carried out on an MTS machine of 250kN capacity under load control and, under two different stress ratios,  $R = 0.1$  for longitudinal and off-axis ( $75^\circ$ ) direction and  $R=-1$  for the longitudinal case. The frequency was kept constant at 10 Hz for all the tests, which were continued until coupon ultimate failure or  $10^6$  cycles, whichever occurred first [5,46].

#### 6.1.4 Plumtree and Shi Data

The composite investigated by Plumtree et al. [47] was Narmco 5245C resin unidirectional reinforced with 58% (Volume fraction) Hercules IM-6 carbon fibers. Fatigue specimens of 2.8 mm thickness were cut to a length of 188 mm and width of 12.7 mm. The orientation of each specimen was  $10^\circ$  off-axis so that matrix shear fracture would be expected, i.e., the off-axis angle,  $\theta$ , satisfied  $3^\circ \leq \theta \leq 27^\circ$  [8]. For cyclic testing, four-point bending was used. The total span was 127 mm with spacing between the two upper loading pins of 37 mm. All the fatigue tests were carried out at room temperature under displacement control with a strain ratio  $R$  (minimum to maximum strain) of 0.1 and a frequency of 1 Hz using a triangular waveform..A computer using an acquisition program written specifically for this project continuously monitored the load and displacement data for each specimen. The fatigue life,  $N_f$ , was taken to be the number of cycles to specimen separation or when the unloading modulus decreased to 80% of its initial value. Optical microscopic observation was carried out on the polished specimen edges during fatigue testing. Cellulose acetate replication tape (22  $\mu\text{m}$  thick) was applied in order to monitor edge micro cracking during cyclic loading. The replicas were sputtered with a thin layer (0.5  $\mu\text{m}$  thick) of gold to enhance contrast for scanning electron microscope (SEM) examination. Schulte and Stinchcomb [55] showed that the micro crack morphology observed on the edges was an accurate representation of the interior of a fatigued specimen. In addition to edge replicas, the fracture surface morphology of failed specimens was studied using scanning electron microscopy.

6.1.5 Oever Data

In Oever’s study [56] a continuous E-glass fiber of PPG industries Fiber Glass BV with a polypropylene compatible sizing (PPG-Tuf Rov 4854,1200 tex) and an isotactic-polypropylene matrix of Shell Chemicals (PP homopolymer VM6100; melt flow index 20) were used. From the obtained plate dog bone specimens were made. Specimens were in accordance with ASTM D638-91.UD laminates with an overall length of 200 mm, a width of 12.5 and a thickness of 2 mm were manufactured by winding fibers on a rectangular mandrel with alternating layers of PP film. After film stacking, the mandrel with layers of polymer film and E-glass fibers was placed in an oven for 60 min at 90°C for drying. PP film with a thickness of approximately 0.02 mm was prepared using film-blowing equipment) Colin 30-25D/400). To avoid the material from adhering to the mandrel, release coated Mylar® sheets were used. Metal shims were used to control the thickness of the laminate. Impregnation was achieved by applying heat (200°C) and pressure (25bar) for 1h. The fiber volume fraction of all composites was approximately 0.5.The R-ratio in all fatigue experiments was 0.1. In order to study the fatigue behavior in longitudinal, shear and transverse loading situations, specimens with a fiber orientation of 0°, 10° and 90° were cut from these laminates. The essential first step to characterize damage during fatigue is to measure the change in stiffness properties. Specimen’s dimensions are listed in Table 6.1.

Table 6.1: Specimen dimensions of the different composites, by Oever [19]

Test Specimen	Thickness (mm)	Width (mm)	Length between tabs (mm)
[0°]	0.4	12	150
[10°]	2.0	12	150
[90°]	4.0	25	75

## 6.2 Variation of Interfacial Efficiency Parameter $f$

### 6.2.1 Variation of Parameter $f$ for Longitudinal Direction ( $\theta = 0^\circ$ )

Fiber-matrix bonding is a very crucial factor in static strength of unidirectional laminates. Many investigators using micro-mechanics models have predicted the influence of the fiber-matrix interface on the tensile strength of unidirectional laminates. Subraminian et al. [44] have introduced the interface efficiency parameter to predict the influence of the matrix-fiber interface on the tensile strength of unidirectional composites. This parameter varied between unity and zero. When the bonding is perfect and there is efficient load transfer from the matrix to the fiber, this parameter is considered to be unity, and for low strength bonding, the load transfer from the matrix is insufficient and this parameter tends to zero.

In the present study, the interface shear strength parameter  $f$  was defined as a function of the number of cycles  $N$  and the constant  $\alpha$  which is dependent on properties of the fiber, matrix and interface and the exponent  $\beta$ , which is the slope of  $f$ - $N$  diagram ( $f = \alpha N^\beta$ ). It is also worth mentioning that the modifications of the damage equation by the parameter  $f$  merely address matrix and matrix-fiber interface cracking and has no impact on the fiber breakage stage.

The trend of the parameter  $f$  for various on-axis ( $\theta = 0$ ) and unidirectional FRP composites has been presented in Figure 6.1, 6.2 and 6.3. This figure compares experimental data of  $f$ - $N$  and the response of parameter  $f$  defined in this study. Table 6.2 tabulates applied cyclic stress, R-ratio and terms involved with parameter  $f$  for five sets of fatigue data performed on unidirectional GRP and CFRP composites with on-axis angle  $\theta = 0$ . The coefficient  $\alpha$  extracted from experimental data and the calculated values presented in this table are found in good agreement.

**Table 6.2:** Variation of  $\alpha$  and  $\beta$  for various sets of GRP and CFRP composite data with on-axis loading direction ( $\theta = 0^\circ$ )

	R ratio	$\sigma_{app}$ (MPa)	$\tau_i$ (MPa)	$\alpha_{Cal.}$	$\alpha_{Exp.}$	$\beta$
GRP Agarwal	-1	69.3	22	2.296	2.3112	-0.103
	-1	79.2	22	2.625	2.201	-0.12
GRP Pauchard	0.7	635.6	41.35	4.35	4.414	-0.18
GRP Philippidis	-1	120	48.26	0.75	0.78	-0.12
	-1	140	48.26	0.87	0.87	-0.17
CFRP Plumtree	0.1	1139	137	1.48	1.382	-0.08
	0.1	1177	137	1.53	1.55	-0.16
GRP Oever	0.1	400	50	2.09	1.7896	-0.09

### 6.2.2 Variation of Parameter $f$ for Off-axis Loading Direction ( $0 < \theta < 90$ )

The parameter  $f$  for off-axis angles  $0 < \theta < 90$  were also found to be a function of the number of fatigue cycles  $N$ . Figure 6.4 compares experimental and calculated values of  $f$  as  $N$  increases. The constants  $\alpha$  and  $\beta$  for unidirectional GRP composites for off-axis angles  $\theta = 10^\circ$  and  $\theta = 75^\circ$  are presented in Table 6.3.

Table 6.3: Variation of  $\alpha$  and  $\beta$  for various sets of GRP composite data with off-axis loading direction ( $0<\theta<90$ )

	R ratio	$\sigma_{app}$ (MPa)	$\tau_i$ (MPa)	$\alpha_{Cal.}$	$\alpha_{Exp.}$	$\beta$
GRP Oever 10°	0.1	40	50	0.306	1.4726	-.0545
GRP Philippidis, 75°	0.1	45	60	1.0894	0.88	-0.04633
	0.1	40	60	2.8699	0.78	-0.19806
	0.1	35	60	0.1	0.1	-4.9682
	0.1	25	60	7.1456	0.38	-0.252

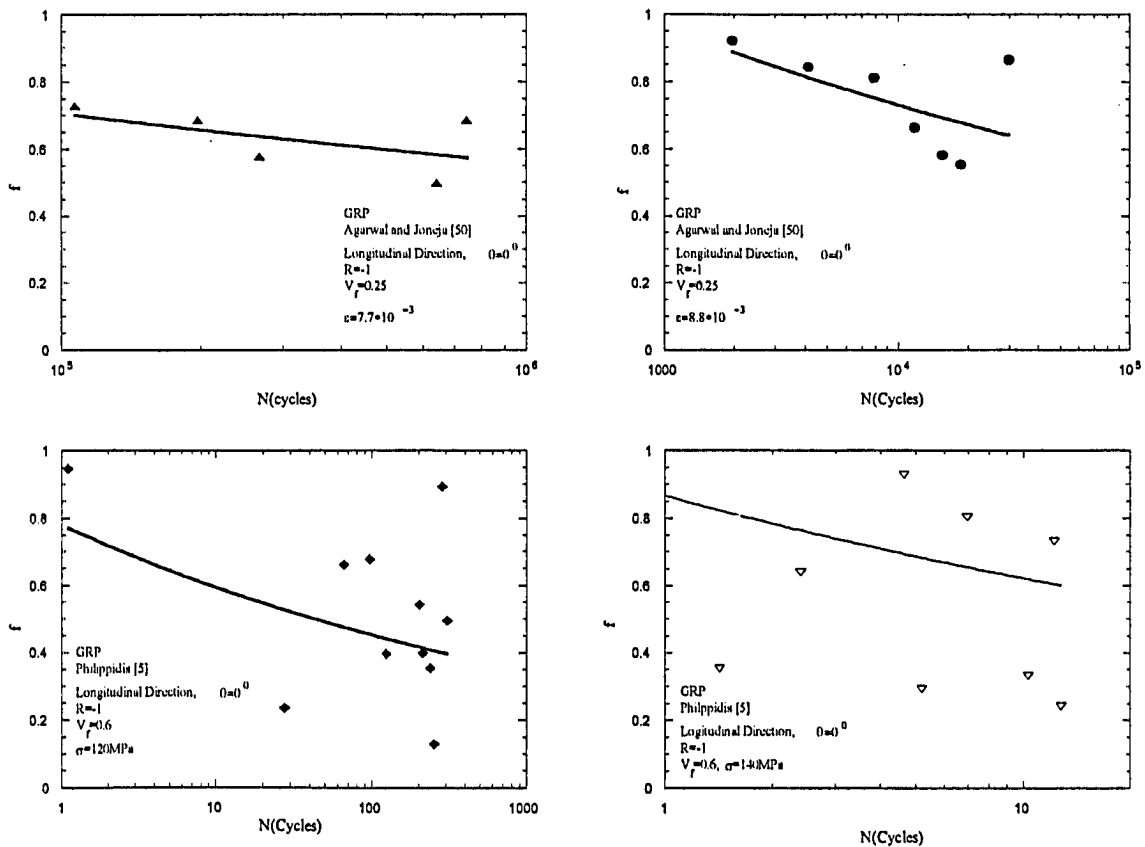


Figure 6.1: Parameter  $f$  versus number of cycles for UD GRP composite ( $\theta = 0^\circ$ ) tested with stress ratio of  $R=-1$ .



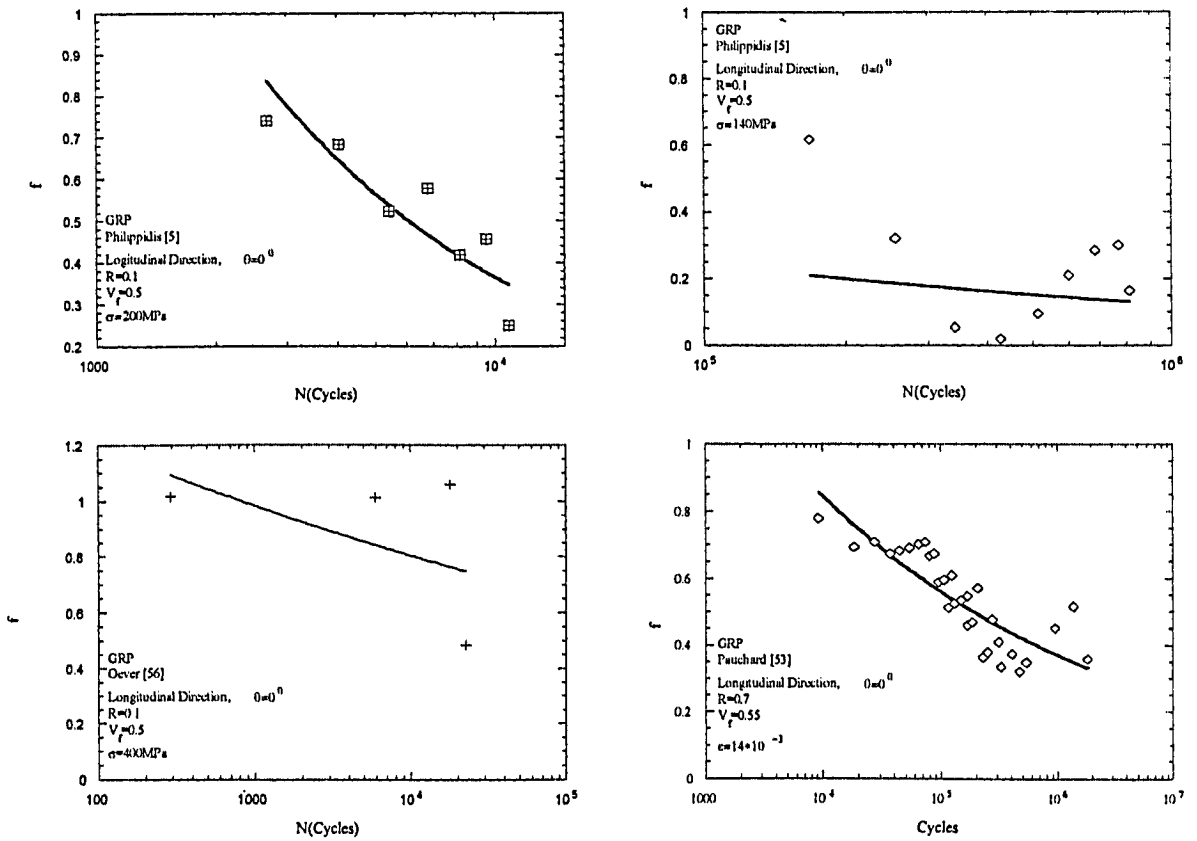


Figure 6.2: Parameter  $f$  versus number of cycles for UD GRP composite ( $\theta = 0^\circ$ ) tested with stress ratios of  $R=0.1$  and  $R=0.7$ .

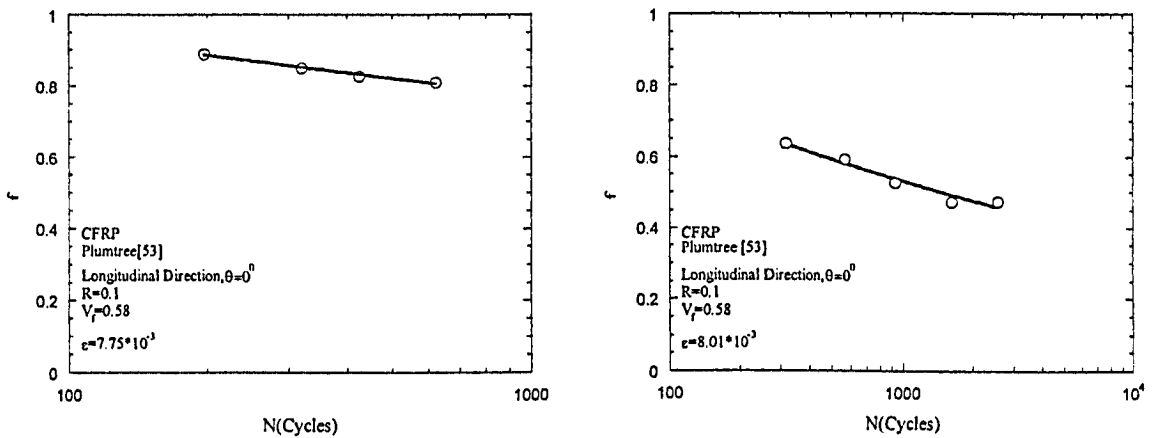
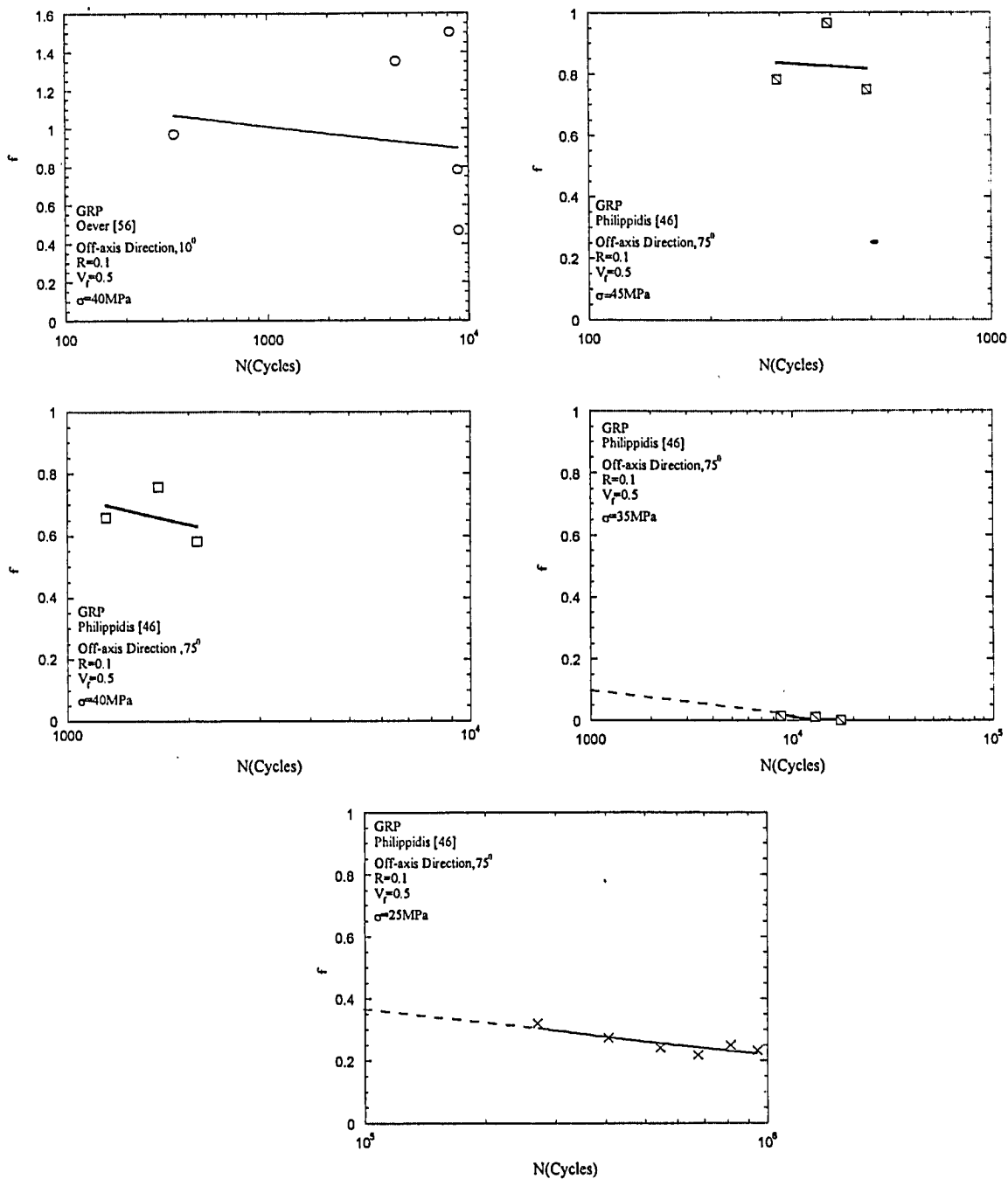


Figure 6.3: Parameter  $f$  versus number of cycles for UD CFRP composite ( $\theta = 0^\circ$ ) tested with stress ratio of  $R=0.1$ .



**Figure 6.4:** Parameter  $f$  versus number of cycles for UD GRP composite with off-axis angles of  $0 < \theta < 90^\circ$  tested with stress ratio of  $R=0.1$ .

### 6.2.3 Variation of Parameter f for Transverse Direction

Results for the parameter f for the transverse direction ( $\theta = 90^\circ$ ) are distinctly different from other off-axis angles discussed earlier. It is found that for this loading direction, the number of cycles has no or very little effect on the parameter f. The value of f stays nearly unchanged as N increases and possesses a value close to zero. Figure 6.5 shows this response

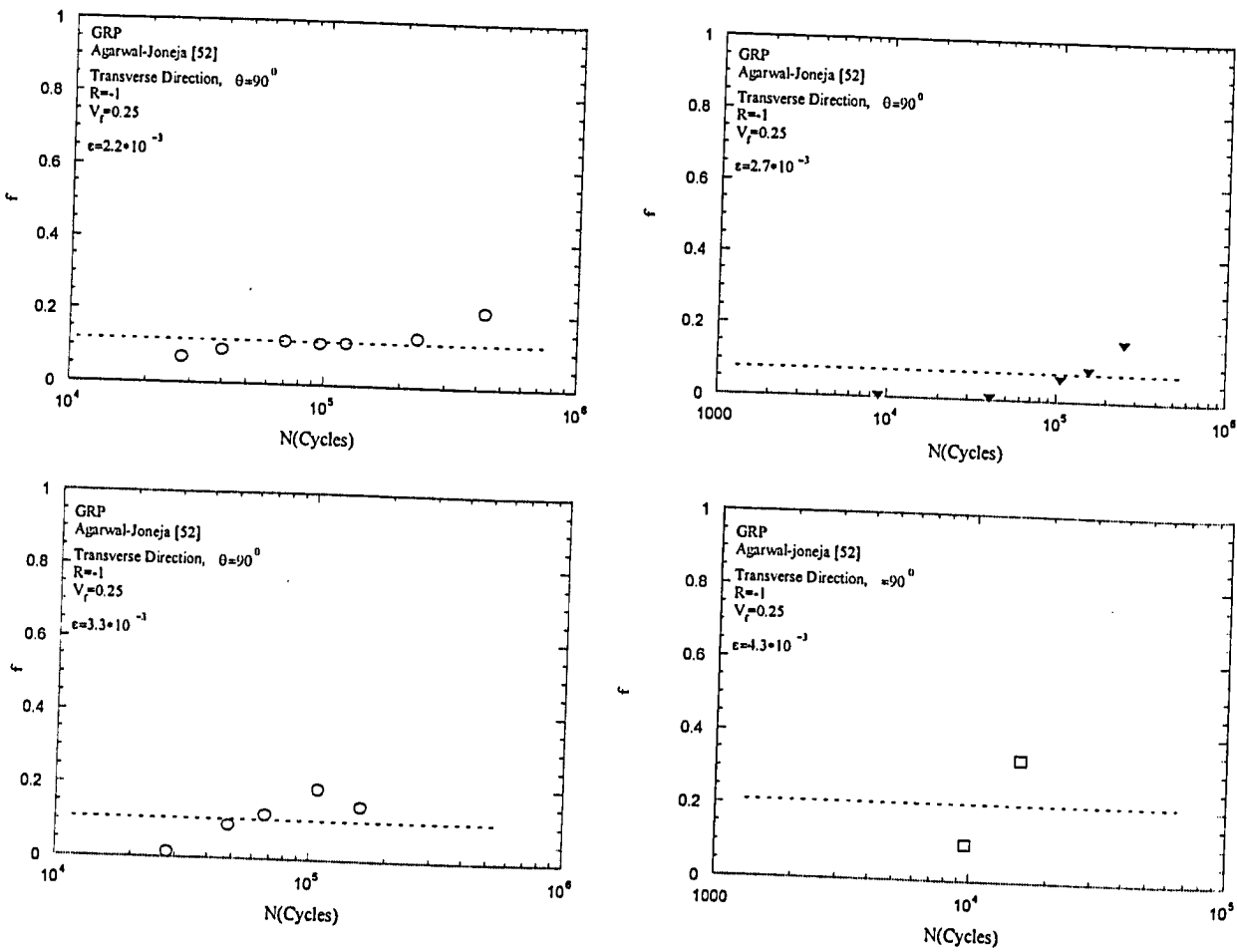


Figure 6.5: Parameter f versus number of cycles for UD GRP composite ( $\theta = 90^\circ$ ) tested with stress ratio of  $R = -1$ .

6.3 Variation of Damage Versus Life

6.3.1 Variation of Damage Parameter for Unidirectional Longitudinal Direction  
( $\theta = 0^\circ$ )

The interfacial shear strength parameter  $f$  defined as “parameter  $f$ ” improves the response of fatigue damage in UD FRP composites. Results of stiffness drop and fatigue damage have been presented in Figures 6.6-6.10. These figures present fatigue damage versus experimental life data for UD GRP and CFRP tested under various stress ratios  $R$ . The dashed line in these figures represent the response of the damage model developed in this study and shows how close the predicted damage curves are the damage values obtained from experiments. The parameter  $n$  that has been explained earlier is also tabulated for each case of experimental data in Table 6.4.

Table 6.4: Variation of  $n$  parameter for various UD GRP and CFRP composite fatigue data with various off-axis angles and stress ratios.

	GRP Agarwal	GRP Agarwal	GRP Pauchard	GRP Philippidis	GRP Philippidis	GRP Philippidis	CFRP Plumtree	GRP Oever	GRP Oever
R-ratio	-1	-1	0.7	-1	0.1	0.1	0.1	0.1	0.1
Direction ( $\theta^\circ$ )	0°	90°	0°	0°	0°	75°	0°	0°	10°
$n$	1	1	2	2	1.25	1.12	2	2	2

In the stiffness-based fatigue damage experiments and the corresponding damage-fatigue cycles curves reported in the literature for GRP and CFRP composites, term  $n$  is specified as a testing condition. Term  $n$  corresponds to the percentage of drop in stiffness recorded for a fatigue test. This mainly shows to what extent stiffness drop versus fatigue cycles has been controlled/measured before final failure. For instance, by considering the degradation up to the half of the real damage life (50%) term  $n=(0.5)^{-1}=2$ .

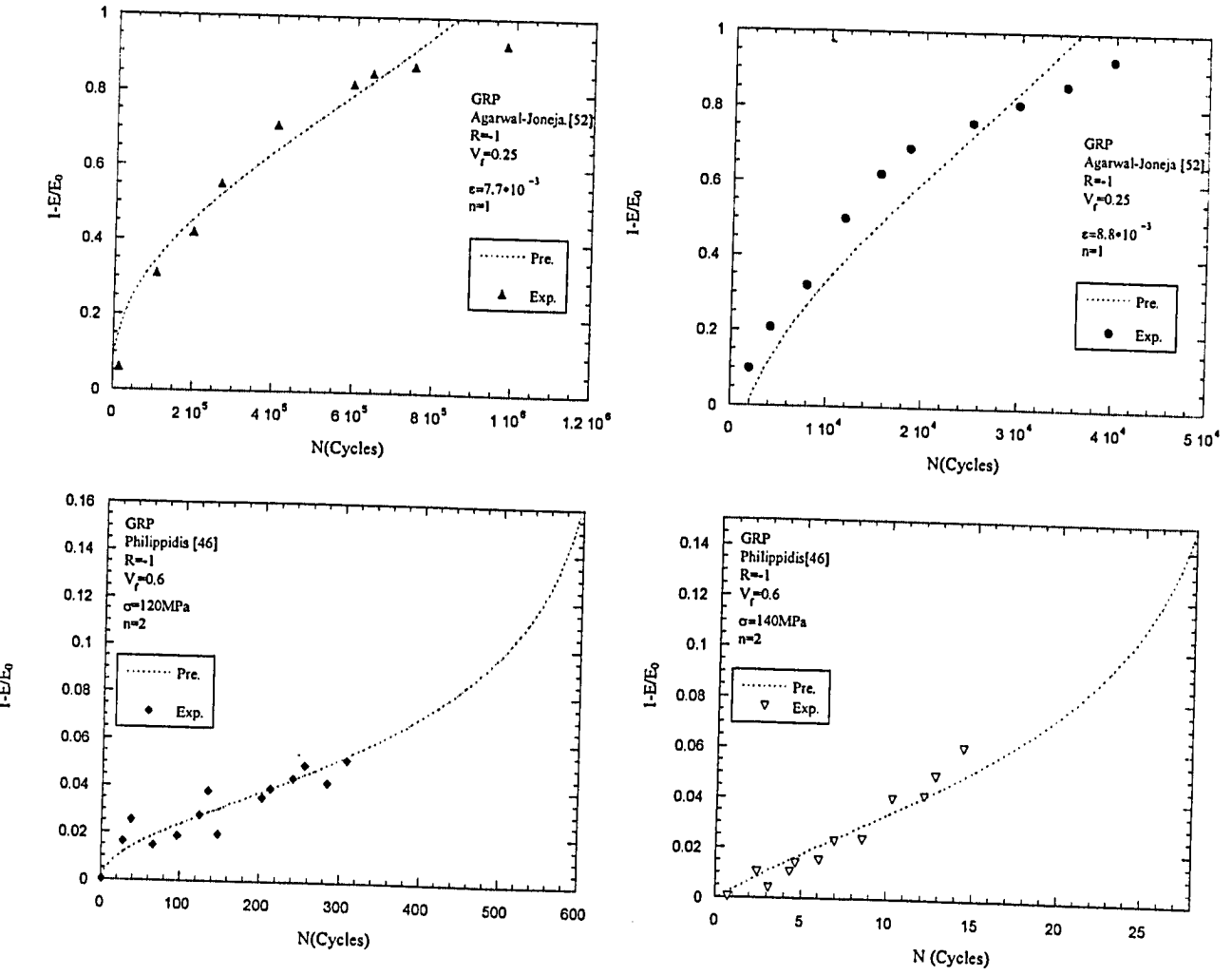


Figure 6.6: Predicted damage-life cycles plotted versus experimental values of damage-life cycles for UD GRP composites tested under various cyclic stress magnitudes when off-axis angle and stress ratio are  $\theta=0^\circ$  and  $R=-1$ , respectively.

### 6.3.2 Variation of Damage Parameter for Off-axis Angles ( $0 < \theta < 90$ )

Figure 6.9 is showing the result from implementing the  $f$  parameter for off-axis directions, into the proposed equation. The experimental data are plotted against the proposed equation to demonstrate the correlation between them. Also, the proposed number  $n$  for individual cases of experimental data can be found in Table 6.4.

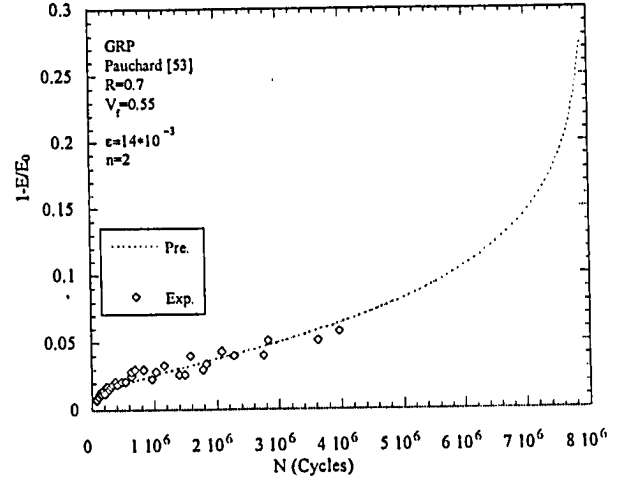
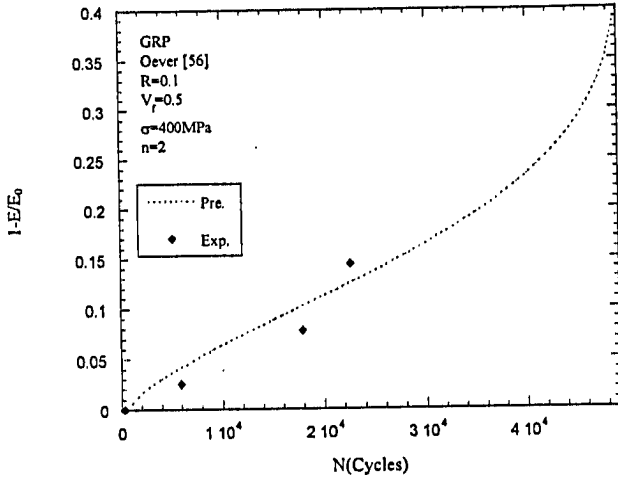
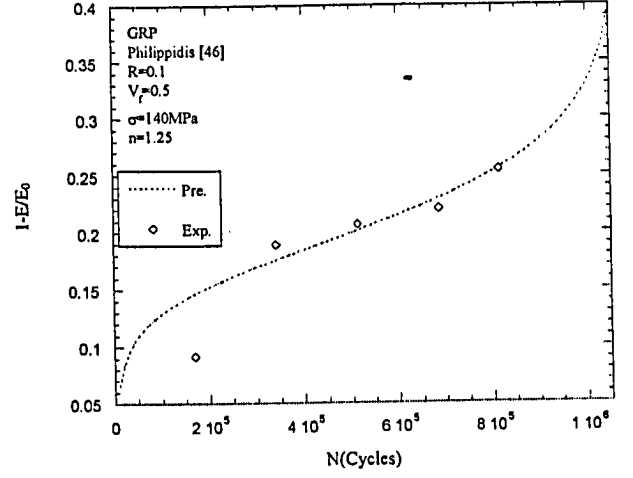
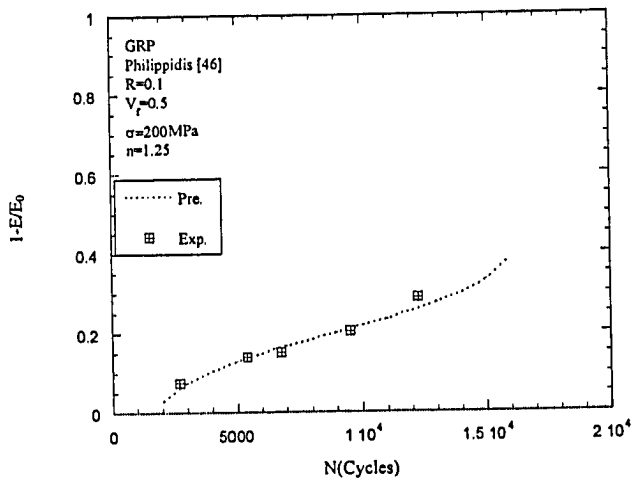
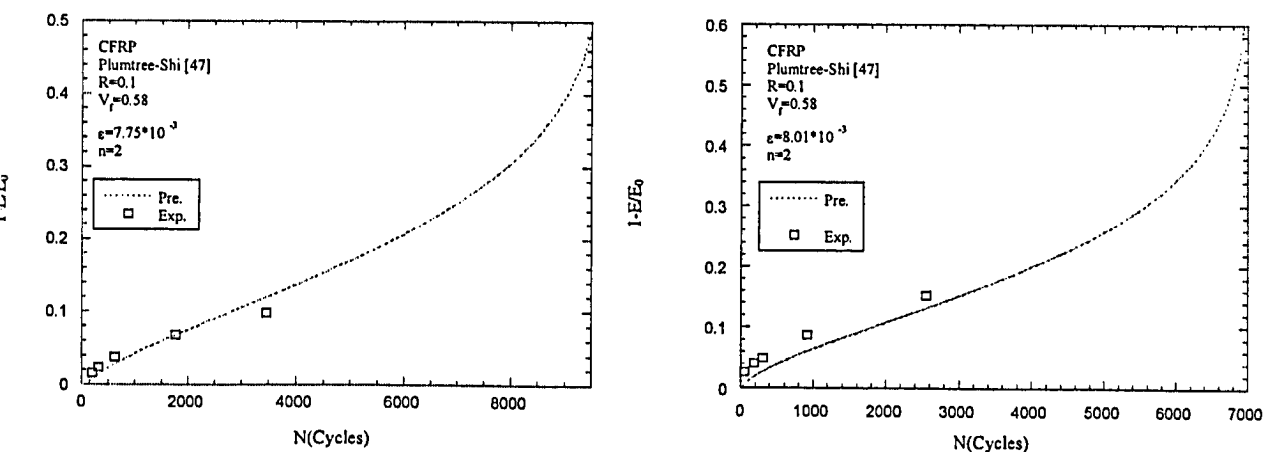


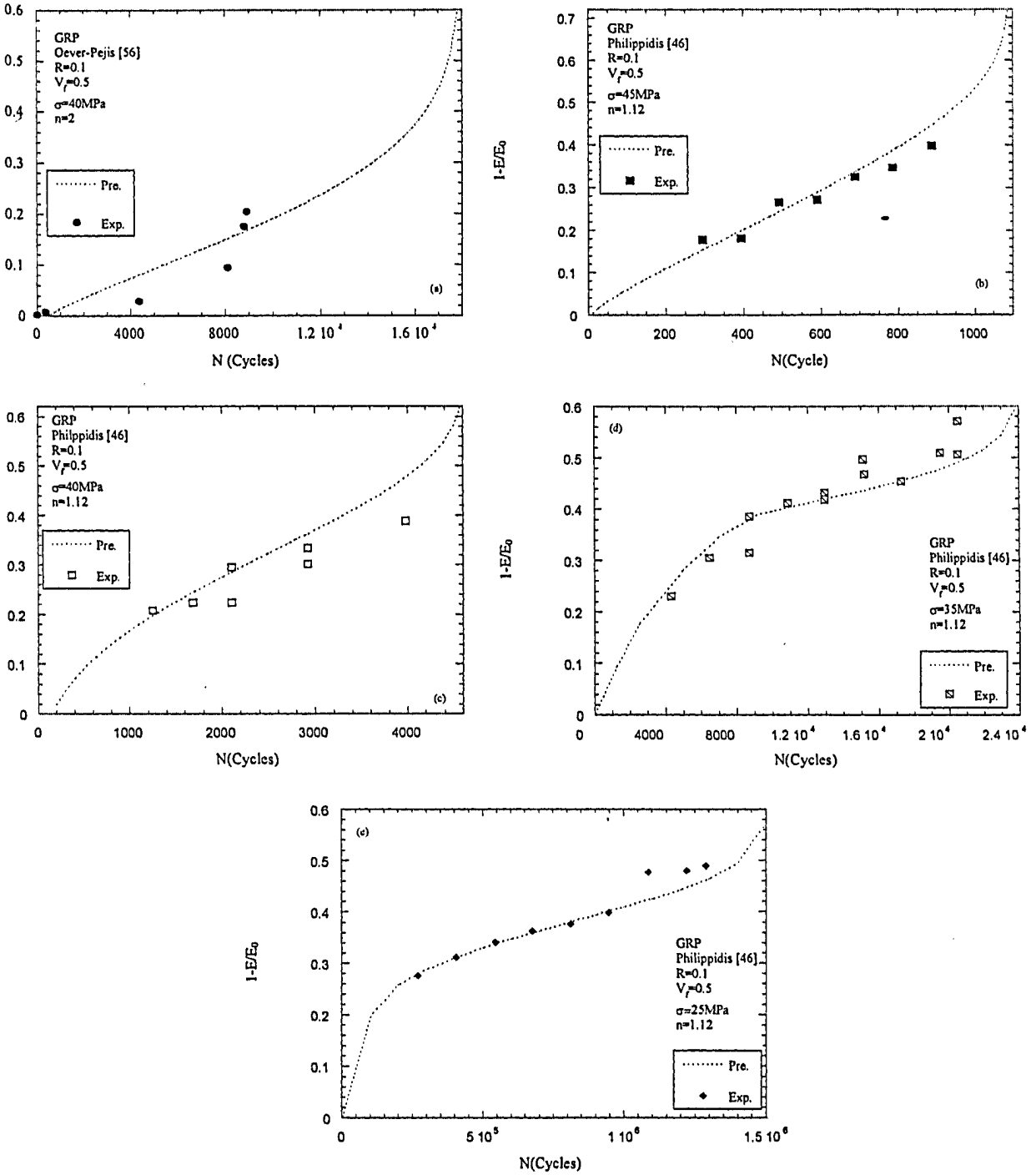
Figure 6.7: Predicted damage-life cycles plotted versus experimental values of damage-life cycles for UD GRP composites tested under various cyclic stress magnitudes when off-axis angle and stress ratios are  $\theta = 0^\circ$  and  $R = 0.1, 0.7$ , respectively.



**Figure 6.8:** Predicted damage-life cycles plotted versus experimental values of damage-life cycles for UD CFRP composites tested under various cyclic stress magnitudes when off-axis angle and stress ratio are  $\theta = 0^\circ$  and  $R = 0.1$ , respectively.

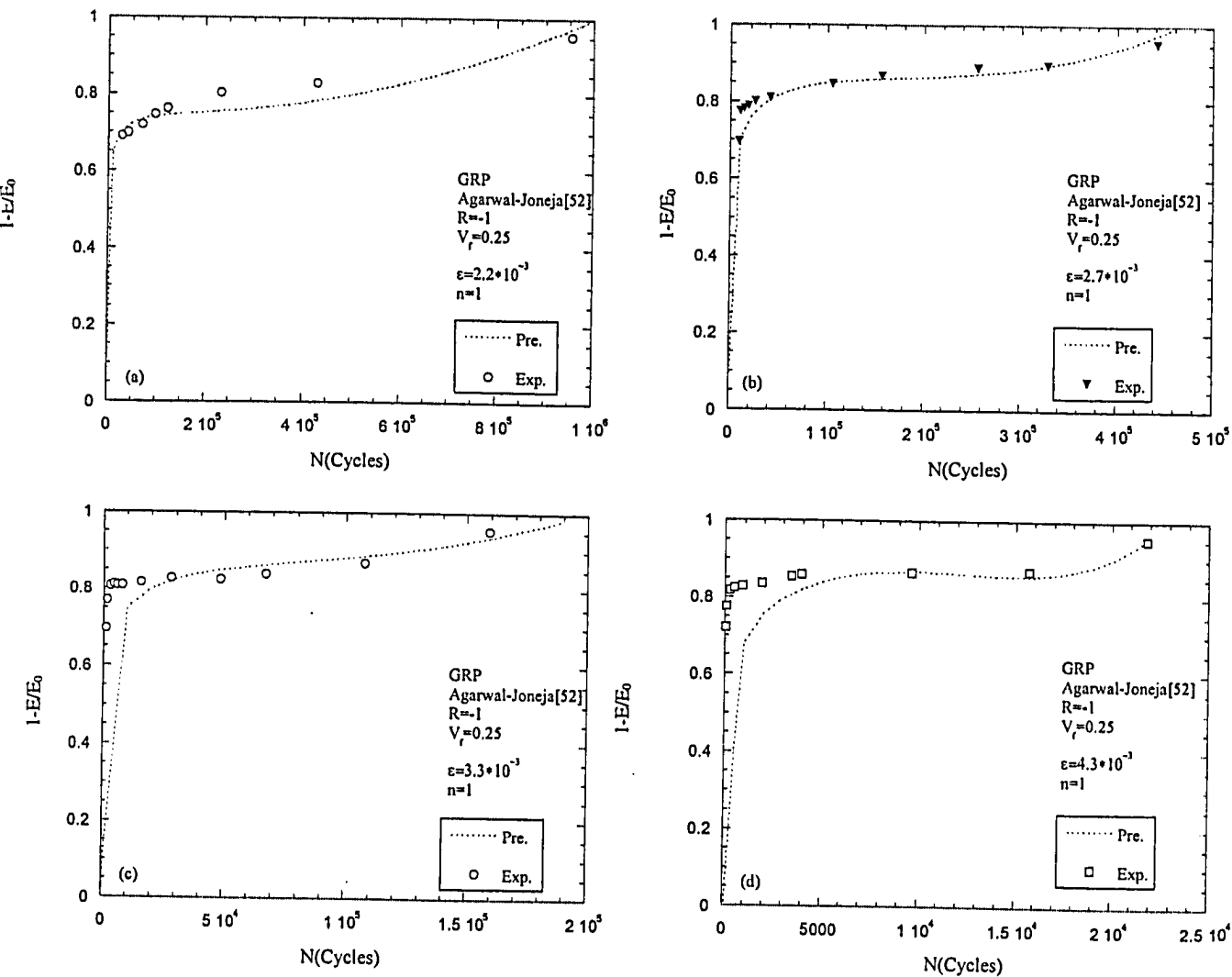
### 6.3.3 Variation of Damage Parameter for Transverse Direction ( $\theta=90^\circ$ )

Figure 6.10 is screening the results from implementing the  $f$  parameter for the transverse direction into the proposed equation. The experimental data are plotted against the proposed equation to demonstrate the correlation between them. Table 6.4 is outlining the values of  $n$  for this experimental case as well.



**Figure 6.9:** Variation of Damage parameter versus life for UD GRP composite, at different cyclic stress magnitude for various off-axis angles of (a)  $\theta=10^\circ$ , (b)  $\theta=75^\circ$ , (c)  $\theta=75^\circ$ , (d)  $\theta=75^\circ$  and (e)  $\theta=75^\circ$ .





**Figure 6.10:** Predicted damage-life cycles plotted versus experimental values of damage-life cycles for UD GRP composites tested under various cyclic strain magnitudes when off-axis angle and stress ratio are  $\theta = 90^\circ$  and  $R=-1$ , respectively, when strain magnitudes are (a)  $\epsilon=2.2 \times 10^{-3}$ , (b)  $\epsilon=2.7 \times 10^{-3}$ , (c)  $\epsilon=3.3 \times 10^{-3}$  and, (d)  $\epsilon=4.7 \times 10^{-3}$ .

## 6.4 Fatigue data and Properties of Cross-Ply GRP and CFRP Composites

To evaluate the fatigue damage analysis proposed in this study, fatigue data of cross-ply GRP and CFRP composites at various R-ratios and cyclic stress magnitudes have been taken from the literature and are presented in Appendix A. The available data are in the form of stiffness degradation (Young's modulus reduction) versus life or cycle ratio, required in the damage analysis.

### 6.4.1 Corum et al. Data

Corum et al. [57] have reported fatigue data for a 0/90° cross-ply consisting of continuous Thomel T300 fibers in a Baydur 420 IMR urethane matrix. A fatigue test has been performed at a stress ratio of  $R = -1$  on 0/90 cross-ply CFRP composite with a fiber volume fraction of 0.427. The carbon-fiber composite addressed here consists of 6K Thornel T300 continuous fibers in a urethane matrix. The material was supplied by ACC (Automotive Composites Consortium) in the form of  $610 \times 610 \times 3$ -mm-thick plaques.

Tensile fatigue tests have been performed at room temperature for specimens having the 0/90 fiber orientations. The stress ratio  $R$  was considered 0.1 in all fatigue tests. A dog-boned-shaped specimen was used. The frequency used varied with stress in accordance with the following relation, recommended by ACC:

$$f = (k \sigma_{uts})(\sigma_{max} - \sigma_{min}) \quad (5.1)$$

where  $k = 3\text{Hz}$ ,  $\sigma_{uts}$  is the ultimate tensile stress of the composite.

### 6.4.2 Daniel et al. Data

Daniel et al. [27] performed fatigue tests on AS4/3501-6 graphite/epoxy cross-ply composite laminates. Tensile fatigue tests have been performed at room temperature in

composite specimens having the [0/90] fiber orientations. The thickness of unidirectional ply has been reported as 0.0127 cm.

#### **6.4.3 Boniface and Ogin Data**

Fatigue tests were performed by Boniface and Ogin [58] on E-glass/epoxy [0/90] laminates with  $R = 0.1$ . These laminates are constituted of a  $90^\circ$  layer of 0.52 thickness between two  $0^\circ$  layers of 0.3 mm thickness, with a volume fraction of fibers approximately 58% for each layer. During fatigue tensile loading, the crack development is studied by Boniface and Ogin for two cyclic stresses 140 MPa and 95 MPa and  $R$  ratio of 0.1.

### **6.5 Variation of Damage Versus Life**

#### **6.5.1 Variation of Parameter $f$ for Plies of $0^\circ$ and $90^\circ$**

As discussed earlier, in the transverse direction ( $\theta = 90^\circ$ ), the number of fatigue cycles has no or very little effect on the parameter  $f$  and the value of  $f$  stays nearly unchanged at close to zero.

In addition to this, the damage analysis results reported in Subramanian et al. [44] indicate that there is very little interfacial damage in the  $0^\circ$  ply of the cross-ply laminate. With this in mind, it is assumed that the matrix-fiber interfacial efficiency parameter,  $f$ , doesn't vary under fatigue loading in experimented cross-ply laminates and stays equal to unity.

## 6.5.2 Variation of Damage Parameter

Results of stiffness drop and fatigue damage have been presented in this section. It has been proved that by using the experimentally determined S-N curve for  $0^\circ$  and  $90^\circ$  laminates the stiffness degradation and fatigue life of cross-ply laminates can be predicted. Available data through literatures [27,57,58] have been used to verify the presented damage model. The dashed line in Figures 6.11-6.15 represents the response of damage model developed in this study and shows how close are the predicted damage curves with damage values obtained from experiments. The parameters  $n$  and  $\eta$  are also tabulated for each case of experimental data, in Table 6.5.

The modified damage Equation (4.25) successfully reflects mechanical properties of fiber, matrix and interface bonding of composite laminates in  $0/90$  degree direction, and holds terms for stress ratio and cyclic stress magnitude.

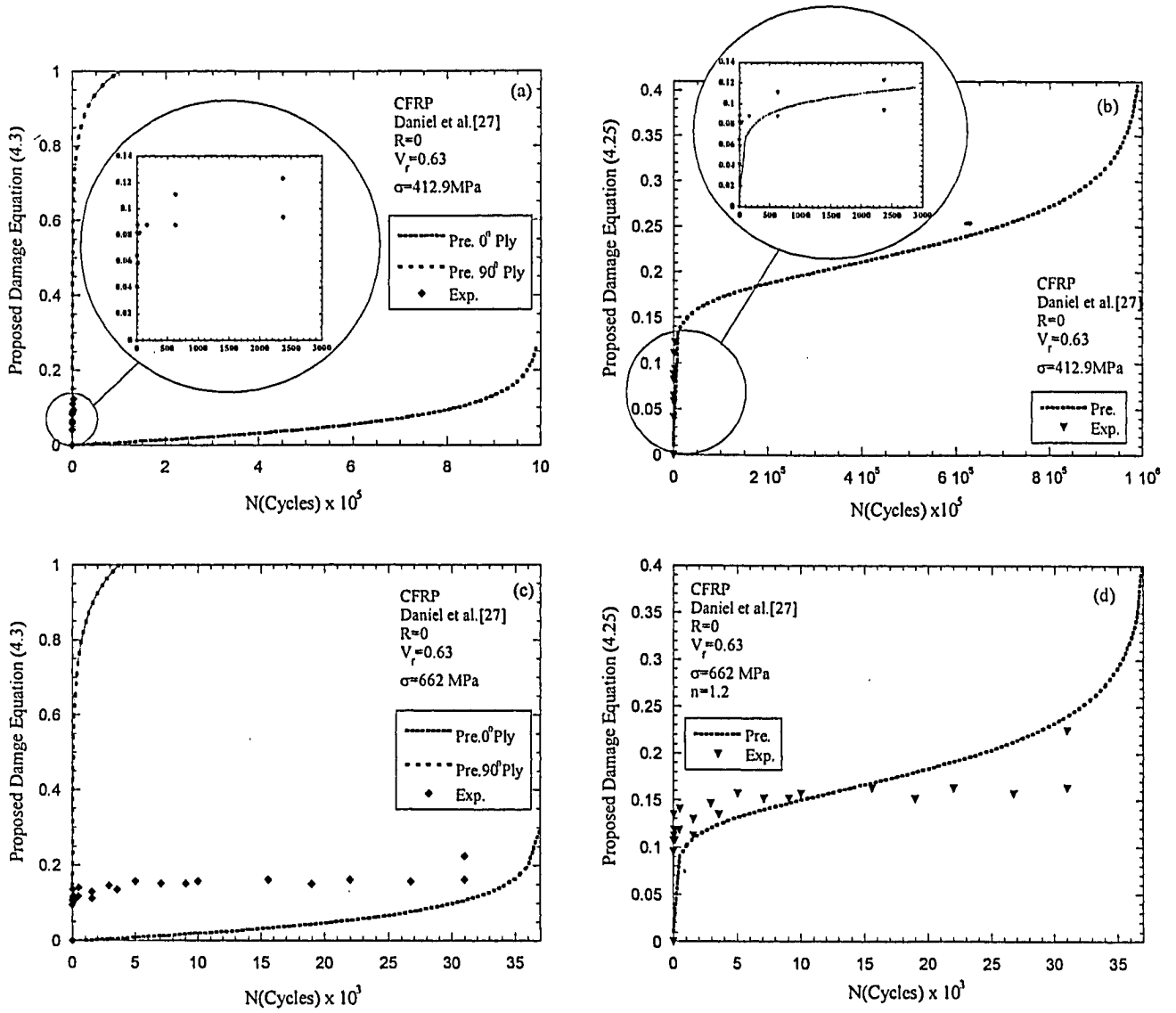
It is also noticed that stiffness reduction mostly occurs during the first 10% of the life of the laminate. During this stage, the crack density increases in the  $90^\circ$  ply. Transverse cracking in the  $90^\circ$  ply results in local stress redistribution in the laminate, with the  $0^\circ$  ply carrying additional load. By considering the damage equation for the  $90^\circ$  ply this phenomena can be implemented into the damage of cross-ply composite. Reaching to this point, so called characteristic damage state in cross-ply composite materials, no additional cracks would be expected to form. Subsequent to the saturation of transverse matrix cracking, the entire load is carried by the  $0^\circ$  ply in the laminate, and the laminate behaves like a  $0^\circ$  ply. Here is when the contribution of damage equation coincided from this ply can be injected into the damage of cross-ply laminate. The delamination, which runs between the  $0/90^\circ$  interfaces, is observed between the two stages of CDS (Characteristic Damage State) and ADV (Advance Damage Development) which develops in cyclic loading subsequent to the development of the CDS [59].

Transverse cracks in the formation of the delamination are that of an aid but not a primary driver. The dominant structures aside from the transverse cracks are longitudinal cracks that are enough evidence to combine only the damage from two stages (stage I and stage III) to predict the damage of the cross-ply laminate. Stage II of damage development exhibits some longitudinal cracks hence the formation of transverse cracks

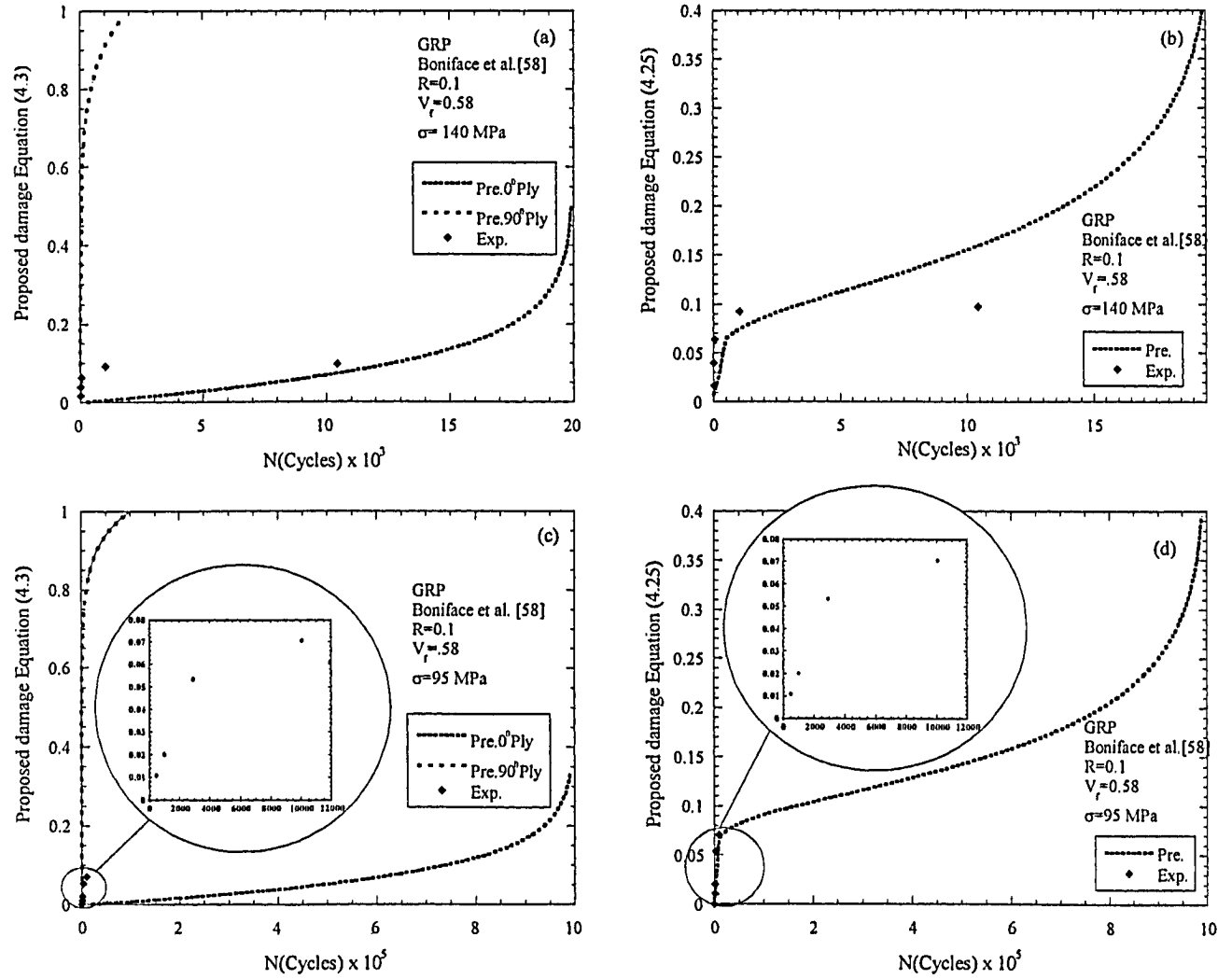
is complete at the beginning of stage II and the other damage modes are only moderately active at this stage, longitudinal cracking predominates. The Figures 6.1-6.5 in this section demonstrates the comparison between the damage equation and the experimental data extracted from the literatures [27,57,58]. In Figure 6.11-6.15, graphs with “b” and “d” notations are damage separately in 0° and 90° plies versus life aside with experimental data. It can be clearly noticed that the damage parameter related to experimental data of cross-ply laminate sits between the damage parameters of 90° at the top and the graph for 0° at the bottom. It is well known that the damage in longitudinal laminate (0° laminate) is much lower than the cross-ply of [0/90] and laminate of 90°. Also graphs with “a” and “c” notations are the one shows the combined graphs of 0/90 degree as the graph predicts the cross-ply damage compared with the experimental data, which also shows very well their agreements.

**Table 6.5:** Variation of  $n$  and  $\eta$  for various cross-ply CFRP and GRP composites.

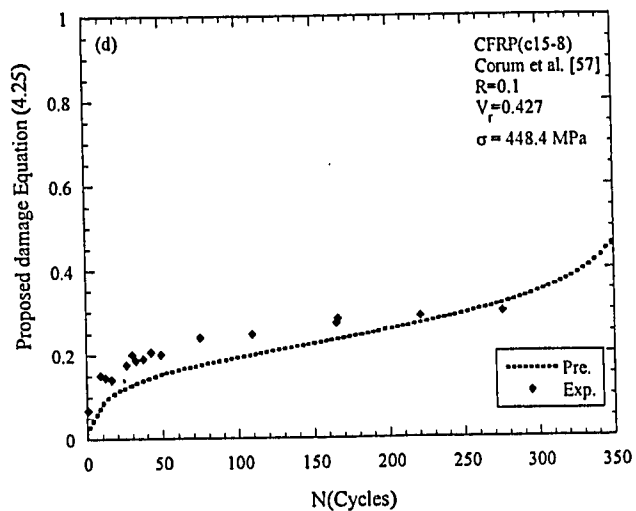
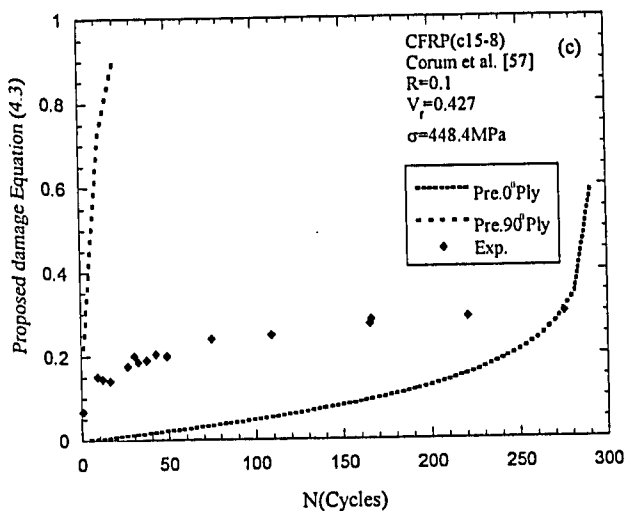
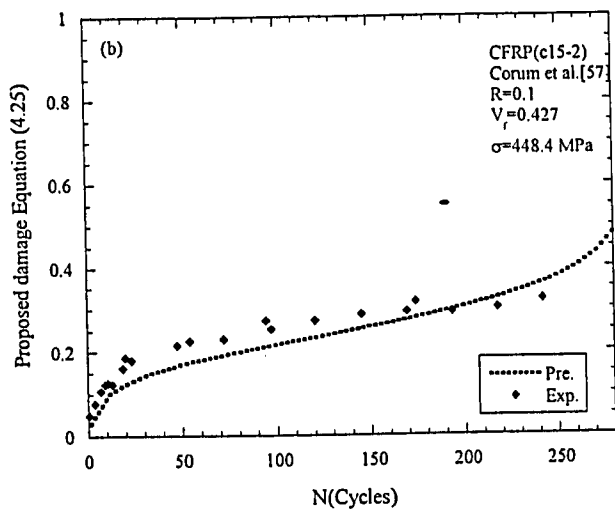
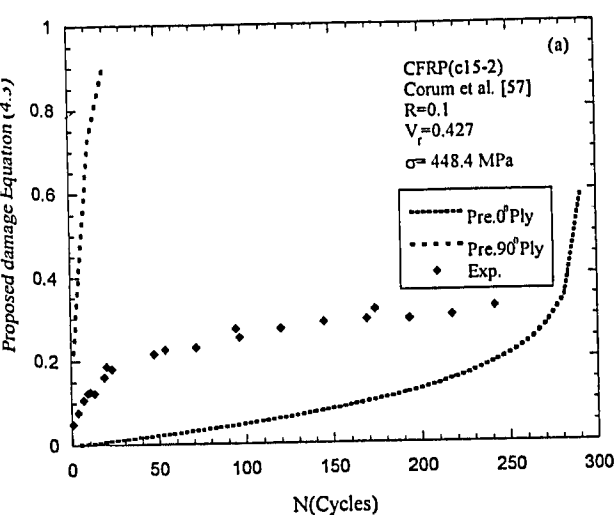
Materials		Stress level (MPa)	R-ratio	$\eta$	$n$
GRP [0/90]		95	0.1	0.1	1
Boniface		140	0.1	0.1	2
CFRP [0/90] Corum	C15-2	448.2	0.1	0.3	1.25
	C15-8	448.2	0.1	0.25	1.25
	C15-3	424.8	0.1	0.4	1.2
	C15-20	424.8	0.1	0.4	1.2
	C15-4	402.9	0.1	0.4	1
	C15-21	402.9	0.1	0.03	1
CFRP [0/90]		412.9	0	0.2	1
Daniel		662	0	0.15	1.2



**Figure 6.11:** (a) Proposed damage of 0° and 90° plies versus experimental values of damage-life tested under 412.9MPa cyclic stress (b) Proposed damage of 0/90 degree cross-ply and experimental values of damage-life tested under 412.9MPa cyclic stress (c) Proposed damage of 0° and 90° plies versus experimental values of damage-life tested under 662MPa cyclic stress (d) Proposed damage of 0/90 degree cross-ply and experimental values of damage-life tested under 662MPa cyclic stress.

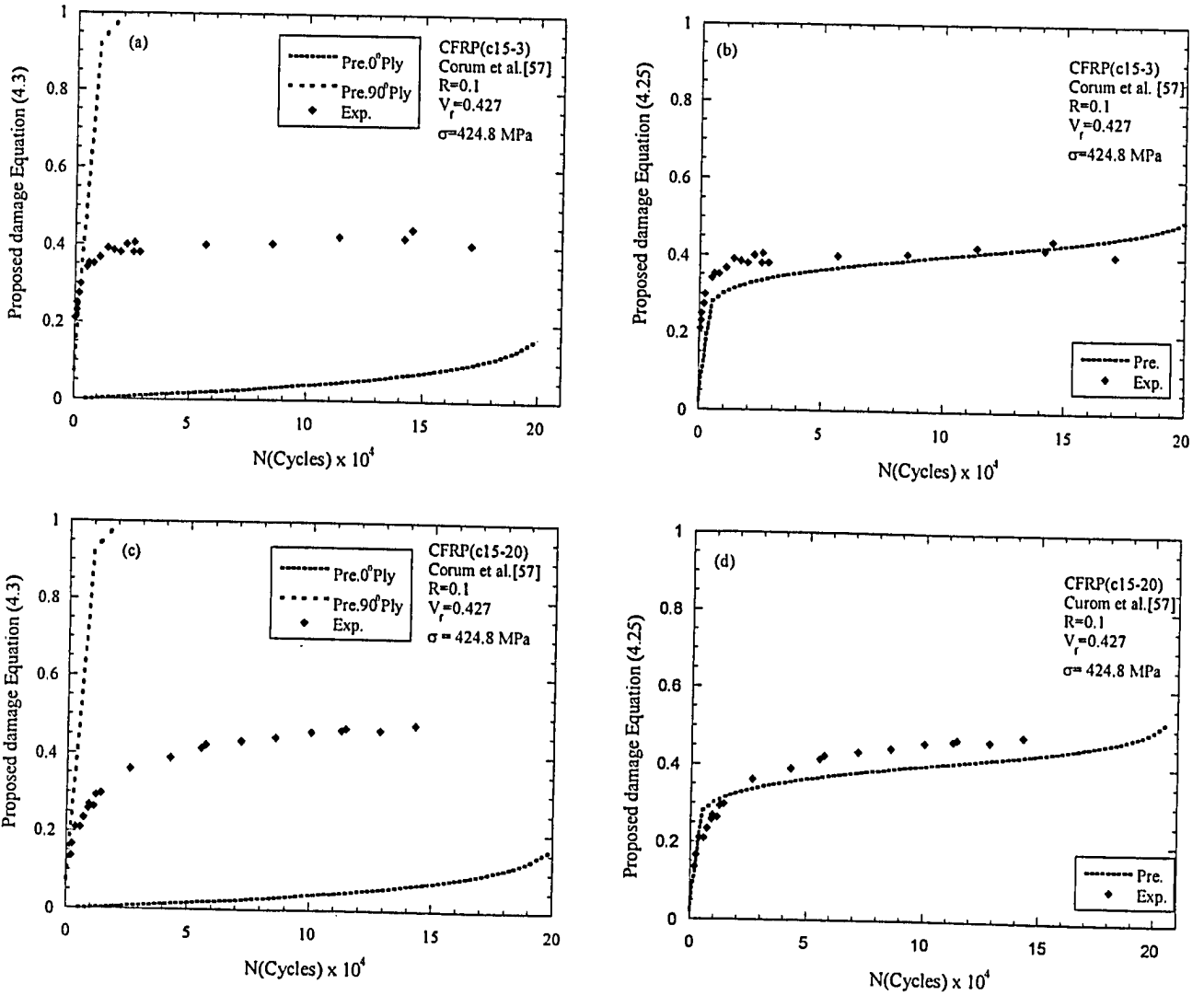


**Figure 6.12:** (a) Proposed damage of  $0^\circ$  and  $90^\circ$  plies versus experimental values of damage-life tested under 140 MPa cyclic stress (b) Proposed damage of 0/90 degree cross-ply and experimental values of damage-life tested under 140 MPa cyclic stress (c) Proposed damage of  $0^\circ$  and  $90^\circ$  plies versus experimental values of damage-life tested under 95 MPa cyclic stress (d) Proposed damage of 0/90 degree cross-ply and experimental values of damage-life tested under 95 MPa cyclic stress.

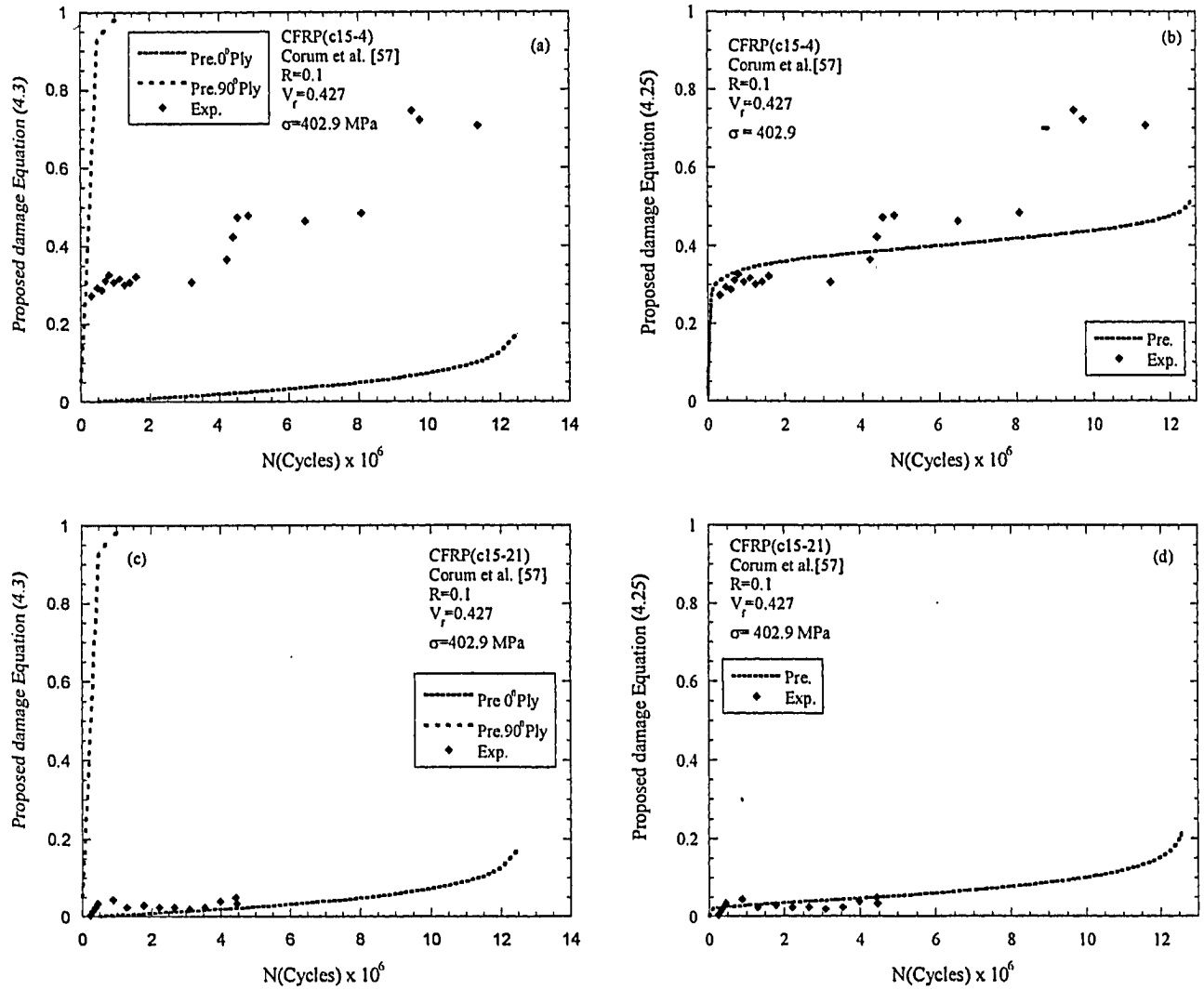


**Figure 6.13:** (a) and (c) Proposed damage of 0° and 90° plies versus experimental values of damage-life tested under 448.4 MPa cyclic stress (b) and (d) Proposed damage of 0/90 degree cross-ply and experimental values of damage-life tested under 448.4 MPa cyclic stress.





**Figure 6.14:** (a) and (c) Proposed damage of 0° and 90° plies versus experimental values of damage-life tested under 424.8 MPa cyclic stress (b) and (d) Proposed damage of 0/90 degree cross-ply and experimental values of damage-life tested under 424.8 MPa cyclic stress.



**Figure 6.15:** (a) and (c) Proposed damage of 0° and 90° plies versus experimental values of damage-life tested under 402.9 MPa cyclic stress (b) and (d) Proposed damage of 0/90 degree cross-ply and experimental values of damage-life tested under 402.9 MPa cyclic stress.

6.6 Variation of Interfacial Efficiency Factor

Figure 6.16 shows the variation of the efficiency factor  $f$  versus life using FEM and the experimental analysis. A very good correlation can be observed from these graphs. Table 6.6 compares and verifies the results for parameter  $\alpha$  which is mathematically defined at  $N=1$ , and  $f$  which represents the interfacial efficiency factor.

Table 6.6: Variation of  $\alpha$  and  $f$  for GRP composite data with on-axis loading direction ( $\theta = 0^\circ$ )

	R ratio	$\sigma_{app}$ (MPa)	$\alpha_{Exp.}$	$\alpha_{FEM}$	$f_{Exp.}$	$f_{FEM} = \frac{U_f}{U_m}$
GRP Philippidis	-1	120	0.806	0.84	0.89-0.49	0.82-0.86
CFRP Plumtree	0.1	1306	0.83	0.82	0.85-0.79	0.85-0.86

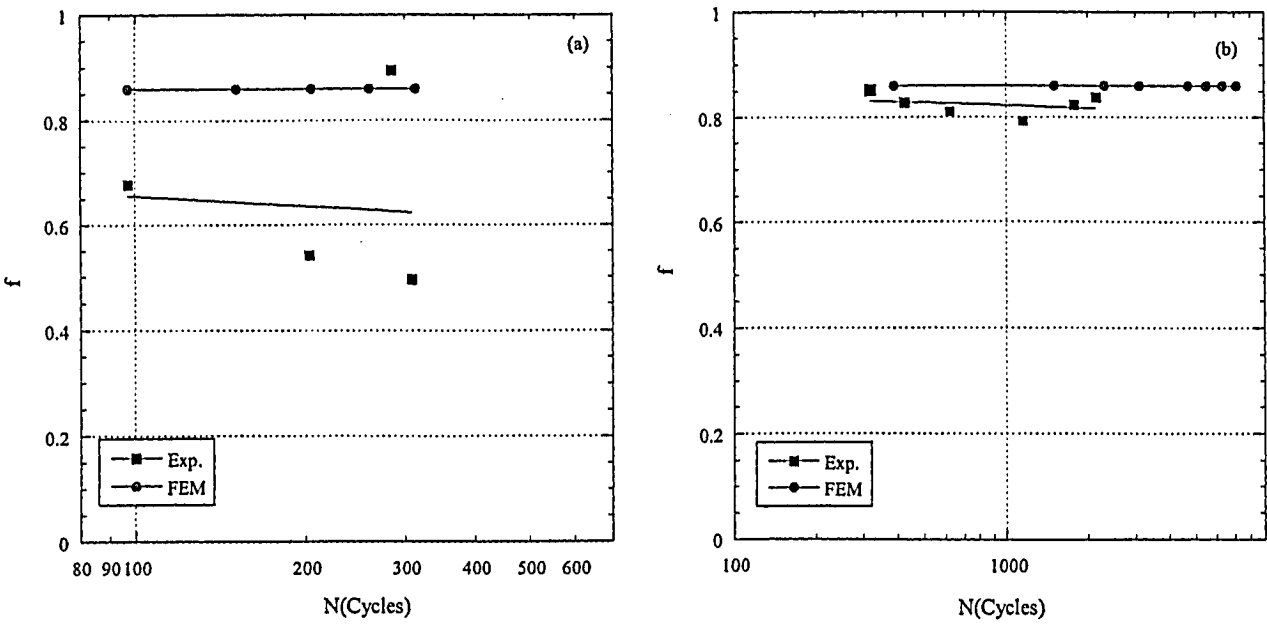


Figure 6.16: Comparison of Interfacial efficiency factor versus life in logarithmic scale for cyclic loads of (a)  $\sigma_a=120\text{MPa}$ , (b)  $\sigma_a=1.306 \text{ GPa}$ , during region II of the damage.

## CHAPTER SEVEN

### Discussion of Results

To predict the fatigue life of composite structures under cyclic loading a cumulative damage model seems a necessity. Researchers have done some work on cumulative damage models both experimentally and analytically [5,18,22]. If the Palmgren-Miner rule (P-M rule) is used for fiber-reinforced plastics (FRP) under cyclic loading, the results of such models show that these predictions are usually not satisfactory. Therefore, a new cumulative damage equation has been developed, e.g., models based on the equivalent damage for multi-stress level loading, models on residual life, models on residual strength, non-linear cumulative damage models, and so forth. Although all these models have some advantages over the P-M rule for the predictive capability, they do not take into account the damage development in the FRP during cyclic loading. The present study attempts to develop a new cumulative-damage model for unidirectional FRP composites based on the consideration of factors affecting the accumulated damage in FRP composites.

The proposed damage analysis in this study takes into account the three regions of the damage development based on physics and the mechanism of cracking in the matrix, the matrix-fiber interface and the fiber. This equation is capable of damage assessment in unidirectional GRP and CFRP composites due to its important damage variables in the on-axis and off-axis loading directions. The proposed damage parameter is not restricted to specific loading conditions (loading direction, stress level, and stress ratio). Stress analysis and damage estimation are the two major components needed for calculating material property degradation.

Utilizing the stresses of each ply, the state of damage is estimated using a normalized damage technique. Then, stiffness degradation is determined using material property degradation rules. Predictions from this model are in good agreement with the experimental data. The proposed damage equation also has a parameter “ $f$ ” to describe the influence of the interfacial shear strength and interfacial efficiency. The parameter  $f$

varies between zero and unity and is a function of number of cycles. The parameter  $f$  consists of a coefficient that is dependent of composite constituents and interfacial strength. The interfacial efficiency determines how strong the interfacial bonding is and how efficient the load is transferred from the matrix to the fiber.

The proposed damage equation in this study also includes terms to take into account the effects of off-axis angle  $\theta$ , mean stress (or R-ratio) on the damage assessment of UD FRP composites.

This section evaluates the proposed damage analysis based on several sets of FRP fatigue data taken from the literature and compares the proposed model with earlier developed fatigue damage models.

This section aims to evaluate and compare the proposed damage model with previously developed fatigue theories for FRP composites. To achieve a quantitative damage assessment, fatigue models by Ramakrishnan- Jayaraman [22] and Philippidis-Vassilopoulos [5] will be examined here. Comparison of fatigue damage assessment based on these models and the proposed equation in this study over several sets of fatigue data on unidirectional GRP and CFRP composites with various off-axis angles and R-ratios will show how capable the proposed equation is in fatigue damage correlation of unidirectional fibrous composites.

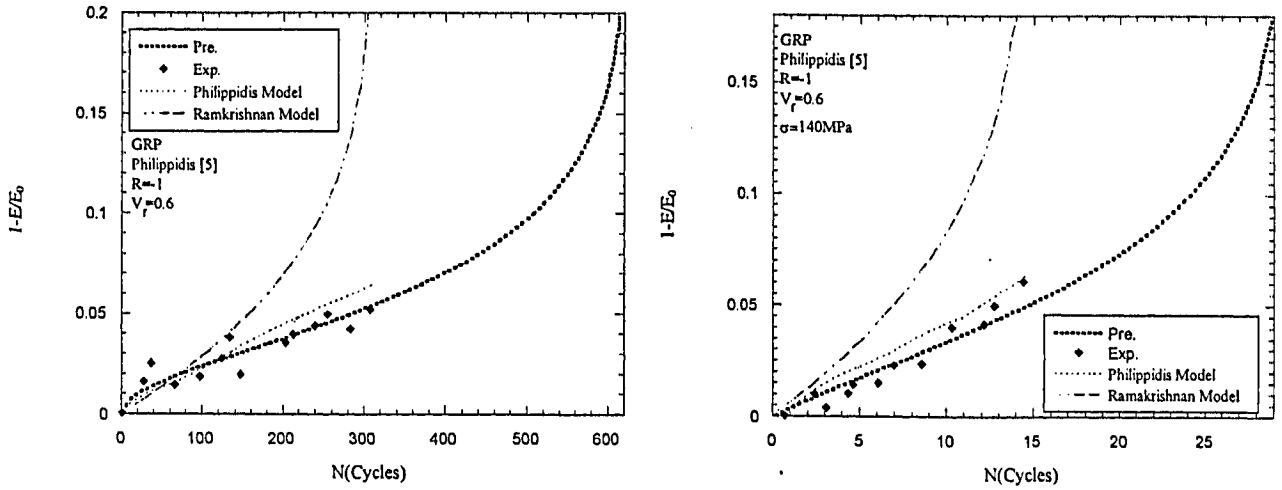
## **7.1 Fatigue Damage Evaluation for GRP Composites**

### **7.1.1 Philippidis-Vassilopoulos GRP Data ( $\theta=0^\circ$ )**

The empirical model of Philippidis and Vassilopoulos [5] was employed to assess the fatigue data of UD GRP composites. Figure 7.1 presents a comparison between predicted damage-fatigue cycles diagrams and experimentally obtained damage-fatigue cycle data for UD GRP composites tested under various cyclic stress magnitudes and off-axis angle  $\theta = 0^\circ$  and stress ratio of  $R = -1$ . This figure shows that predicted damage curve based on the proposed damage analysis in this study is in a very close agreement with experimental

data, while predicted curves by Philippidis-Vassilopoulos, Ramakrishnan-Jayaraman are found in less agreement with experimental values.

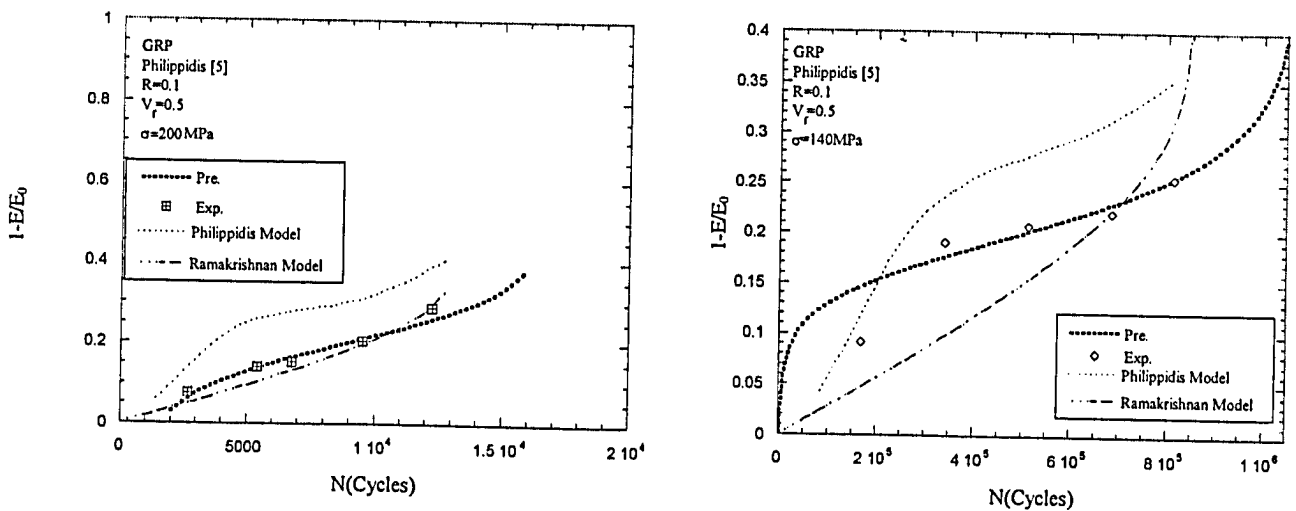
Figure 7.2 also presents a very good agreement of the proposed model with experimental data for UD GRP ( $\theta=0^\circ$ ) tested at various cyclic stress magnitudes of 150 MPa and 200 MPa with stress ratio of  $R=0.1$ . In this figure, the Philippidis- Vassilopoulos model presents an up bound and the Ramakrishnan-Jayaraman model correspond to a lower bound when compared with experimental data.



**Figure 7.1:** Comparison between predicted damage-life cycles plotted versus experimental values of damage-life cycles for UD GRP composites tested under various cyclic stress magnitudes when off-axis angle and stress ratio are  $\theta= 0^\circ$  and  $R=-1$ , respectively.

### 7.1.2 Philippidis-Vassilopoulos GRP Data ( $\theta=75^\circ$ )

Figure 7.3 represents the prediction of fatigue damage progress of UD GRP composites with off-axis angle  $\theta=75^\circ$  as number of cycles increases. This figure shows fatigue response of GRP composites tested at various stress magnitudes of 25, 35, 40, and 45MPa with a stress ratio of  $R=0.1$ . The proposed model prediction curve shows a very

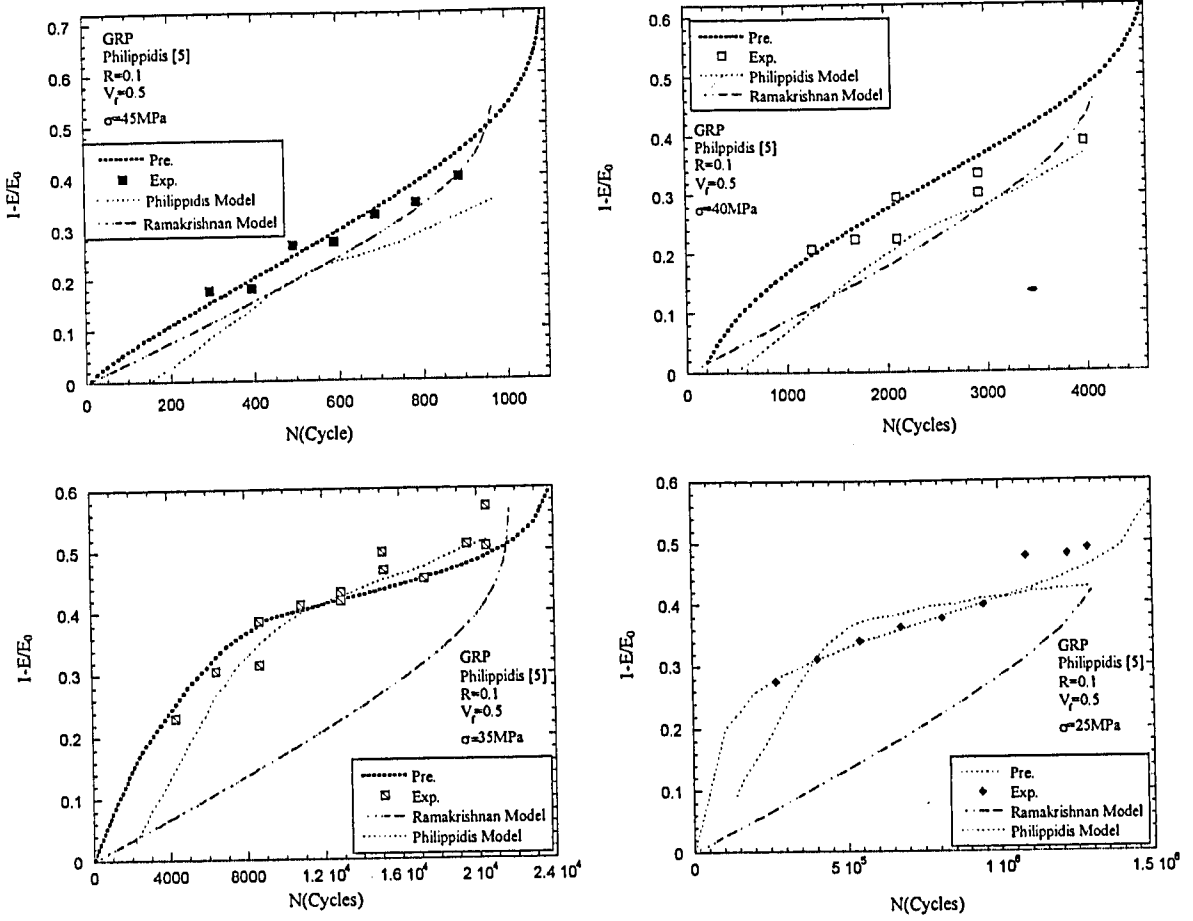


**Figure 7.2:** Comparison between predicted damage-life cycles plotted versus experimental values of damage-life cycles for UD GRP composites tested under various cyclic stress magnitudes when off-axis angle and stress ratio are  $\theta=0^\circ$  and  $R=0.1$ , respectively.

good agreement with experimental fatigue data of various stress magnitudes. In cyclic stress magnitudes of 25, 35 and 40 Mpa, the Philippidis model may present the next best prediction. Ramakrishnan's model shows slightly better response as compared with Philippidis at a stress magnitude of 45 MPa

### 7.1.3 Agarwal- Joneja GRP Composite Fatigue Data ( $\theta=0^\circ$ )

Agarwal- Joneja [52] have performed several fully reversed fatigue tests on UD GRP composite specimens ( $\theta=0^\circ$ ) for different cyclic strain amplitudes of 0.77% and 0.88%. The fiber volume fraction in this material was  $V_f=25\%$ . Figure 7.4 presents the experimental data of Agarwal-Joneja and the predicted curves based on Ramakrishnan's damage model and the model proposed in this study. The comparison of predicted curves with experimental data shows a higher degree of correlation of the proposed damage equation over Ramakrishnan's.

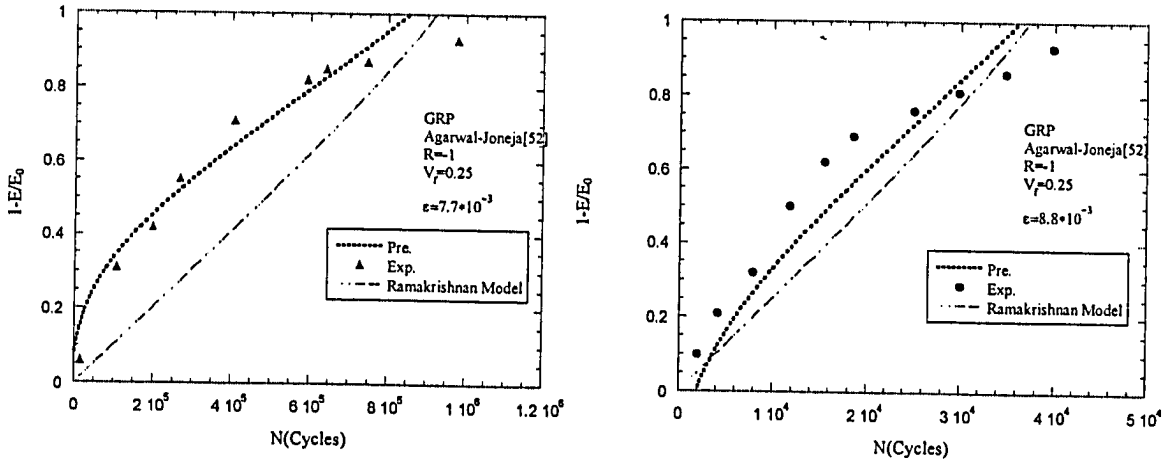


**Figure 7.3:** Comparison between predicted damage parameter versus life for UD GRP composite, at different cyclic stress magnitude for off-axis angle of  $\theta=75^\circ$  and stress ratio of  $R=0.1$ .

#### 7.1.4 Pauchard and Oever GRP Composite Fatigue Data ( $\theta=0^\circ$ )

Pauchard et al. [53] and Oever-Peijis [56] have performed fatigue tests on UD GRP composite specimens ( $\theta=0^\circ$ ) respectively under cyclic strain amplitude of 0.14% and a cyclic stress amplitude of 400 MPa. The fiber volume fraction in Pauchard's material was  $V_f=55\%$ , while GPR specimens tested by Oever contained 50% fiber. Pauchard's fatigue tests performed with a stress ratio of  $R=0.7$  and Oever's tests contained a stress ratio of  $R=0.1$ .



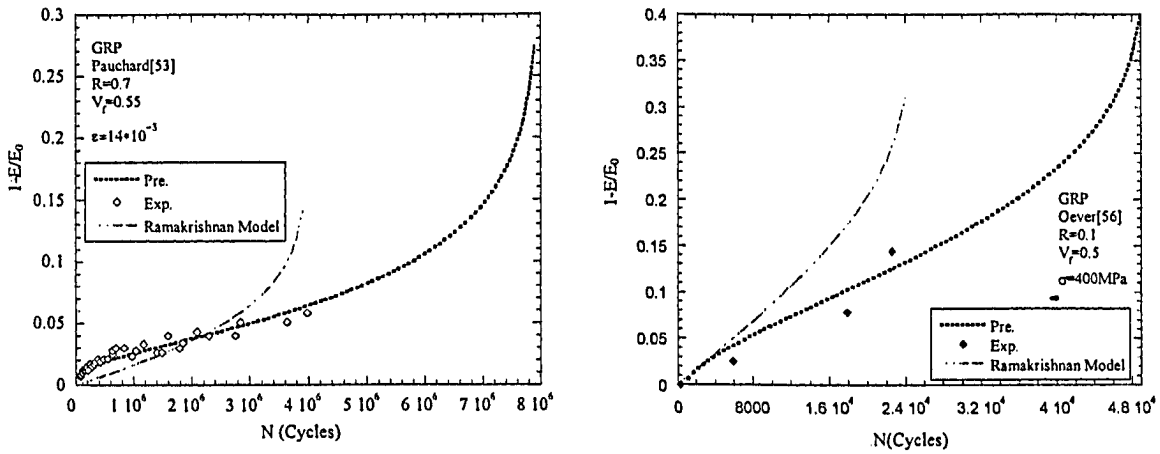


**Figure 7.4:** Comparison between predicted damage-life cycles plotted versus experimental values of damage-life cycles for UD GRP composites tested under various cyclic strain magnitudes when off-axis angle and stress ratio are  $\theta= 0^\circ$  and  $R=-1$ , respectively.

Figure 7.5 presents the experimental data of Pauchard and Oever and the predicted curves based on Ramakrishnan's damage model and the model proposed in this study. The comparison of predicted curves with experimental data shows a higher degree of correlation of the proposed damage equation over Ramakrishnan's.

#### 7.1.5 Agarwal- Joneja GRP Composite Fatigue Data ( $\theta=90^\circ$ )

Agarwal- Joneja [52] have performed several fully reversed fatigue tests on UD GRP composite specimens ( $\theta=90^\circ$ ) for different cyclic strain amplitudes of 0.22, 0.27, 0.33, and 0.43%. The fiber volume fraction in this material was  $V_f=25\%$ . Figure 7.6 presents the experimental data of Agarwal-Joneja and the predicted curves based on Ramakrishnan's damage model and the model proposed in this study. The comparison of predicted curves with experimental data shows a higher degree of correlation of the proposed damage equation over Ramakrishnan's.

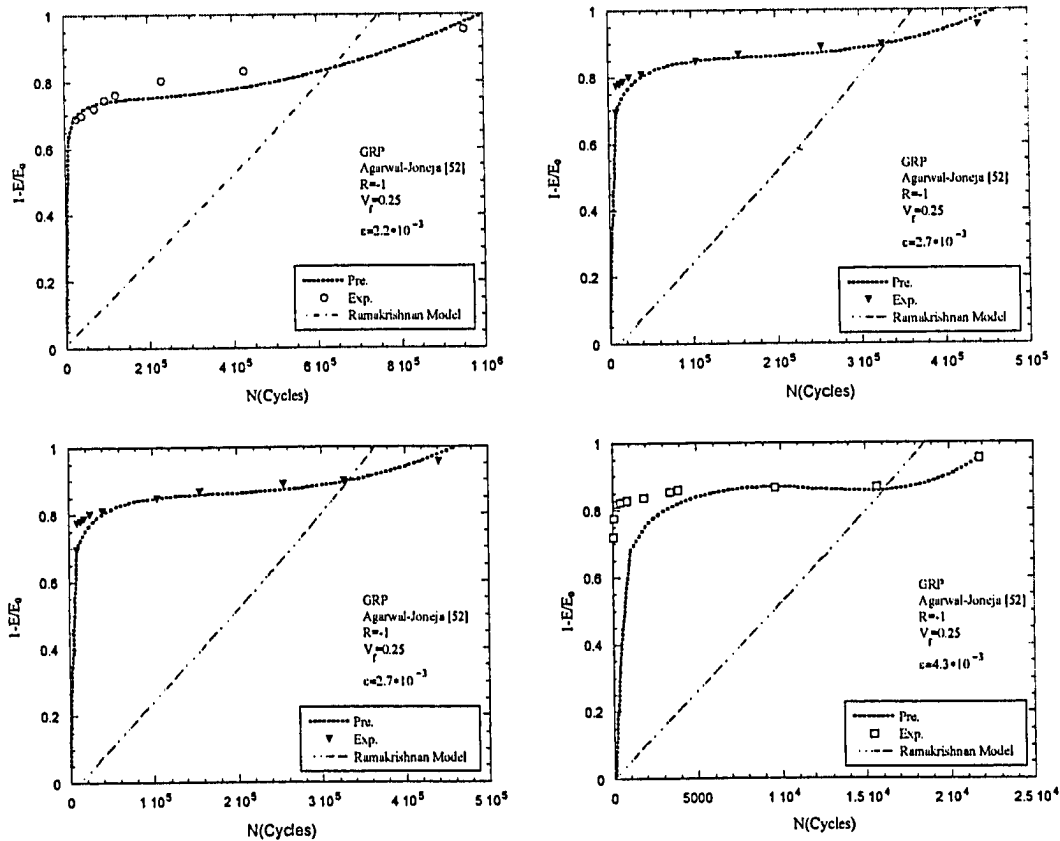


**Figure 7.5:** Comparison between predicted damage-life cycles plotted versus experimental values of damage-life cycles for UD GRP composites tested under various cyclic stress/strain magnitudes when off-axis angle and stress ratios are  $\theta=0^\circ$  and  $R=0.1, 0.7$ , respectively.

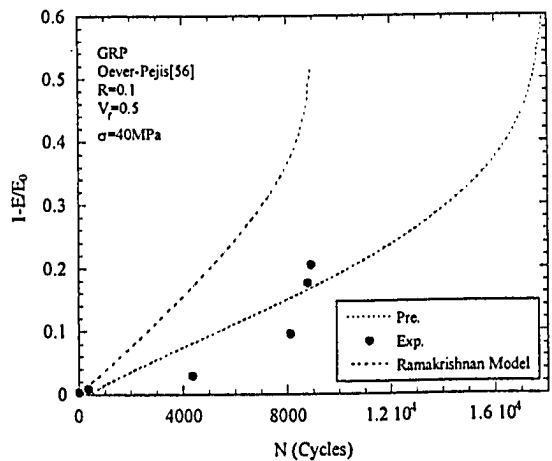
As it is depicted in Figure 6.6, for all strain magnitudes the slope of proposed damage model in Stage II is nearly zero and is in a good agreement with experimental data. This may suggest that the parameter  $f$  in the proposed damage equation is very close to zero and the interfacial shear strength at  $(\theta = 90^\circ)$  is weak. This response is not evident based on Ramakrishnan's approach.

#### 7.1.6 Oever GRP Composite Fatigue Data ( $\theta=10^\circ$ )

Oever-Peijis [56] have performed fatigue tests on UD GRP composite specimens ( $\theta=10^\circ$ ) under a cyclic stress magnitude of 40 MPa. The fiber volume fraction in the GRP specimen tested by Oever contained 50% fiber. Oever's fatigue test contained a stress ratio of  $R = 0.1$ . Figure 7.7 presents the experimental data of Oever and the predicted curves based on Ramakrishnan's damage model and the model proposed in this study. The comparison of predicted curves with experimental data shows a higher degree of correlation of the proposed damage equation over Ramakrishnan's.



**Figure 7.6:** Comparison between predicted damage-life cycles plotted versus experimental values of damage-life cycles for UD GRP composites tested under various cyclic strain magnitudes when off-axis angles and stress ratio are  $\theta = 90^\circ$  and  $R = -1$  respectively.

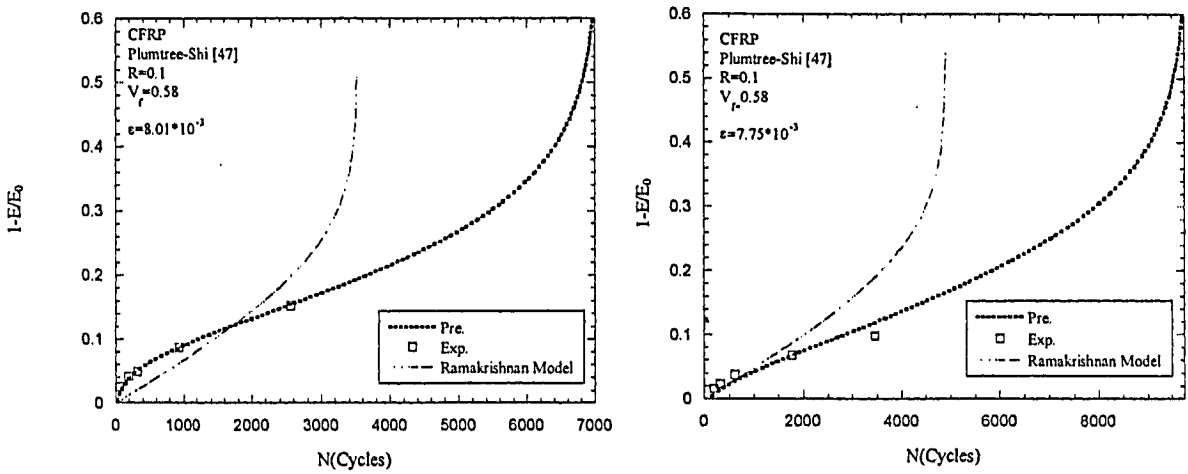


**Figure 7.7:** Comparison between predicted damage-life cycles plotted versus experimental values of damage-life cycles for UD GRP composites tested under cyclic stress magnitudes when off-axis angle and stress ratio are  $\theta= 10^\circ$  and  $R=0.1$ , respectively

## 7.2 Fatigue Damage Evaluation for CFRP Composites

### 7.2.1 Plumtree-Shi CFRP Composite Fatigue Data ( $\theta=0^\circ$ )

Plumtree-Shi [16] has performed several fatigue tests on UD CFRP composite specimens ( $\theta=0^\circ$ ) for different cyclic strain amplitudes of 0.775 and 0.801%. The fiber volume fraction in this material was  $V_f=58\%$ . Figure 7.8 presents the experimental data of Plumtree-Shi and the predicted curves based on Ramakrishnan's model and the damage model proposed in this study. The comparison of predicted curves with experimental data shows a higher degree of correlation of the proposed damage equation over Ramakrishnan's.



**Figure 7.8:** Comparison between predicted damage-life cycles plotted versus experimental values of damage-life cycles for UD CFRP composites tested under various cyclic strain magnitudes when off-axis angle and stress ratio are  $\theta= 0^\circ$  and  $R=0.1$  respectively.

## **CHAPTER EIGHT**

### **Conclusion and Recommendations**

#### **8.1 Conclusions**

The characteristics of damage accumulation in unidirectional GRP and CFRP composite materials have been studied. The experimental results of earlier studies in damage growth show that there are three different regions during the damage evolution in composites under fatigue loading. Region I involves the cracking mechanism and damage progress in the matrix, the matrix-Fiber interface in Region II and the Fiber in Region III. The total damage parameters in unidirectional GRP and CFRP were calculated by damage accretion in the three regions (I, II, and III). The damage parameter was proposed to capture the characteristics of damage growth in composite materials subject to fatigue loading based on the corresponding stiffness reduction of composite laminate as the number of cycles progresses.

The proposed fatigue damage model successfully correlated fatigue damage of unidirectional GRP and CFRP composites at different  $\theta$ , R-ratio and different loading levels. The results of fatigue damage assessment revealed that the proposed damage equation correlated the data with a higher degree of success as compared with fatigue damage developed by Ramakrishnan [22] and Philippidis [5]. Several experimental data series of GRP and CFRP composites were taken from the literature and have been used to evaluate the proposed damage model. Results of the prediction of fatigue damage as the number of cycles increases showed a very good agreement between the proposed model and the experimental data. The proposed damage equation has also shown a higher degree of success in correlating experimental damage data as compared with other earlier developed damage models.

Further, it has been found that, for laminates of a [0/90] cross-ply composite under cyclic load, the relationship between stiffness drop and number of cycles also exhibits three distinct regions. Results of the prediction of fatigue damage as the number of cycles increases showed a very good agreement between the proposed equation and the experimental data. Based on the present study, the fatigue performance of any [0/90] cross-ply laminate can be evaluated from the present model, knowing the fatigue behavior of unidirectional laminates in both axial and transverse directions. The superiority of this damage model over other models is that it includes the parameter  $R$ , mean stress, number of cycles to failure, off-axis angle  $\theta$  and  $f$  parameter as bonding principle, as well as the physics of cracking in micro-constituents of cross-ply.

The present study also has provided an analysis of the interface crack problem in continuous fiber reinforced polymer matrix composites. The finite element mesh has been formed for a cylindrical element of the matrix with a single fiber. A ring-shaped crack was assumed between fiber and matrix. A finite element approach was developed to employ the fatigue damage model in ANSYS 8.0 Education Version software that proves to be capable of simulating the observed experimental results. Variation of the efficiency factor  $f$  versus life was found in a consistent and good agreement when evaluating both FEM analysis and experimental values.

## 8.2 Recommendations

Further modeling of the fatigue damage accumulation is useful in several aspects. Parametric simulation can be undertaken to elucidate the interaction of constituent properties in fatigue degradation, which could provide valuable insight for micro structural tailoring for optimal fatigue performance. More specifically, the presented damage assessment could be generalized to embrace the behavior of the cross-ply composite laminate under various stacking and complicated fatigue load. Calibration of such a model by more experimental data would hopefully validate the model and characterize the microstructural properties and damage behavior of constituents in a composite framework.

Finally, vital attempts to extend the models for service applications are legitimate. In a distant perception, this should include multidirectional laminates, variable amplitude loading, elevated temperature, and environmental fatigue, variable frequency which all influences the fatigue behavior of composite material when used in real application.

## REFERENCES

1. Sendeckyj G.P., Life prediction for resin-matrix composite materials. In: Reifsnider K.L, editor. *Fatigue of Composite Materials*, Composite Materials Series, 4. Elsevier, 1991.
2. Highsmith A.L., Reifsnider K.L, Stiffness reduction mechanisms in composite laminates. In: Reifsnider KL, editor. *Damage in Composite Materials*, ASTM STP 775. American Society for Testing and Materials, pp.103–17, 1982.
3. Talreja R., *Fatigue of Composite Materials*. Lancaster Pennsylvania: Technomic, 1987.
4. Andersen S.I., Brondsted P., Lilholt H., Fatigue of polymeric composites for wing blades and the establishment of stiffness-controlled fatigue diagrams In: *Proceedings of 1996 European Union Wind Energy Conference*, Gutenberg Sweden, pp.950–53, 20–24 May 1996.
5. Philippidis T.P., Vassilopoulos A.P., Fatigue design allowable for GRP laminates based on stiffness degradation measurements, *Composites Science and Technology*, 60, pp.2819-2828, 2000.
6. Middleton D.H., *Composite materials in aircraft structures*. Longman Scientific & Technical, New York, J. Wiley, 1990.
7. Jones R.M., *Mechanics of composite materials*. Ann Arbor, MI: Edwards Brothers; 1999.
8. Croquette, Potential Applications of Composites Offshore, *Proc. Of Composite Materials in the Petroleum Industry*, Institut Français du Pétrole, November 3-4, 1994.
9. Gibson A.G., *Composites in Offshore Structures*, Chapter 3 of *Composite Materials in Maritime Structures*, Volume 2, eds: R. A. Shenoi, J. F. Wellicome, Cambridge Ocean Technology Series, 1993.
10. Wang S.S., Williams J.G. and Lo K.H. (eds.), *Proceedings of Composite Materials for Offshore Operations*, Houston TX 77060, 2000.
11. Stringfellow W.D. (ed.), *Fiberglass Pipe Handbook*, Fiberglass Pipe Institute, 355 Lexington Ave., New York 10017, 1992.



12. ISO/DIS 14692-1, Petroleum and natural gas industries - Glass reinforced (GRP) piping – Parts 1-4, 2000.
13. ASTM 2992-96e1, Standard Practice for Obtaining Hydrostatic or Pressure Design Basics for “Fiberglass” (Glass-Fiber-Reinforced Thermosetting-Resin) Pipe and Fittings.
14. ISO 109281: Plastics pipe systems – glass reinforced thermosetting plastic (GRP) pipes and fittings – methods of regression analysis and their use, 1997.
15. Anisdahl L., Wang D.T., Stokke R., Composite Materials for Offshore Operations-2, Eds. S.S. Wang, J.G. Williams and K.H. Lo, American Bureau of Shipping, Houston TX 77060, ISBN 0-943870-01-1. pp 261-274, 1999.
16. BS 4994: Design and Construction of Vessels and Tanks in Reinforced Plastics, British Standards Institution, London UK, 1987.
17. ASME Boiler and Pressure Vessel Code, Section X: Fibre Reinforced Plastic Pressure Vessels, The American Society of Mechanical Engineers, 1992.
18. Shokrieh M.M. and Lessard L.B., Multiaxial fatigue behavior of unidirectional plies based on uniaxial fatigue experiments, International Journal of fatigue, 19,3,209-217, 1997.
19. Shokrieh M.M., Progressive Fatigue Damage Modeling of Composite Materials, Ph.D. Thesis, Department of Mechanical Engineering, McGill University, Montreal, Canada, Feb. 1996.
20. Shokrieh M.M. and Lessard L.B., Progressive Fatigue Damage Modeling of Composite Materials, Part I: Modeling, J. Composite Materials, Vol.34, No.13, pp. 1056-1080, 2000.
21. Adam T., Dickson R.F., Jones C.J., Reiter H. and Harris B., A Power Low Fatigue Damage Model for Fiber-Reinforced Plastic Laminates, Proc. Instn Mech. Engineers, Vol.200, No.C3, pp. 155-166, 1986.
22. Ramakrishnan V., Jayaraman N., Mechanistically based fatigue-damage evolution model for brittle matrix fibre-reinforced composites, Journal of Materials Science 28, 5592-5602, 1993.
23. Hyer M.W., Stress Analysis of fiber reinforced Composite Materials, WCB/McGraw-Hill, ISBN 0-07-016700-1, 1997.

24. Haplin J.C., Primer on Composite Materials: ANALYSIS, Technomic Pub. Co., 1984.
25. Johnson A.F., Engineering Design Properties of GRP, British plastics Federation, 1978.
26. Reifsnider K.L., Fatigue of Composite Materials, Elsevier, Amsterdam, 1991.
27. Daniel I.M., Lee J.W., Yaniv G., Damage Mechanisms and stiffness degradation in graphite/epoxy composite. Proceedings of ICCM-6 and ECCM-2, Elsevier Applied Science, London, PP. 4129-38, 1987.
28. King J., Advanced composite materials, Material World, Vol.5, No 6, pp.324-327, 1997.
29. Varvani-Farahani A., Haftchenari H. and Panbechi M., A Fatigue Damage parameter for Life Assessment of Off-Axis Unidirectional Glass Fiber-Reinforced composites, Journal of Composite Materials, 2005.
30. Reifsnider K.L., Highsmith A.L., Materials Experimentation and Design in Fatigue, Wesbury House, Guildford, pp.246-260, 1981.
31. Crossman F.W., Wang A.S.D., Damage in Composite Materials, ASTM STP 775, pp.118-139, 1982.
32. Batdorf S.B., Reinforced J., Plast.Compos, 1, PP.153-14, 1982.
33. Bailey J.E., Curtis P.T, and Parvizi A., Proc.R.Soc.London, A 366, 1977, pp.599.
34. Harlow D.G., Phoenix S.L., Int.J.Fracture, 15, PP.321-336, 1979.
35. Jamison R.D., Schulte K., Reifsnider K.L., Stinchcomb W.W., NASA, Effects of Defects in Composite Materials, ASTM STP 836, pp.21-25, 1984.
36. Bakisand C.E., Stinchcomb W.W., Composite Materials: Fatigue and Fracture, ASTM STP 907, pp.314-334, 1986.
37. Tamuz V., Proc. 2<sup>nd</sup> U.S.A.-U.S.S.R. Symp. On Fracture of Composite Materials, Lehigh University, 1981.
38. Subramanian S., Reifsnider K.L., Stinchcomb W.W. , A Cumulative damage model to predict the fatigue life of composite laminates including the effect of a fiber-matrix interphase. Int J Fatigue, PP.17 (5): 343-51, 1995.

39. Reifsnider K.L., Damage and Damage Mechanics, in K. L. Reifsnider (ed), Fatigue of Composite Materials, Composite Materials, Series ed R. B. Pipes, Elsevier and Science Publishers, pp. 11–77, 1990.
40. Gao Z., Reifsnider K.L., J. Compos. Technol, Res., 14,201, 1990.
41. Gao Z., Reifsnider K.L., and Carman G.P., J.Composite. Mater, 26,1578, 1992.
42. Qing-Dun Z., Zhi-Li W. and Ling L., A study of the influence of Interfacial Damage on stress concentration in unidirectional composites, Composites Science and Technology, 57, PP.129-135, 1997.
43. Papanikos P., Tserpes KI. , Pantelakis Sp., Modeling of fatigue damage progression and life in CFRP laminates. Fatigue Fract. Eng. Mater. Struct. , 26:37–47, 2003.
44. Subramanian S., Reifsnider K.L., Stinchcomb W.W., Tensile Strength of Unidirectional Composites: The Role of Efficiency and Strength of Fiber-Matrix Interface. Journal of Composites Technology and Research, Vol.17, No.4, pp.289-300, 1995.
45. ANSYS Software Release 8, Theory Reference (<http://www.ansys.com>).
46. Philippidis T.P., Vassilopoulos A.P., Fatigue of composite Laminates under off-axis loading, International Journal of Fatigue 21, 253-262, 1999.
47. Plumtree A., Shi L., Fatigue damage evolution in off-axis unidirectional CFRP, International Journal of Fatigue 24, PP.155-159, 2002.
48. Tserpes K.I., Papanikos P., Labeas G., Pantelakis Sp., Fatigue damage accumulation and residual strength assessment of CFRP laminates, Composite Structures, 63, PP.219–230, 2004.
49. Paepegem W.V., “Fatigue of Composites: Finite Elements Implementation of Fatigue Degradation Model for Fiber Reinforced Composite Materials“, Dept. of Mech. Construction and Production Ghent University, Belgium, 2001.
50. Agarwal B.D., Joneja S.K., Flexural Fatigue of a Unidirectional Composite in the Longitudinal Direction, Material Science and Engineering, 46, PP. 63-68, 1980.
51. Agarwal B.D., Joneja S.K., Progressive Damage in GFRP Under Constant Deflection Flexural Fatigue, Fibre Science and technology, 12 (5), PP. 341-352, 1979.

52. Agarwal B. D., Joneja S.K., Flexural fatigue properties of Unidirectional GRP in the transverse direction, *Composites*, 10 (1), PP.28-30, 1979.
53. Pauchard V., Grosjean F., Campion-Boulharts H., Chateauminios A., Application of a stress-corrosion-cracking model to an analysis of the durability of glass composites in wet environment, *Composites Science and Technology*, 62,PP. 493-498, 2002.
54. Lee S., Scott R.F., Gaudert P.C., Ubbink W.H., Poon C. Mechanical testing of toughened composite materials. *Composites*, 19,PP.300–10,1988.
55. Schulte K., Stinchcomb W.W., Damage near the edges of a composite specimen during quasi-static and fatigue loading. *Composite Technol Rev*; 6,PP.3–9,1984.
56. Oever M. van den and Peijs T., Continuous-glass-fibre-reinforced polypropylene composites II influence of maleic-anhydride modified polypropylene on fatigue behaviour, *Composites Part, A* 29A,PP. 227-239, 1998.
57. Corum, J.M., Battiste R.L., Liu K.C., Ruggles M.B., Basic Properties of Reference Cross ply Carbon-Fiber Composite, Oak Ridge National Laboratory, ORNL/TM-2000.
58. Boniface L, Ogin SL., Application of the Paris equation to the fatigue growth of transverse ply cracks. *Journal of Composite Materials*, 23:PP.735–54, 1989.
59. Berthelot J., El Mahi A., Le Corre D J.F., Development of transverse cracking in cross-ply laminates during fatigue tests *Composites Science and Technology* 61, PP.1711–1721, 2001.
60. Data bank for composite properties ([www.lampro.co.uk](http://www.lampro.co.uk)).
61. Khashaba U.A., In-plane shear properties of cross-ply composite laminates with different off-axis angles, *Composite structures* 65, PP.167-177, 2004.
62. Data bank for composite properties ([www.mathweb.com](http://www.mathweb.com)).

## APPENDIX A

Appendix A tabulates the material properties and fatigue data for unidirectional and cross-ply FRP composites tested.

Table (A1-1) through Table (A1-5) present fatigue tests performed for UD FRP composites at various off-axis angles  $\theta$  and stress ratio  $R$ . Also Table (A1-6) through Table (A1-8) list fatigue tests performed for cross-ply FRP composites at various stress ratio  $R$ .

Table (A2-1) through Table (A2-10) tabulate mechanical properties of unidirectional FRP composites. Table (A2-11) through Table (A2-13) list the Mechanical Properties of cross-ply FRP composites.

All the stiffness degradation data are tabulated in Table (A3-1) through Table (A3-32) as fatigue life ratio on UD GRP specimens varies for various off-axis angles and  $R$  ratios. Table (A3-33) through Table (A3- 42) present stiffness ratio versus stress cycles for cross-ply FRP.

Table (A4-1) and Table (A4-2) introduce nodal displacement in  $x$  direction for the selected nodes for FRP unidirectional composites, used in FEM analysis.

Table A1-1: Fatigue tests performed by Agarwal and Joneja [50-52] for UD GRP composites with off-axis angles of 0°, 45° and 90°, R= -1 and  $V_f=0.25$ .

Longitudinal Direction 0°		Off-axis angle 45°		Transverse Direction 90°	
Max. Strain ( $\times 10^{-3}$ )	Life (Cycles)	Max. Strain ( $\times 10^{-3}$ )	Life (Cycles)	Max. Strain ( $\times 10^{-3}$ )	Life (Cycles)
7.7	1,070,000	2.2	$10^6$	2.2	$10^6$
8.8	43,525	2.8	135,953	2.7	462,550
10.7	2,960	3.8	13,616	3.3	198,076
13.5	25	5.3	652.5	4.3	22,870.5

Table A1-2: Fatigue testing condition for longitudinal direction, by Pauchard [53], R=0.7 and  $V_f=0.55$ .

Longitudinal Direction 0°	
Max. Strain ( $\times 10^{-3}$ )	Life (Cycles)
14	$4 \times 10^6$

Table A1-3: Fatigue testing conditions for 0°, 75° directions, by Philippidis et al. [5,46], R= -1 and 0.1 and  $V_f=0.6$ .

R=-1		R=0.1			
Longitudinal Direction 0°		Longitudinal Direction 0°		Off-axis angle 75°	
Applied Stress (MPa)	Life (Cycles)	Applied Stress (MPa)	Life (Cycles)	Applied Stress (MPa)	Life (Cycles)
90	$97 \times 10^3$	200	13,577	45	980
120	313	180	46,158	40	4,175
140	14.5	150	383,613	35	21,574
160	1	140	854,867	25	1,353,056

Table A1-4: Fatigue testing condition for 0°direction, by Plumtree et al. [47], R=0.1 and  $V_f=0.58$ .

Longitudinal Direction 0°	
Max. Strain ( $\times 10^{-3}$ )	Life (Cycles)
8.01	3,351
7.75	4908
7.55	534,718
6.45	3,140

Table A1-5: Fatigue testing conditions for 0°, 75° directions, by Oever study [56],  
R= -1 and 0.1 and  $V_f=0.6$ .

R=-1		R=0.1			
Longitudinal Direction 0°		Longitudinal Direction 10°		Off-axis angle 90°	
Applied Stress (MPa)	Life (Cycles)	Applied Stress (MPa)	Life (Cycles)	Applied Stress (MPa)	Life (Cycles)
90	$97 \times 10^3$	200	13,577	45	980
120	313	180	46,158	40	4,175
140	14.5	150	383,613	35	21,574
160	1	140	854,867	25	1,353,056

Table A1-6: Stress-life data (R = -1) on cross-ply CFRP composite [0/90], by Corum et al. [57], with  $V_f=0.427$ .

Max. Stress (MPa)	Life (Cycles)
448.4	292
424.8	174586
402.9	$12.7 \times 10^6$



Table A1-7: Stress-life data ( $R=0$ ) on cross-ply CFRP composite [0/90/0] by Daniel et al. [27], with  $V_f=0.63$ .

Max. Stress (MPa)	Life (Cycles)
412.9	$1 \times 10^6$
662	31,000

Table A1-8: Stress-life data ( $R=0.1$ ) on cross-ply GRP composite [0/90/0] by Boniface and Ogin [58], with  $V_f=0.58$ .

Max. Stress (MPa)	Life (Cycles)
140	$10^4$
95	$10^6$

Table A2-1: Mechanical Properties of GRP of Agarwal and Joneja [50-52] for longitudinal direction 0°.

Material Properties	Values
Matrix Modulus of Elasticity in Direction 1	$E_m=4.73\text{GPa}$
Fiber Modulus of Elasticity in Direction 1	$E_f=72.4\text{GPa}$ -
Modulus of Elasticity in Direction 1[11]	$E_c=9\text{ GPa}$
Matrix Shear Modulus	$G_m=1.822\text{ GPa}^b$
Fiber Shear Modulus	$G_f=30\text{ GPa}^b$
Shear Modulus in Direction 1-2	$G_{12}=2.381\text{ GPa}^a$
Ultimate Tensile Strength of GRP	$\sigma_{uts}=125\text{ MPa}$
Interface shear Strength of GRP [a]	$\tau_i=22\text{ MPa}$
Volume Fraction of E-glass Fiber	$V_f=0.25$

<sup>a</sup> $1/G_{12}=V_f/G_f+V_m/G_m$

<sup>b</sup> [62]

Table A2-2: Mechanical Properties of GRP of Agarwal and Joneja [50-52] for 45° off-axis angles.

Material Properties	Values
Matrix Modulus of Elasticity in Direction 1	$E_m=4.73\text{GPa}$
Fiber Modulus of Elasticity in Direction 1	$E_f=72.4\text{GPa}$
Modulus of Elasticity in Direction x	$E_x=7.34\text{ GPa}^a$
Matrix Shear Modulus	$G_m=1.822\text{ GPa}^d$
Fiber Shear Modulus	$G_f=30\text{ GPa}^d$
Shear Modulus in Direction 1-2	$G_{12}=2.381\text{ GPa}^c$
Ultimate Tensile Strength of GRP	$\sigma_{uts}=62.5\text{ MPa}^b$
Shear Strength of GRP	$\tau_i=62.5\text{ MPa}^b$
Volume Fraction of E-glass Fiber	$V_f=0.25$

<sup>a</sup>  $E_x$  is calculated based on the  $E_1$  and  $E_2$  that comes from ROM.[61]

<sup>b</sup>  $\sigma_{uts(45)}=\tau_{ult(45)}=1/2\sigma_{uts(0)}$ [23]

<sup>a</sup> $1/G_{12}=V_f/G_f+V_m/G_m$

<sup>d</sup> [62]

Table A2-3: Mechanical Properties of GRP of Agarwal and Joneja [50-52], for 90° direction.

Material Properties	Values
Matrix Modulus of Elasticity in Direction 1	$E_m=4.73\text{GPa}$
Fiber Modulus of Elasticity in Direction 1	$E_f=72.4\text{GPa}$
Modulus of Elasticity in Transverse Direction	$E_x=8.423\text{ GPa}^a$
Matrix Shear Modulus	$G_m=1.822\text{ GPa}^d$
Fiber Shear Modulus	$G_f=30\text{ GPa}^d$
Shear Modulus in Direction 1-2	$G_{12}=2.381\text{ GPa}^c$
Ultimate Tensile Strength of GRP	$\sigma_{uts}=44\text{ MPa}^b$
Shear Strength of GRP	$\tau_i=44\text{ MPa}^b$
Volume Fraction of E-glass Fiber	$V_f=0.25$

<sup>a</sup>  $E_x$  is calculated based on the  $E_1$  and  $E_2$  that comes from R.M.[61]

<sup>b</sup> Iso-stress condition[23]

$$^a 1/G_{12}=V_f/G_f+V_m/G_m$$

<sup>d</sup> [62]

Table A2-4: Mechanical Properties of GRP of Pauchard [53 ], for longitudinal direction

Material Properties	Values
Matrix Modulus of Elasticity in Direction 1	$E_m=4.73 \text{ GPa}$
Fiber Modulus of Elasticity in Direction 1	$E_f=80 \text{ GPa}$
Modulus of Elasticity in Direction 1	$E_c=45.4 \text{ GPa}^a$
Matrix Shear Modulus	$G_m=1.822 \text{ GPa}^b$
Fiber Shear Modulus	$G_f=30 \text{ GPa}^b$
Shear Modulus in Direction 1-2	$G_{12}=3.77 \text{ GPa}$
Ultimate Tensile Strength of GRP	$\sigma_{uts}=1203 \text{ MPa}$
Shear Strength of GRP	$\tau_i=41.35 \text{ MPa}^a$
Volume Fraction of E-glass Fiber	$V_f=0.55$

<sup>a</sup>[62]

<sup>b</sup>[62]

Table A2-5: Mechanical Properties of GRP of Philippidis [5], for longitudinal direction 0°.

Material Properties	Values
Matrix Modulus of Elasticity in Direction 1	$E_m=4.73 \text{ GPa}$
Fiber Modulus of Elasticity in Direction 1	$E_f=80 \text{ GPa}^a$
Modulus of Elasticity in Direction 1	$E_c= 44.8 \text{ GPa}$
Matrix Shear Modulus	$G_m=1.822 \text{ GPa}^b$
Fiber Shear Modulus	$G_f=30 \text{ GPa}^b$
Shear Modulus in Direction 1-2	$G_{12}=4.4 \text{ GPa}$
Ultimate Tensile Strength of GRP	$\sigma_{uts}=166 - 499.4 \text{ MPa}$
Shear Strength of GRP	$\tau_i=48.26 \text{ MPa}^a$
Volume Fraction of E-glass Fiber	$V_f=0.5-0.6$

<sup>a</sup>[62]

<sup>b</sup>[62]

Table A2-6: Mechanical Properties of GRP of Philippidis [46], for 75° direction.

Material Properties	Values
Matrix Modulus of Elasticity in Direction 1	$E_m=4.73 \text{ GPa}$
Fiber Modulus of Elasticity in Direction 1	$E_f=80 \text{ GPa}$
Modulus of Elasticity in Direction 1	$E_c=13.77 \text{ GPa}^a$
Matrix Shear Modulus	$G_m=1.822 \text{ GPa}^b$
Fiber Shear Modulus	$G_f=30 \text{ GPa}^b$
Shear Modulus in Direction 1-2	$G_{12}=3.77 \text{ GPa}$
Ultimate Tensile Strength of GRP	$\sigma_{uts}=87.93 \text{ MPa}$
Shear Strength of GRP	$\tau_i=60 \text{ MPa}^c$
Volume Fraction of E-glass Fiber	$V_f=0.5$

<sup>a</sup> Based on rule of mixture  $E_c=38.5 \text{ GPa}$ ,  $E_c=44.8 \text{ GPa}$  [62]

<sup>b</sup> [62]

<sup>c</sup> [61]

Table A2-7: Mechanical Properties of CFRP of Plumtree [47]., for longitudinal direction 0°.

Material Properties	Values
Matrix Modulus of Elasticity in Direction 1	$E_m=3.3 \text{ GPa}$
Fiber Modulus of Elasticity in Direction 1	$E_f=296 \text{ GPa}$
Modulus of Elasticity in Direction 1	$E_c=173 \text{ GPa}^a$
Matrix Shear Modulus	$G_m=2.9 \text{ GPa}^c$
Fiber Shear Modulus	$G_f=5.5 \text{ GPa}^c$
Shear Modulus in Direction 1-2	$G_{12}=5 \text{ GPa}^d$
Ultimate Tensile Strength of CFRP	$\sigma_{uts}=2610 \text{ MPa}^b$
Shear Strength of CFRP	$\tau_i=137 \text{ GPa}^c$
Volume Fraction of carbon Fiber	$V_f=0.58$

<sup>a</sup> Based on rule of mixture,  $E_c=147 \text{ GPa}$  [61]

<sup>b</sup> Based on rule of mixture,  $E_c=2004 \text{ GPa}$  [61]

<sup>c</sup> [5]

<sup>d</sup>  $1/G_{12}=V_f/G_f+V_m/G_m$



Table A2-8: Mechanical Properties of GRP of Oever [56], for longitudinal direction 0°.

Material Properties	Values
Matrix Modulus of Elasticity in Direction 1	$E_m=1.5 \text{ GPa}$
Fiber Modulus of Elasticity in Direction 1	$E_f=72.4 \text{ GPa}$
Modulus of Elasticity in Direction 1	$E_c=42.65 \text{ GPa}$
Matrix Shear Modulus	$G_m=1.822 \text{ GPa}^b$
Fiber Shear Modulus	$G_f=30 \text{ GPa}^b$
Shear Modulus in Direction 1-2	$G_{12}=3.77 \text{ GPa}$
Ultimate Tensile Strength of GRP	$\sigma_{uts}=1025 \text{ MPa}$
Shear Strength of GRP	$\tau_i=50 \text{ MPa}^a$
Volume Fraction of E-glass Fiber	$V_f=0.5$

<sup>a</sup>[61]

<sup>b</sup>[62]

Table A2-9: Mechanical Properties of GRP of Oever [56], for 10° direction.

Material Properties	Values
Matrix Modulus of Elasticity in Direction 1	$E_m=1.5 \text{ GPa}$
Fiber Modulus of Elasticity in Direction 1	$E_f=72.4 \text{ GPa}$
Modulus of Elasticity in Direction 1	$E_c=28.3 \text{ GPa}$
Matrix Shear Modulus	$G_m=1.822 \text{ GPa}^b$
Fiber Shear Modulus	$G_f=30 \text{ GPa}^b$
Shear Modulus in Direction 1-2	$G_{12}=3.77 \text{ GPa}$
Ultimate Tensile Strength of GRP	$\sigma_{uts}=64 \text{ MPa}$
Shear Strength of GRP	$\tau_i=52 \text{ MPa}^a$
Volume Fraction of E-glass Fiber	$V_f=0.6$

<sup>a</sup>[21], <sup>b</sup>[62]

Table A2-10: Mechanical Properties of GRP of Oever [56], for 90° direction.

Material Properties	Values
Matrix Modulus of Elasticity in Direction 1	$E_m=1.5 \text{ GPa}$
Fiber Modulus of Elasticity in Direction 1	$E_f=72.4 \text{ GPa}$
Modulus of Elasticity in Direction 1	$E_c=6.85 \text{ GPa}$
Matrix Shear Modulus	$G_m=1.822 \text{ GPa}^b$
Fiber Shear Modulus	$G_f=30 \text{ GPa}^b$
Shear Modulus in Direction 1-2	$G_{12}=3.77 \text{ GPa}$
Ultimate Tensile Strength of GRP	$\sigma_{uts}=4.5 \text{ MPa}$
Shear Strength of GRP	$\tau_i=50 \text{ MPa}^a$
Volume Fraction of E-glass Fiber	$V_f=0.6$

<sup>a</sup>[61], <sup>b</sup>[18]

Table A2-11: Mechanical Properties of cross-ply CFRP composite [0/90] reported by Corum et al. [57].

Material Properties	Values
Matrix Modulus of Elasticity in Direction 1	$E_m=3.3\text{ GPa}$
Fiber Modulus of Elasticity in Direction 1	$E_f=228\text{ GPa}$
Modulus of Elasticity of UD CFRP in Direction 1	$E_c=99.24\text{ GPa}^a$
Modulus of Elasticity of UD CFRP in Direction 2	$E_c=10.17\text{ GPa}$
Modulus of Elasticity of Cross-ply Composite	$E_c=46.2\text{ GPa}$
Shear Modulus in Direction 1-2	$G_{12}=2.96\text{ GPa}$
Ultimate Tensile Strength of UD CFRP in Direction 1	$\sigma_{uts}=1.389\text{ GPa}^a$
Ultimate Tensile Strength of UD CFRP in Direction 2	$\sigma_{uts}=44\text{ GPa}$
Ultimate Tensile Strength of Cross-ply	$\sigma_{uts}=474\text{ GPa}$
Volume Fraction of E-glass Fiber	$V_f=0.427$

<sup>a</sup>Rule of Mixture

Table A2-12: Mechanical Properties of cross-ply CFRP composite [0/90/0] reported by Daniel et al. [27].

Material Properties	Values
Matrix Modulus of Elasticity in Direction 1	$E_m=3.3 \text{ GPa}$
Fiber Modulus of Elasticity in Direction 1	$E_f=228 \text{ GPa}$
Modulus of Elasticity of UD CFRP in Direction 1	$E_c=142 \text{ GPa}$
Modulus of Elasticity of UD CFRP in Direction 2	$E_c=10.3 \text{ GPa}$
Modulus of Elasticity of Cross-ply	$E_c=54.2 \text{ GPa}$
Shear Modulus in Direction 1-2	$G_{12}=7.6 \text{ GPa}$
Ultimate Tensile Strength of UD CFRP in Direction 1	$\sigma_{uts}=2.372 \text{ GPa}$
Ultimate Tensile Strength of UD CFRP in Direction 2	$\sigma_{uts}=57.2 \text{ MPa}$
Ultimate Tensile Strength of Cross-ply	$\sigma_{uts}=779 \text{ MPa}$
Volume Fraction of E-glass Fiber	$V_f=0.63$

Table A2-13: Mechanical Properties of cross-ply GRP composite reported by Boniface and Ogin [58].

Material Properties	Values
Fiber Modulus of Elasticity in Direction 1	$E_f=72.4\text{ GPa}$
Modulus of Elasticity of UD CFRP in Direction 1	$E_c=42.3\text{ GPa}$
Modulus of Elasticity of UD CFRP in Direction 2	$E_c=13.2\text{ GPa}$
Modulus of Elasticity of Cross-ply	$E_c=36.2\text{ GPa}^a$
Shear Modulus in Direction 1-2	$G_{12}=4.4\text{ GPa}$
Ultimate Tensile Strength of Cross-ply	$\sigma_{uts}=1.2\text{ GPa}$
Volume Fraction of E-glass Fiber	$V_f=0.58$

<sup>a</sup>  $E_c=(\alpha E_{11}+E_{22})/(1+\alpha)$  [4]

Table A3-1: Stiffness ratio  $E/E_0$  versus life of UD GRP tested by Agarwal and Joneja [52] for longitudinal direction.

$\sigma_{app}$ (MPa)	$N_f$ (Cycles)	$R^*$	$E_m^*$	$E_f^*$	R
69.3	1070000	0.446	1.011	2.011 <sup>a</sup>	-1
$E/E_0$		$N$ (Cycles)			
0.94		16050			
0.69		107000			
0.58		197950			
0.45		267500			
0.29		406600			
0.18		593850			
0.15		642000			
0.13		746325			
0.07		979050			

<sup>a</sup> Based on  $E_c=9$  GPa.

Table A3-2: Stiffness ratio  $E/E_0$  versus life of UD GRP tested by Agarwal and Joneja [52] for longitudinal direction.

$\sigma_{app}$ (MPa)	$N_f$ (Cycles)	$R^*$	$E_m^*$	$E_f^*$	R
79.2	43525	0.366	1.011	2.011 <sup>a</sup>	-1
$E/E_0$		N (Cycles)			
0.9		1959			
0.79		4135			
0.68		7835			
0.5		11752			
0.38		15451			
0.31		18498			
0.24		25027			
0.19		29815			
0.14		34820			
0.07		39825			

<sup>a</sup> Based on  $E_c=9$  GPa.

Table A3-3: Stiffness ratio  $E/E_0$  versus life of UD GRP tested by Agarwal and Joneja [52] for longitudinal direction.

$\sigma_{app}(\text{MPa})$	$N_f(\text{Cycles})$	$R^*$	$E_m^*$	$E_f^*$	$R$
96.3	2960	0.230	1.011	2.011 <sup>a</sup>	-1
$E/E_0$		$N(\text{Cycles}) -$			
0.93		207			
0.82		474			
0.74		710			
0.67		873			
0.57		1214			
0.51		1554			
0.42		1998			
0.26		2649			
0.14		2901			

<sup>a</sup> Based on  $E_c=9\text{ GPa}$ .



Table A3-4: Stiffness ratio  $E/E_0$  versus life of UD GRP tested by Agarwal and Joneja [52] for longitudinal direction.

$\sigma_{app}(MPa)$	$N_f(Cycles)$	$R^*$	$E_m^*$	$E_f^*$	R
121.5	25	.028	1.011	2.011 <sup>a</sup>	-1
$E/E_0$		$N(Cycles)$			
0.97		2			
0.9		4			
0.84		6			
0.76		8			
0.68		11			
0.51		16			
0.38		21			
0.26		24			

<sup>a</sup> Based on  $E_c=9\text{ GPa}$ .

Table A3-5: Stiffness ratio  $E/E_0$  versus life of UD GRP tested by Agarwal and Joneja [52], for  $45^\circ$  direction.

$\sigma_{app}$ (MPa)	$N_f$ (Cycles)	$R^*$	$E_m^*$	$E_f^*$	$R$
15.1	1000000	0.7584	0.865	1.865	-1
$E/E_0$		$N$ (Cycles) *			
0.9961		110687			
0.9961		162214			
0.9922		272901			
0.9922		446565			
0.9767		692748			
0.9302		864504			
0.4341		879771			
0.0000		998092			

Table A3-6: Stiffness ratio  $E/E_0$  versus life of UD GRP tested by Agarwal and Joneja [52], for 45° direction.

$\sigma_{app}$ (MPa)	$N_f$ (Cycles)	$R^*$	$E_m^*$	$E_f^*$	R
19.21	135953	0.693	0.865	1.865	-1
$E/E_0$		$N$ (Cycles)			
0.9961		15048			
0.9961		22053			
0.9922		37102			
0.8915		89770			
0.8217		107932			
0.4264		110527			
0.3217		119867			
0.2287		132061			
0.1512		134915			
0.0000		135696			

Table A3-7: Stiffness ratio  $E/E_0$  versus life of UD GRP tested by Agarwal and Joneja [52], for  $45^\circ$  direction.

$\sigma_{app}(\text{MPa})$	$N_f(\text{Cycles})$	$R^*$	$E_m^*$	$E_f^*$	$R$
26.1	13616	0.5824	0.865	1.865	-1
$E/E_0$		$N(\text{Cycles})$			
0.9961		1507			
0.9961		2209			
0.9922		3716			
0.9147		7873			
0.7519		9277			
0.4419		9381			
0.3256		10082			
0.2868		11226			
0.1628		12421			
0.1550		13382			
0.0000		13590			

Table A3-8: Stiffness ratio  $E/E_0$  versus life of UD GRP tested by Agarwal and Joneja [52], for 45° direction.

$\sigma_{app}(\text{MPa})$	$N_f(\text{Cycles})$	$R^*$	$E_m^*$	$E_f^*$	$R$
36.36	652.5	0.418	0.865	1.865	-1
$E/E_0$		$N(\text{Cycles})$			
0.9961		72			
0.9961		106			
0.9922		178			
0.9922		291			
0.9806		349			
0.9457		386			
0.6357		388			
0.5000		401			
0.3333		468			
0.2326		609			
0.0000		651			

Table A3-9: Stiffness ratio  $E/E_0$  versus life of UD GRP tested by Agarwal and Joneja [52], for 90° direction.

$\sigma_{app}$ (MPa)	$N_f$ (Cycles)	$R^*$	$E_m^*$	$E_f^*$	$R$
18.53	1000000	0.578	1	0	-1
$E/E_0$		$N$ (Cycles) *			
0.309524		27890			
0.301587		40020			
0.280423		70425			
0.253968		96403			
0.238095		122001			
0.195767		232225			
0.169312		428369			
0.044974		953994			

Table A3-10: Stiffness ratio  $E/E_0$  versus life of UD GRP tested by Agarwal and Joneja [52], for 90° direction.

$\sigma_{app}(\text{MPa})$	$N_f(\text{Cycles})$	$R^*$	$E_m^*$	$E_f^*$	$R$
22.74	462550	0.483	1	0	-1

$E/E_0$	$N(\text{Cycles})$
0.304233	8991
0.224868	9879
0.219577	13737
0.21164	17939
0.201058	25339
0.190476	40583
0.153439	105742
0.132275	156568
0.111111	254723
0.103175	327460
0.044974	441269

Table A3-11: Stiffness ratio  $E/E_0$  versus life of UD GRP tested by Agarwal and Joneja [52], for 90° direction.

$\sigma_{app}$ (MPa)	$N_f$ (Cycles)	$R^*$	$E_m^*$	$E_f^*$	$R$
27.8	198076	0.368	1	0	-1
$E/E_0$		$N$ (Cycles)			
0.304233		908			
0.230159		1409			
0.193122		2683			
0.187831		4036			
0.190476		5438			
0.190476		7682			
0.18254		15327			
0.171958		27833			
0.174603		48216			
0.15873		67047			
0.12963		107380			
0.044974		158993			



Table A3-12: Stiffness ratio  $E/E_0$  versus life of UD GRP tested by Agarwal and Joneja [52], for 90° direction.

$\sigma_{app}(\text{MPa})$	$N_f(\text{Cycles})$	$R^*$	$E_m^*$	$E_f^*$	$R$
36.22	22870.5	0.178	1	0	-1
$E/E_0$		$N(\text{Cycles})$			
0.280423		50			
0.224868		80			
0.18254		230			
0.177249		466			
0.171958		887			
0.164021		1884			
0.145503		3422			
0.140212		3941			
0.134921		9644			
0.12963		15691			
0.047619		21818			

Table A3-13: Stiffness ratio  $E/E_0$  versus life of GRP of Pauchard et al. [53], for longitudinal direction  $0^\circ$ .

$\sigma_{app}$ (MPa)	$N_f$ (Cycles)	$R^*$	$E_m^*$	$E_f^*$	R
635.6	$4 \times 10^6$	0.925	0.0308	0.969	0.7
$E/E_0$	N (Cycles)		$E/E_0$	N (Cycles)	
0.996	9404.449		0.986	184785	
0.994	18478.5		0.988	208930	
0.994	27542		0.983	229087	
0.993	37440		0.983	251189	
0.993	45013		0.985	275423	
0.993	54117		0.983	311411	
0.993	65063		0.981	331131	
0.993	73564		0.981	410519	
0.992	80662		0.979	478630	
0.992	88444		0.979	541170	
0.990	96977		0.977	969765	
0.990	106333		0.974	1401737	
0.988	116591		0.974	1490505	
0.990	123975		0.970	1791981	
0.988	131826		0.966	1847850	
0.988	149051		0.960	2754229	
0.988	168525		0.949	3630781	
0.986	168526		0.942	3981072	

Table A3-14: Stiffness ratio  $E/E_0$  versus life of GRP of Philippidis et al. [5], for longitudinal direction  $0^\circ$ .

$\sigma_{app}(\text{MPa})$	$N_f(\text{Cycles})$	$R^*$	$E_m^*$	$E_f^*$	R
90	$97 \times 10^3$	0.455	0.035	0.965	-1
$E/E_0$		N (Cycles)			
0.977895		9563			
0.970526		9905			
0.979298		19127			
0.962456		19468			
0.98		30398			
0.970175		33130			
0.954386		39620			
0.958246		46792			
0.971579		51574			
0.964561		58405			
0.963509		65577			
0.952281		68310			
0.965263		74799			
0.958246		84021			
0.944561		94609			

Table A3-15: Stiffness ratio  $E/E_0$  versus life of GRP of Philippidis et al. [5], for longitudinal direction  $0^\circ$ .

$\sigma_{app}(\text{MPa})$	$N_f(\text{Cycles})$	$R^*$	$E_m^*$	$E_f^*$	$R$
120	313	0.273	0.035	0.965	-1

$E/E_0$	$N(\text{Cycles})$	$E/E_0$	$N^*(\text{Cycles})$
0.999649	1	0.935088	193
0.999649	7	0.964561	203
0.98386	28	0.960702	213
0.974737	38	0.937895	235
0.985263	66	0.95614	240
0.999298	74	0.950526	255
0.960702	85	0.934386	256
0.981404	97	0.935789	274
0.985614	109	0.931228	282
0.972281	125	0.957895	284
0.962105	135	0.933333	290
0.980351	148	0.94807	308
0.942456	154	0.929123	310
0.975439	178		

Table A3-16: Stiffness ratio  $E/E_0$  versus life of GRP of Philippidis et al. [5], for longitudinal direction  $0^\circ$ .

$\sigma_{app}(\text{MPa})$	$N_f(\text{Cycles})$	$R^*$	$E_m^*$	$E_f^*$	$R$
140	14.5	0.151	0.035	0.965	-1
$E/E_0$	$N(\text{Cycles})$		$E/E_0$	$N(\text{Cycles})$	
0.999649	1		0.946667	8	
0.982456	2		0.976491	9	
0.96386	3		0.94386	10	
0.989474	4		0.929474	11	
0.964211	5		0.958596	12	
0.956491	6		0.922105	13	
0.977193	7		0.936842	14	

Table A3-17: Stiffness ratio  $E/E_0$  versus life of GRP of Philippidis et al. [46], for longitudinal direction  $0^\circ$ .

$\sigma_{app}$ (MPa)	$N_f$ (Cycles)	$R^*$	$E_m^*$	$E_f^*$	$R$
200	13577	0.82	0.192	0.808	0.1

$E/E_0$	$N$ (Cycles)	$E/E_0$	$N^*$ (Cycles)
0.925424	2681	0.813559	8156
0.725424	2682	0.60339	8157
0.671186	2683	0.79661	9525
0.898305	4051	0.59322	9526
0.715254	4052	0.762712	10840
0.647458	4053	0.59661	10893
0.861017	5419	0.576271	10840
0.630508	5420	0.711864	12262
0.847458	6788	0.559322	12263
0.694915	6789	0.542373	12919
0.613559	6790	0.491525	12920

Table A3-18: Stiffness ratio  $E/E_0$  versus life of GRP of Philippidis et al.[46], for longitudinal direction  $0^\circ$ .

$\sigma_{app}(\text{MPa})$	$N_f(\text{Cycles})$	$R^*$	$E_m^*$	$E_f^*$	$R$
180	46158	0.838	0.192	0.808	0.1

$E/E_0$	$N(\text{Cycles})$	$E/E_0$	$N(\text{Cycles})$
0.911864	9119	0.684746	27731
0.742373	9120	0.630508	27732
0.820339	13773	0.772881	32384
0.698305	13960	0.613559	32385
0.789831	18426	0.701695	36851
0.671186	18612	0.664407	36852
0.783051	23079	0.671186	41691
0.657627	23079	0.423729	43924
0.776271	27546	0.535593	43925

Table A3-19: Stiffness ratio  $E/E_0$  versus life of GRP of Philippidis et al. [46], for longitudinal direction  $0^\circ$ .

$\sigma_{app}$ (MPa)	$N_f$ (Cycles)	$R^*$	$E_m^*$	$E_f^*$	$R$
150	383613	0.865	0.192	0.808	0.1

$E/E_0$	$N$ (Cycles)	$E/E_0$	$N$ (Cycles)
1	37124	0.725424	230475
0.833898	75794	0.664407	230477
0.759322	75795	0.579661	230478
0.640678	75796	0.715254	269147
0.755932	114465	0.674576	269148
0.728814	114466	0.572881	269149
0.59322	114467	0.684746	306272
0.745763	153136	0.630508	307818
0.694915	154683	0.559322	306272
0.586441	153136	0.620339	346488
0.738983	190260	0.538983	346489
0.674576	191806	0.583051	365050
0.579661	191807	0.454237	365051



Table A3-20: Stiffness ratio  $E/E_0$  versus life of GRP of Philippidis et al. [46], for longitudinal direction  $0^\circ$ .

$\sigma_{app}$ (MPa)	$N_f$ (Cycles)	$R^*$	$E_m^*$	$E_f^*$	$R$
140	854867	0.874	0.192	0.808	0.1

$E/E_0$	$N$ (Cycles)	$E/E_0$	$N$ (Cycles)
0.908475	168905	0.79	599785
0.854237	255081	0.701695	599786
0.810169	341257	0.6	599787
0.79661	427433	0.779661	685962
0.722034	427434	0.762712	768691
0.650847	427435	0.657627	772138
0.79322	513609	0.745763	813502
0.616949	513610	0.515254	813503

Table A3-21: Stiffness ratio  $E/E_0$  versus life of GRP of Philippidis et al. [46], for 75° direction.

$\sigma_{app}$ (MPa)	$N_f$ (Cycles)	$R^*$	$E_m^*$	$E_f^*$	$R$
45	980	0.77	0.41	0.58	0.1

$E/E_0$	$N$ (Cycles)	$E/E_0$	$N$ (Cycles)
1	196	0.727568	588
0.821622	294	0.734054	685
0.818378	391	0.675676	686
0.737297	392	0.701622	783
0.811892	489	0.652973	784
0.734054	490	0.704865	885
0.721081	491	0.601081	886
0.747027	587		

Table A3-22: Stiffness ratio  $E/E_0$  versus life of GRP of Philippidis et al. [46],for 75° direction.

$\sigma_{app}(MPa)$	$N_f$ (Cycles)	$R^*$	$E_m^*$	$E_f^*$	R
40	4175	0.795	0.41	0.58	0.1
$E/E_0$		$N$ (Cycles)			
0.977297		835			
0.87027		1253			
0.844324		1686			
0.8111		2104			
0.798919		2505			
0.743784		2923			
0.737297		3340			
0.688649		3774			
0.610811		3982			

Table A3-23: Stiffness ratio  $E/E_0$  versus life of GRP of Philippidis et al. [46], for 75° direction.

$\sigma_{app}$ (MPa)	$N_f$ (Cycles)	$R^*$	$E_m^*$	$E_f^*$	$R$
35	21574	0.821	0.41	0.58	0.1

$E/E_0$	$N$ (Cycles)	$E/E_0$	$N^*$ (Cycles)
0.76973	4315	0.503784	15102
0.695135	6472	<del>0.545946</del>	17259
0.685405	8712	0.490811	19500
0.614054	8713	0.494054	20495
0.588108	10870	0.429189	20496
0.581622	12944	<del>0.503784</del>	15102
0.568649	12945	<del>0.545946</del> 40	17259
0.532973	15185		

Table A3-24: Stiffness ratio  $E/E_0$  versus life of GRP of Philippidis et al. [46], for 75° direction.

$\sigma_{app}$ (MPa)	$N_f$ (Cycles)	$R^*$	$E_m^*$	$E_f^*$	$R$
30	143673	0.846	0.41	0.58	0.1
$E/E_0$		$N$ (Cycles)			
0.662703		28735			
0.601081		43102			
0.558919		58022			
0.536216		72389			
0.497297		86756			
0.500541		101676			
0.487568		116596			
0.474595		130964			
0.458378		142568			

Table A3-25: Stiffness ratio  $E/E_0$  versus life of GRP of Philippidis et al. [46], for 75° direction.

$\sigma_{app}$ (MPa)	$N_f$ (Cycles)	$R^*$	$E_m^*$	$E_f^*$	R
25	1353056	0.872	0.41	0.58	0.1
$E/E_0$		$N$ (Cycles) -			
0.724324		270611			
0.688649		405917			
0.659459		546427			
0.636757		676528			
0.623784		811834			
0.601081		947139			
0.607568		1134485			
0.523243		1087649			
0.52		1222954			
0.51027		1290607			

Table A3-26: Stiffness ratio  $E/E_0$  versus life of CFRP of Plumtree et al. [47], for longitudinal direction  $0^\circ$ .

$\sigma_{app}$ (MPa)	$N_f$ (Cycles)	$R^*$	$E_m^*$	$E_f^*$	R
1177	3531	0.413	0.168	1.168	0.1
$E/E_0$		$N$ (Cycles)			
0.0259		54			
0.0345		120			
0.0414		185			
0.0491		316			
0.0655		567			
0.0871		926			
0.1181		1613			
0.1526		2561			

Table A3-27: Stiffness ratio  $E/E_0$  versus life of CFRP of Plumtree et al. [47], for longitudinal direction  $0^\circ$ .

$\sigma_{app}$ (MPa)	$N_f$ (Cycles)	$R^*$	$E_m^*$	$E_f^*$	$R$
1139	4908	0.432	0.168	1.168	0.1

$E/E_0$	$N$ (Cycles)	$E/E_0$	$N$ (Cycles)
0.006667	92	0.073333	1227
0.026667	276	0.078333	1288
0.036667	429	0.081667	1411
0.041667	490	0.086667	1595
0.046667	675	0.09	1748
0.05	736	0.096667	1963
0.055	798	0.1	2055
0.058333	859	0.101667	2086
0.061667	920	0.11	2454
0.066667	982	0.131667	3344
0.07	1043	0.153333	4202
0.071667	1135	0.168333	4693



Table A3-28: Stiffness ratio  $E/E_0$  versus life of CFRP of Plumtree et al. [47], for longitudinal direction  $0^\circ$ .

$\sigma_{app}$ (MPa)	$N_f$ (Cycles)	$R^*$	$E_m^*$	$E_f^*$	R
1110	534718	0.446	0.168	1.168	0.1
$E/E_0$		N (Cycles)			
0.0155		21455			
0.0198		26406			
0.0233		34658			
0.0293		46210			
0.0371		67665			
0.0543		125428			
0.0681		193093			
0.0767		232701			
0.0983		376283			
0.1259		509963			

Table A3-29: Stiffness ratio  $E/E_0$  versus life of CFRP of Plumtree et al. [47], for longitudinal direction,  $0^\circ$ .

$\sigma_{app}(\text{MPa})$	$N_f(\text{Cycles})$	$R^*$	$E_m^*$	$E_f^*$	$R$
948	3140	0.473	0.168	1.168	0.1

$E/E_0$	$N(\text{Cycles})$	$E/E_0$	$N(\text{Cycles})$
0.0034	68	0.1672	1211
0.0345	194	0.1733	1512
0.0707	252	0.1784	1812
0.1121	310	0.1845	2113
0.1319	426	0.1888	2403
0.1440	552	0.1940	2704
0.1552	669	0.2000	3004
0.1586	785	0.2000	3140
0.1638	1018		

Table A3-30: Stiffness ratio  $E/E_0$  versus life GRP of Oever et al. [56], for longitudinal direction  $0^\circ$ .

$\sigma_{app}(MPa)$	$N_f$ (Cycles)	$R^*$	$E_m^*$	$E_f^*$	$R$
400	25000	0.824	0.152	0.848	0.1
$E/E_0$		$N$ (Cycles)			
0.999958		293			
0.974936		5938			
0.922112		17889			
0.855386		22581			
0.719154		24413			
0.54956		25000			

Table A3-31: Stiffness ratio  $E/E_0$  versus life GRP of Oever et al. [56], for 10° direction.

$\sigma_{app}(\text{MPa})$	$N_f(\text{Cycles})$	$R^*$	$E_m^*$	$E_f^*$	$R$
40	9000	0.71875	0.279	1.279	0.1
$E/E_0$		$N(\text{Cycles})$			
0.996971		0			
0.991362		345			
0.970329		4354			
0.904425		8097			
0.824499		8788			
0.795053		8894			

Table A3-32: Stiffness ratio  $E/E_0$  versus life GRP of Oever et al. [56], for 90° direction

$\sigma_{app}(\text{MPa})$	$N_f(\text{Cycles})$	$R^*$	$E_m^*$	$E_f^*$	$R$
3.6	320	0.64	1	0	0.1
$E/E_0$		$N(\text{Cycles})$			
0.99892		0			
0.99892		17			
0.975689		155			
0.958266		240			
0.910353		295			
0.815978		318			

Table A3-33: Stiffness ratio  $E/E_0$  versus stress cycles for cross-ply CFRP (C15-2) reported by Corum et al. [57].

$\sigma_{app}$ (MPa)	$N_f$ (Cycles)	$R^*$	$R$
448.2	292	0.5725	0.1

$E/E_0$	$N$ (Cycles)	$E/E_0$	$N$ (Cycles)
0.985366	0	0.77561	54
0.95122	1	0.770732	72
0.921951	4	0.726829	95
0.892683	7	0.746341	97
0.878049	9	0.726829	121
0.873171	11	0.712195	145
0.878049	13	0.707317	169
0.839024	19	0.682927	174
0.814634	20	0.707317	193
0.819512	23	0.697561	218
0.785366	48	0.678049	242

Table A3-34: Stiffness ratio  $E/E_0$  versus stress cycles for cross-ply CFRP (C15-18) reported by Corum et al. [57].

$\sigma_{app}$ (MPa)	$N_f$ (Cycles)	$R^*$	$R$
448.2	292	0.5725	0.1

$E/E_0$	$N$ (Cycles)	$E/E_0$	$N$ (Cycles)
0.931707	1	0.8	49
0.84878	9	0.760976	75
0.853659	13	0.75122	106
0.858537	16	0.726829	165
0.82439	27	0.717073	166
0.8	31	0.712195	221
0.814634	33	0.702439	276
0.809756	38	0.75122	110
0.795122	43		

Table A3-35: Stiffness ratio  $E/E_0$  versus stress cycles for cross-ply CFRP (C15-3) reported by Corum et al. [57].

$\sigma_{app}$ (MPa)	$N_f$ (Cycles)	$R^*$	$R$
424.8	174586	0.595	0.1
$E/E_0$	N (Cycles)	$E/E_0$	N (Cycles)
0.853659	0	0.614634	16850
0.829268	0	0.619512	19658
0.790244	468	0.6	22467
0.770732	936	0.595122	25743
0.75122	936	0.619512	25275
0.726829	1872	0.619512	28084
0.702439	2340	0.6	56635
0.658537	5149	0.595122	85187
0.64878	6085	0.57561	113738
0.64878	7957	0.580488	141822
0.634146	10765	0.556098	145098
0.609756	14042	0.595122	170842



Table A3-36: Stiffness ratio  $E/E_0$  versus stress cycles for cross-ply CFRP (C15-20) reported by Corum et al. [57].

$\sigma_{app}(\text{MPa})$	$N_f$ (Cycles)	$R^*$	$R$
424.8	174586	0.595	0.1

$E/E_0$	$N$ (Cycles)	$E/E_0$	$N$ (Cycles)
0.863415	1872	0.609756	42593
0.834146	2340	0.585366	55231
0.790244	3744	0.57561	57103
0.790244	5617	0.565854	71613
0.765854	7021	0.556098	85655
0.741463	8893	0.541463	100165
0.731707	9361	0.536585	112334
0.736585	11233	0.531707	114206
0.707317	12170	0.536585	128248
0.702439	14042	0.521951	142758
0.639024	26211		

Table A3-37: Stiffness ratio  $E/E_0$  versus stress cycles for cross-ply CFRP (C15-4) reported by Corum et al. [57].

$\sigma_{app}$ (MPa)	$N_f$ (Cycles)	$R^*$	$R$
402.9	$12.7 \times 10^6$	0.6175	0.1
$E/E_0$	N (Cycles)	$E/E_0$	N (Cycles)
0.726829	306434	0.692683	3200536
0.707317	476676	0.634146	4221984
0.712195	612867	0.57561	4392225
0.687805	715013	0.526829	4528418
0.673171	817158	0.521951	4834853
0.692683	953351	0.536585	6469169
0.682927	1123592	0.517073	8069437
0.697561	1259786	0.253659	9499464
0.692683	1430027	0.278049	9737802
0.678049	1600268	0.292683	11372118

Table A3-38: Stiffness ratio  $E/E_0$  versus stress cycles for cross-ply CFRP (C15-21) reported by Corum et al. [57].

$\sigma_{app}$ (MPa)	$N_f$ (Cycles)	$R^*$	$R$
402.9	$12.7 \times 10^6$	0.6175	0.1

$E/E_0$	$N$ (Cycles)	$E/E_0$	$N$ (Cycles)
0.995122	238338	0.97561	2213137
0.985366	306434	0.97561	2655764
0.97561	374531	0.980488	3098391
0.965854	442627	0.97561	3541019
0.956098	885255	0.960976	3983646
0.97561	1293834	0.95122	4426273
0.970732	1770509	0.965854	4460322

Table A3-39: Stiffness ratio  $E/E_0$  versus stress cycles for cross-ply CFRP composite reported by Daniel et al. [27].

$\sigma_{app}(\text{MPa})$	$N_f(\text{Cycles})$	$R^*$	$R$
412.9	1e6	0.735	0

$E/E_0$	$N$ (Cycles)	$E/E_0$	$N$ (Cycles)
0.959064	1	0.918129	47
0.935673	2	0.912281	166
0.935673	3	0.912281	628
0.918129	4	0.888889	628
0.94152	12	0.906433	2371
0.912281	13	0.877193	2372

Table A3-40: Stiffness ratio  $E/E_0$  versus stress cycles for cross-ply CFRP composite reported by Daniel et al. [27].

$\sigma_{app}(\text{MPa})$	$N_f$ (Cycles)	$R^*$	$R$
662	31,000	0.575	0
$E/E_0$	$N$ (Cycles)	$E/E_0$	$N$ (Cycles)
0.893258	1	0.853933	2949
0.893258	7	0.865169	3587
0.88764	11	0.842697	5056
0.865169	10	0.848315	7125
0.882022	50	0.848315	9104
0.882022	58	0.842697	10041
0.882022	128	0.837079	15608
0.893258	156	0.848315	18989
0.882022	458	0.837079	21997
0.859551	505	0.842697	26761
0.88764	1559	0.837079	30600
0.870787	1560	0.775281	31001

Table A3-41: Stiffness ratio  $E/E_0$  versus stress cycles for cross-ply GRP composite reported by Boniface and Ogin [58].

$\sigma_{app}$ (MPa)	$N_f$ (Cycles)	$R^*$	$R$
140	$10^4$	0.92	0.1

$E/E_0$	$N$ (Cycles)
0.983824	10
0.960294	20
0.936765	53
0.907843	1029
0.902941	10444

Table A3-42: Stiffness ratio  $E/E_0$  versus stress cycles for cross-ply GRP composite reported by Boniface and Ogin [58].

$\sigma_{app}$ (MPa)	$N_f$ (Cycles)	$R^*$	$R$
95	$10^6$	0.964	0.1

$E/E_0$	$N$ (Cycles)
1	11
0.989216	464
0.979902	993
0.946569	2941
0.929412	10073
0.919608	1000000

Table A4-1: Nodal displacement in x direction for the selected nodes in cyclic applied load of 120MPa for GRP composite for 5 cyclic intervals.

		$U_{n1}$ $\times 10^{-6}$	$U_{n2}$ $\times 10^{-6}$	$U_{n3}$ $\times 10^{-6}$	$U_{n4}$ $\times 10^{-6}$	$U_{n5}$ $\times 10^{-6}$
Nodes fiber Face	100	2.26	2.27	2.28	2.3	2.31
	94	2.07	2.08	2.09	2.11	2.12
	167	1.61	1.62	1.63	1.64	1.65
Nodes fiber face	443	1.94	1.95	1.96	1.97	1.99
	449	1.97	1.98	1.99	2	2.01
	536	1.4	1.41	1.41	1.42	1.43



Table A4-2: Nodal displacement in x direction for the selected nodes in cyclic applied load of 140MPa for CFRP composite for 8 cyclic intervals.

		U <sub>n1</sub> ×10 <sup>-6</sup>	U <sub>n2</sub> ×10 <sup>-6</sup>	U <sub>n3</sub> ×10 <sup>-6</sup>	U <sub>n4</sub> ×10 <sup>-6</sup>	U <sub>n5</sub> ×10 <sup>-6</sup>	U <sub>n6</sub> ×10 <sup>-6</sup>	U <sub>n7</sub> ×10 <sup>-6</sup>	U <sub>n8</sub> ×10 <sup>-6</sup>
Node matrix Face	100	5.39	5.43	5.48	5.54	5.61	5.69	5.8	5.93
	94	4.94	4.98	5.03	5.08	5.15	5.22	5.32	5.44
	167	3.85	3.88	3.91	3.96	4	4.06	4.14	4.24
Node fiber face	443	4.63	4.67	4.71	4.76	4.82	4.89	4.98	5.1
	449	4.69	4.72	4.77	4.82	4.88	4.95	5.04	5.16
	536	3.33	3.36	3.39	3.43	3.47	3.52	3.59	3.67

## APPENDIX B

### B.1 MATLAB-Programming of Fatigue Damage Analysis

Appendix A contains the program listing for the fatigue damage analysis of unidirectional and cross-ply CFRP and GRP composites based on the fatigue damage approach developed in this thesis. In this program, the algorithm included following analysis:

1. Calculation  $E_m^*$ ,  $E_f^*$ ,  $R^*$  and  $N_f$  as the input to the program
2. Calculation of the fatigue damage in region I, II and III
3. Calculation of  $f$  parameter for individual experimental data
4. Calculation of  $f$  based on the proposed model for each set of experimental data
5. Calculation of fatigue damage for separate lamina of cross-ply composite based on the proposed equation
6. Calculation of total fatigue damage accumulation for cross-ply composite in regions I, II and III

**B.2 Symbols and Description in the Program**

Symbols (In Code)	Symbols (In Text)	Variable Description
X	N	Cycles before failure
Y	D	Fatigue Damage
f	f	Matrix/fibre Interfacial coefficient
n	n	Fatigue life modification Factor
m	$\eta$	Weighting Factor
a,b	-	Array of Material Properties
Em	$E_m^*$	Modified Matrix Young's Modulus
Ef	$E_f^*$	Modified Fiber Young's Modulus
r	$R^*$	Effect of Mean stress factor
Nf	$N_f$	Modified fatigue life

## Fatigue Damage Assessment of Unidirectional GRP and CFRP

Clear

```
%%%%%%%%%%%%%%%%%%%%%%%%%%%%%%%%%%%%%%%%%%%%%%%%%%%%%%%%%%%%%%%%%%%%%%%%%
% Correlation of Proposed Equation with experimental data
%%%%%%%%%%%%%%%%%%%%%%%%%%%%%%%%%%%%%%%%%%%%%%%%%%%%%%%%%%%%%%%%%%%%%%%%%
```

```
%%%%%%%%%%%%%%%%%%%%%%%%%%%%%%%%%%%%%%%%%%%%%%%%%%%%%%%%%%%%%%%%%%%%%%%%%
%Experimental Data, Damage (Y), versus Life (X)
%%%%%%%%%%%%%%%%%%%%%%%%%%%%%%%%%%%%%%%%%%%%%%%%%%%%%%%%%%%%%%%%%%%%%%%%%
```

```
a=input(Em,Ef,r,Nf);
```

```
%%%%%%%%%%%%%%%%%%%%%%%%%%%%%%%%%%%%%%%%%%%%%%%%%%%%%%%%%%%%%%%%%%%%%%%%%
X=input (N); %fatigue life data
%%%%%%%%%%%%%%%%%%%%%%%%%%%%%%%%%%%%%%%%%%%%%%%%%%%%%%%%%%%%%%%%%%%%%%%%%
```

```
%%%%%%%%%%%%%%%%%%%%%%%%%%%%%%%%%%%%%%%%%%%%%%%%%%%%%%%%%%%%%%%%%%%%%%%%%
Y=input (D); %fatigue damage data
%%%%%%%%%%%%%%%%%%%%%%%%%%%%%%%%%%%%%%%%%%%%%%%%%%%%%%%%%%%%%%%%%%%%%%%%%
```

```
n=length(X);
```

```
%%%%%%%%%%%%%%%%%%%%%%%%%%%%%%%%%%%%%%%%%%%%%%%%%%%%%%%%%%%%%%%%%%%%%%%%%
%Function to plot Experimental Data
%%%%%%%%%%%%%%%%%%%%%%%%%%%%%%%%%%%%%%%%%%%%%%%%%%%%%%%%%%%%%%%%%%%%%%%%%
```

```
for i=1:n
    plot(X,1-Y,'k*');
    hold on
end
```

```
%%%%%%%%%%%%%%%%%%%%%%%%%%%%%%%%%%%%%%%%%%%%%%%%%%%%%%%%%%%%%%%%%%%%%%%%%
% Function to plot the proposed equation (Y) versus life (x) in a
% defined range f parameter
%%%%%%%%%%%%%%%%%%%%%%%%%%%%%%%%%%%%%%%%%%%%%%%%%%%%%%%%%%%%%%%%%%%%%%%%%
```

```
for f=0:.1:1 %%%%%%%%%%%%%%%%%%%%%%%%%%%%%%%%%%%%%%%%%%%%%%%%%%%%%%%%%%%%%%%%%%%%%%%%%%
for x=1:100000:n*a(4) %Modified fatigue life by factor n
    %%%%%%%%%%%%%%%%%%%%%%%%%%%%%%%%%%%%%%%%%%%%%%%%%%%%%%%%%%%%%%%%%%%%%%%%%%
```

```
-Y=1-[a(1)*[(1-f)*((log2(x+1))/(log2(n*a(4))))]+f*(x/(n*a(4)))]+a(2)*a(3)*[(log2(1-
x/(n*a(4))))/log2(1/(n*a(4))))];
```

```
plot(x,1-Y,'k+-');
hold on;
xlabel('Number of cycles'); ylabel('1-E/Ec,int');
```

```
end
end

clear

%%%%%%%%%%%%%%%%%%%%%%%%%%%%%%%%%%%%%%%%%%%%%%%%%%%%%%%%%%%%%%%%%%%%%%%%
%Method to define f parameter for individual experimental data
%%%%%%%%%%%%%%%%%%%%%%%%%%%%%%%%%%%%%%%%%%%%%%%%%%%%%%%%%%%%%%%%%%%%%%%%

a=input (Em, Ef,r,Nf);

%%%%%%%%%%%%%%%%%%%%%%%%%%%%%%%%%%%%%%%%%%%%%%%%%%%%%%%%%%%%%%%%%%%%%%%%
%Experimental Data, Damage (Y), versus Life (X)
%%%%%%%%%%%%%%%%%%%%%%%%%%%%%%%%%%%%%%%%%%%%%%%%%%%%%%%%%%%%%%%%%%%%%%%%

                %%%%%%%%%
X=input (N); %fatigue life data
                %%%%%%%%%

                %%%%%%%%%
Y=input (D); %fatigue damage data
                %%%%%%%%%

n=length(X);
w=zeros(n,1);

%%%%%%%%%%%%%%%%%%%%%%%%%%%%%%%%%%%%%%%%%%%%%%%%%%%%%%%%%%%%%%%%%%%%%%%%
%Computing f parameter for each set of (X, Y) values, based on the %proposed equation
%%%%%%%%%%%%%%%%%%%%%%%%%%%%%%%%%%%%%%%%%%%%%%%%%%%%%%%%%%%%%%%%%%%%%%%%

for i=1:n
    q=(log2(1-X(i)/(n*a(4))))/(log2(1/(n*a(4))));
    s=(log2(X(i)+1))/(log2((n*a(4))));
    t=X(i)/(n*a(4));
    f=(1-Y(i)-a(2)*a(3)*q-a(1)*s)/(-a(1)*s+a(1)*t);
    w(i,1)=f;
    plot(log(X(i)),f,'k*-');
    hold on;
    xlabel('Number of Cycles'); ylabel('f');
end

w
```

## Fatigue Damage Assessment of Cross-ply GRP and CFRP Composite

clear

%%  
%%

% Correlation of Proposed Equation with experimental data

%%  
%%

n= 1;

m= 0.1;

a=input(Em,Ef,r,Nf);

f=1;

w=zeros(j,1);

z=zeros(j,1);

i=1;

%%

% Function to plot the proposed equation (Y) versus life (x) in a defined f parameter, in

% 0° direction

%%

for x=1.1:10:a(4)

Y=[a(1)\*[(1-f)\*((log2(x+1))/(log2(a(4))))]+f\*(x/a(4))]+

a(2)\*a(3)\*((log2(1-x/a(4)))/log2(1/a(4)))];

w(i,1)=Y;

z(i,1)=x;

i=i+1;

plot(x,Y,'rd');

hold on;

xlabel('Number of cycles'); ylabel('1-E/Ec,int');

title('Oak ridge Vf=42.7%,Sigma=95%UTS');

```
end
w
z
a=input(Em,Ef,r,Nf);
w=zeros(j,1);
z=zeros(j,1);
i=1;
f=0;
%%%%%%%%%%%%%%%%%%%%%%%%%%%%%%%%%%%%%%%%%%%%%%%%%%%%%%%%%%%%%%%%%%%%%%%%
% Function to plot the proposed equation (Y) versus life (x) in a defined f parameter, in
% 90° direction
%%%%%%%%%%%%%%%%%%%%%%%%%%%%%%%%%%%%%%%%%%%%%%%%%%%%%%%%%%%%%%%%%%%%%%%%
for x=1.1:10:a(4)
    Y=[a(1)*[(1-f)*[(log2(x+1))/(log2(a(4)))]+f*(x/a(4))]+
a(2)*a(3)*[(log2(1-x/a(4)))/log2(1/a(4))]];
    w(i,1)=Y;
    z(i,1)=x;
    i=i+1;
    plot(x,Y,'bs');
    hold on;
    xlabel('Number of cycles'); ylabel('1-E/Ec,int');
    title('Oak ridge Vf=42.7%,Sigma=95%UTS');
end
w
z
%%%%%%%%%%%%%%%%%%%%%%%%%%%%%%%%%%%%%%%%%%%%%%%%%%%%%%%%%%%%%%%%%%%%%%%%
%Experimental Data, Damage (Y), versus Life (X)
%%%%%%%%%%%%%%%%%%%%%%%%%%%%%%%%%%%%%%%%%%%%%%%%%%%%%%%%%%%%%%%%%%%%%%%%
                                %%%%%%%%%
X=input (N); %fatigue life data
                                %%%%%%%%%
```

```

%%%%%%%%%%%%%%%%%%%%%%%%%%%%%%%%%%%%%%%%
Y=input (D); %fatigue damage data
%%%%%%%%%%%%%%%%%%%%%%%%%%%%%%%%%%%%%%%%

%%%%%%%%%%%%%%%%%%%%%%%%%%%%%%%%%%%%%%%%
%Function to plot Experimental Data
%%%%%%%%%%%%%%%%%%%%%%%%%%%%%%%%%%%%%%%%

n=length(X);
for i=1:n
    plot(X,Y,'k*');
    hold on
end

clear

%%%%%%%%%%%%%%%%%%%%%%%%%%%%%%%%%%%%%%%%
% Correlation of Proposed Equation with experimental data
%%%%%%%%%%%%%%%%%%%%%%%%%%%%%%%%%%%%%%%%

n=1.25;
m=.1;
a=input(Em,Ef,r,Nf);
b=input(Em,Ef,r,Nf);
f1=0;
f=1;
w=zeros(j,1);
z=zeros(j,1);
i=1;
%%%%%%%%%%%%%%%%%%%%%%%%%%%%%%%%%%%%%%%%
% Function to plot the proposed equation (Y) versus life (x) in a defined f parameter, by
% combining 0 and 90 degree
%%%%%%%%%%%%%%%%%%%%%%%%%%%%%%%%%%%%%%%%

```



```

for x=1.1:10:a(4)
%%%%%%%%%%%%%%%%%%%%%%%%%%%%%%%%%%%%%%%%%%%%%%%%%%%%%%%%%%%%%%%%%%%%%%%%
%Damage related to 0 degree ply
%%%%%%%%%%%%%%%%%%%%%%%%%%%%%%%%%%%%%%%%%%%%%%%%%%%%%%%%%%%%%%%%%%%%%%%%

Y1=[a(1)*[(1-f)*[(log2(x+1))/(log2(a(4)))]+f*(x/a(4))]+
a(2)*a(3)*[(log2(1-x/a(4)))/log2(1/a(4))]];

%%%%%%%%%%%%%%%%%%%%%%%%%%%%%%%%%%%%%%%%%%%%%%%%%%%%%%%%%%%%%%%%%%%%%%%%
%Damage related to 90 degree ply
%%%%%%%%%%%%%%%%%%%%%%%%%%%%%%%%%%%%%%%%%%%%%%%%%%%%%%%%%%%%%%%%%%%%%%%%

Y2=[b(1)*[(1-f1)*[(log2(x+1))/(log2(a(4)))]+f1*(x/a(4))]+
b(2)*b(3)*[(log2(1-x/a(4)))/log2(1/a(4))]];

%%%%%%%%%%%%%%%%%%%%%%%%%%%%%%%%%%%%%%%%%%%%%%%%%%%%%%%%%%%%%%%%%%%%%%%%
D=0.7*Y1+0.3*Y2; %combining of damage of o degree and 90 degree plies
%%%%%%%%%%%%%%%%%%%%%%%%%%%%%%%%%%%%%%%%%%%%%%%%%%%%%%%%%%%%%%%%%%%%%%%%

w(i,1)=D;
z(i,1)=x;
i=i+1;

plot(x,D,'b+');
hold on;
xlabel('Number of cycles'); ylabel('1-E/Ec,int');
title('Oak ridge Vf=42.7%,Sigma=95%UTS');
end
w
z

```

```

%%%%%%%%%%%%%%%%%%%%%%%%%%%%%%%%%%%%%%%%%%%%%%%%%%%%%%%%%%%%%%%%%%%%%%%%
%Experimental Data, Damage (Y), versus Life (X)
%%%%%%%%%%%%%%%%%%%%%%%%%%%%%%%%%%%%%%%%%%%%%%%%%%%%%%%%%%%%%%%%%%%%%%%%

```

```

%%%%%%%%%%%%%%%%%%%%%%%%%%%%%%%%%%%%%%%%%%%%%%%%%%%%%%%%%%%%%%%%%%%%%%%%
X=input(N); %fatigue life data
%%%%%%%%%%%%%%%%%%%%%%%%%%%%%%%%%%%%%%%%%%%%%%%%%%%%%%%%%%%%%%%%%%%%%%%%

```

```

%%%%%%%%%%%%%%%%%%%%%%%%%%%%%%%%%%%%%%%%%%%%%%%%%%%%%%%%%%%%%%%%%%%%%%%%
Y=input(D); %fatigue damage data
%%%%%%%%%%%%%%%%%%%%%%%%%%%%%%%%%%%%%%%%%%%%%%%%%%%%%%%%%%%%%%%%%%%%%%%%

```

```

%%%%%%%%%%%%%%%%%%%%%%%%%%%%%%%%%%%%%%%%%%%%%%%%%%%%%%%%%%%%%%%%%%%%%%%%
%Function to plot Experimental Data
%%%%%%%%%%%%%%%%%%%%%%%%%%%%%%%%%%%%%%%%%%%%%%%%%%%%%%%%%%%%%%%%%%%%%%%%
n=length(X);
for i=1:n
    plot(X,Y,'k*');
    hold on
end

```